HAL
open science

Transport quantique dans les verres de spin

Thibaut Capron

To cite this version:

Thibaut Capron. Transport quantique dans les verres de spin. Systèmes mésoscopiques et effet Hall quantique [cond-mat.mes-hall]. Université de Grenoble, 2011. Français. NNT : . tel-00686330

HAL Id: tel-00686330

https://theses.hal.science/tel-00686330

Submitted on 9 Apr 2012

HAL is a multi-disciplinary open access archive for the deposit and dissemination of scientific research documents, whether they are published or not. The documents may come from teaching and research institutions in France or abroad, or from public or private research centers.

L'archive ouverte pluridisciplinaire **HAL**, est destinée au dépôt et à la diffusion de documents scientifiques de niveau recherche, publiés ou non, émanant des établissements d'enseignement et de recherche français ou étrangers, des laboratoires publics ou privés.

UNIVERSITÉ DE GRENOBLE

THÈSE

Pour obtenir le grade de

DOCTEUR DE L'UNIVERSITÉ DE GRENOBLE

Spécialité : **Physique de la Matière Condensée et du Rayonnement**

Arrêté ministériel : 7 août 2006

Présentée par

Thibaut CAPRON

Thèse dirigée par **Laurent SAMINADAYAR**

préparée au sein de l'**Institut Néel**
dans l'**École Doctorale de Physique**

TRANSPORT QUANTIQUE DANS LES VERRES DE SPIN

Thèse soutenue publiquement le **30 Mars 2011**
devant le jury composé de :

Mr Eric VINCENT
DR CEA Saclay, Président du Jury
Mme Hélène BOUCHIAT
DR LPS Orsay, Rapporteur
Mr Giorgio PARISI
PR Université de Rome, Rapporteur
Mr David CARPENTIER
CR ENS Lyon, Membre
Mr Daniel ESTÈVE
DR CEA Saclay, Membre
Mr Laurent LÉVY
PR Université de Grenoble, Membre
Mr Laurent SAMINADAYAR
PR Université de Grenoble, Membre

Quantum transport in spin glasses

Thibaut Capron

March 30, 2011

Contents

Remerciements **iii**

Introduction **v**

I Theoretical introduction and related concepts **1**

1 Spin glasses, a model for glassy systems **3**
1.1 The intriguing glass phase . . . 3
1.2 Spin glasses . . . 4
1.2.1 Disorder and frustration . . . 5
1.2.2 Canonical spin glasses . . . 6
1.2.3 Spin glass phase space . . . 7
1.2.4 Towards an order parameter . . . 8
1.3 Models for spin glass systems . . . 9
1.3.1 Replica symmetry breaking: the Parisi solution . . . 10
1.3.2 Scaling theories . . . 12

2 Coherent electron transport: an original probe for disorder **15**
2.1 Electron transport in solids . . . 15
2.2 Universal Conductance Fluctuations . . . 17
2.2.1 Quantitative description . . . 19
2.2.2 Effect of the temperature . . . 20
2.3 Onsager symmetries . . . 21

3 Universal conductance fluctuations and spin glasses **23**
3.1 A first attempt, noise experiments . . . 23
3.2 Pioneering work on universal conductance fluctuations . . . 24
3.3 A recent renewal . . . 25

II Experimental implementation **29**

4 Experimental implementation **31**
4.1 Experimental setup . . . 31
4.1.1 Samples fabrication . . . 31
4.1.2 Experimental setup . . . 35
4.2 Measurement implementation . . . 38

4.2.1 Rapid quench strategy 38
4.2.2 Correlations 40
4.2.3 Calibration of the reproducibility 42

III Experimental study of spin glasses 45

5 Experimental calibration on pure Ag 47
5.1 Weak-localization measurements 47
5.2 Universal conductance fluctuations 48
5.3 Onsager relations 51

6 Remanence in the resistivity of AgMn spin glass 55
6.1 Size effects in spin glasses 55
6.2 Experimental signatures of the spin glass phase 56
6.2.1 Temperature dependence of the resistivity 56
6.2.2 Magnetic irreversibilities 60

7 Universal conductance fluctuations in AgMn spin glass 65
7.1 Measurement of universal conductance fluctuations 65
7.2 Magnetic excitations 68
7.3 Temperature dependence of the phase coherence length 71

8 Measurement of the magnetofingerprints correlations 77
8.1 Scaling effects: the route to overlaps 77
8.2 Field effects: spin glass rigidity? 79
8.3 Temperature effects: a determination of the overlaps? 83

Conclusion 88

A Wiring of the fridge 91

B Extraction of the phase coherence length from the universal conductance fluctuations 97

Bibliography 99

Remerciements

L'expérience de la thèse est une formidable aventure scientifique. J'ai eu le plaisir de pouvoir la mener à bien grâce à l'aide et au soutien de nombreuses personnes dans mon entourage. Je tiens à leur exprimer ma profonde gratitude.

Merci aux directeurs successifs de l'Institut Néel, Alain Fontaine et Alain Schuhl, de m'avoir accueilli dans leur laboratoire à Grenoble durant près de quatre ans.

Je tiens à exprimer toute ma reconnaissance envers Laurent Saminadayar, merci d'avoir guidé mes premiers pas dans la recherche, merci pour tes nombreux et riches enseignements, ta bienveillance et la confiance que tu m'as témoignée au fil des années. Un grand merci également pour tes nombreuses relectures du manuscrit, pour ta patience et pour tout le travail que nous avons fourni ensemble dans cette préparation de thèse.

Merci, Christopher Bäuerle, pour ton engagement au quotidien, ton soutien sur la durée et tes nombreux enseignements expérimentaux. Merci à Tristan Meunier, pour m'avoir fait partager ton enthousiasme et ta vision de la physique.

Je souhaite remercier vivement Hélène Bouchiat et Giorgio Parisi d'avoir accepté d'être les rapporteurs de ce travail de thèse. J'exprime également ma gratitude à l'égard de David Carpentier, Daniel Estève, Laurent Lévy et Eric Vincent qui m'ont honoré de leur participation à mon jury de thèse. Merci, Laurent Lévy, de m'avoir soutenu tout au long de ce projet et de m'avoir fait profiter de ton savoir et de ton expérience. Merci, David Carpentier, d'avoir su me transmettre les tenants et aboutissants de vos travaux avec autant de pédagogie et merci de ta disponibilité.

Lors de ce travail de recherches, nous avons bénéficié de nombreuses collaborations. Merci à Christophe Peaucelle et Angela Perat-Mabilon pour avoir permis l'utilisation de l'implanteur ionique dans les meilleurs délais. Merci au groupe d'Hélène Bouchiat, d'avoir mis à notre disposition votre bâti d'évaporation d'or. Merci à Hugues Pothier et le groupe Quantronics, pour l'utilisation du bâti d'évaporation d'argent. Votre contribution nous a permis d'élaborer les échantillons adéquats pour ce travail de thèse. J'ai également eu la chance de pouvoir présenter ce travail et avoir des discussions fructueuses avec de nombreux chercheurs : Gilles Montambaux, Christophe Texier, Leonid Glazman... Et, merci aux chercheurs de l'Institut Néel avec qui j'ai eu des discussions plus informelles : Olivier Buisson, Klaus Hasselbach, Olivier Bourgeois, Wolfgang Wernsdorfer...

De nombreuses personnes ont eu un rôle primordial dans la réalisation technique de ce projet. Alors, un grand merci aux personnels des pôles de l'Institut : le pôle Cryogénie, Pierre Perrier et le pôle Ingéniérie expérimentale, Thierry Fournier, Thierry Crozes, le pôle Nanofab

et la Plateforme Technologique Amont située tout près au CEA, le pôle électronique et enfin le liquéfacteur. Merci également aux services informatique et administratif du laboratoire.

Un grand merci aux membres de l'équipe Cohérence Quantique, avec lesquels j'ai travaillé au quotidien. Merci, en particulier à Yasuhiro Niimi, for your kindness and for all the interesting discussions we have shared, about physics and other topics. A Sylvain Hermelin, pour ta disponibilité et nos discussions scientifiques enflammées. A Soumen Mandal, for your jokes and positive mood. Et, à Tobias Bautze, for your great kindness. Merci, Guillaume Forestier, pour l'aide précieuse que tu m'as apportée durant mon dernier mois de thèse.

Merci aux autres doctorants que j'ai cotoyés durant ces quelques années, pour tous les bons moments que nous avons partagés : Guillaume Paulin, Nicolas Roch, Aurélien Bideaud, Pascale Diener, Marton Karsaï, Pierre Delplace, Samuel Tardif, Fabien Bonnet, Ulisse Ferrari, et bien d'autres...

Enfin, merci aux amis proches et à la famille, qui sont d'une aide précieuse pour mener à bien une entreprise telle que la thèse. La joyeuse bande du "FC" qui m'a suivi de près depuis le début : Zouille, Pierrot, Kael, Rémi, Jojo, Jc, Fred, Raynald... Les amis "retournakéens", qui m'ont toujours soutenu, bien qu'ils n'y comprenaient pas grand chose : Julien, Xav, Patrice, Sofy, Sylv, Cedrick, Stéphane... Mon ami d'enfance Greg, mais aussi Seb, Aurélien, mes conscrits, et tous ceux que j'oublie...

Merci à mes parents, pour votre affection et votre soutien sans faille depuis toujours. Merci à ma grand-mère, Evelyne, pour ton enthousiasme. Merci à mes frères et soeurs, Flavien, Marjorie et Chloé, d'avoir été là. Merci, Jeanne, de votre bonne humeur et votre affection. Et enfin, merci à celle qui partage ma vie et prend soin de moi, merci pour tes conseils et ton sourire, merci Elodie.

Introduction

The fascinating glassy state

Glass is a ubiquitous material in our daily life; however, it is one of the most complex states of matter. It is frequently used in various forms (optical glasses, glass wool...) for its numerous physical properties.

The specificity of this peculiar state of matter is that it is between a liquid state and a solid state. The atoms in the glass are disordered like in a liquid, but are trapped, under a very fast cooling procedure called a quench, in a solid state. As with a liquid, the matter flows, but on extremely long time scales, that can be counted in thousands of years. Thus, the material appears solid for daily handling. After the success of solid state physics in describing crystallized materials in which the atoms are ordered, physicists have paid attention to these disordered systems, that require new concepts.

From the seventies, one type of glasses, called spin glass, has received the attention of physicists. It is a magnetic glass, composed of magnetic atoms randomly distributed in space. Such systems are frequently encountered in the study of magnetic materials, and one understands rather well some of the underlying mechanisms leading to the formation of this phase. Spin glass is thus considered as a model system for the study of glassy state.

During the seventies and eighties, this glass was extensively studied, both theoretically and experimentally. The experimental approaches have revealed fascinating properties: a non conventional order of matter, memory features... And the theoretical works have converged towards two main descriptions of the spin glass fundamental state. Two visions that are clearly antagonist and still heavily debated. On the one hand, a "mean-field" point of view with coexisting multiple fundamental states. On the other hand, a "droplet" vision, with a unique fundamental state. In order to discriminate between these two theories, it is required to know in details, that is at the microscopic level, the fundamental states obtained after, for example, two independent quenches.

The input of mesoscopic physics

Mesoscopic physics deals with the electronic properties of conductors in the quantum regime, that is, when these properties are governed by the wave nature of electrons. To reach such a regime, one needs samples below the micrometer size, and cryogenic temperatures. This explains why the study of mesoscopic physics soared during the eighties and nineties, with the development of adequate experimental techniques.

In particular, in this regime, electrons interfere while they diffuse in the system. This gives rise to fluctuations in the conductance that reflect the detailed paths of the electrons

in the sample, *i.e.*, the disorder configuration. A measurement of these fluctuations gives a "fingerprint" of the disorder. The idea of using such a property in the study of disordered systems emerged simultaneously with mesoscopic physics, but only a few really conclusive experiments have been achieved so far.

Purpose of this work

In this PhD work, we propose to implement such measurements of the conductance fluctuations in spin glasses. This original mesoscopic approach provides a tool which has a unique sensitivity to the disorder. We have elaborated mesoscopic spin glass samples, and prepared the experimental setup required for the measurement. The comparison between results obtained in a pure Ag sample, and in a AgMn alloy allows to highlight experimental signatures of the spin glass phase. We have addressed the study of the resistivity of the spin glass, of the amplitude of the conductance fluctuations in field and temperature, and of the correlations between different fingerprints of the disorder configuration. Such measurements open a new way to an experimental determination of the spin glass order parameter, that may allow characterization of the ground state of the system.

Manuscript outline

This manuscript is divided into three parts. The first part gives an introduction to the physics we are dealing with. Chapter 1 introduces the spin glass physics and the problematic of the ground state in such systems. Chapter 2 details concepts of the mesoscopic physics and in particular universal conductance fluctuations used in our study of spin glasses. Chapter 3 describes the state of the art of experimental and theoretical attempts to link mesoscopic fluctuations and spin glasses.

The second part deals with the implementation of the experiment. In chapter 4, we present the experimental setup and the measurement implementation.

The third part is dedicated to the results of the measurements made in mesoscopic spin glasses. Chapter 5 presents the experimental calibration of the technique performed on a non magnetic sample, which will serve as a reference. In chapter 6, we present the experimental signatures of the spin glass phase on the resistivity. Our low-noise setup reveals characteristic irreversibilities that allow to determine the freezing temperature T_g. Chapter 7 presents measurements of the conductance fluctuations in spin glasses. Their dependence on the magnetic field yields new trends towards a freezing of magnetic excitations in a spin glass. Chapter 8 deals with the analysis of the correlations between different disorder configurations. The experimental conductance fluctuations are shown to be sensitive to the magnetic disorder. We thus study the effect of an external parameter which acts on the disorder: an additional magnetic field seems to modify the fingerprints in a reversible way, whereas a temperature cycle affects them irreversibly. These results allow for a direct determination of the spin glass order parameter.

Part I

Theoretical introduction and related concepts

L'ordre est le plaisir de la raison, mais le désordre est le délice de l'imagination.
Paul Claudel, Le Soulier de satin

Chapter 1
Spin glasses, a model for glassy systems

In this chapter, we outline the basics on spin glasses, and the theoretical concepts linked to the description of the ground state in these systems.

1.1 The intriguing glass phase

Condensed matter physics has been built around the success of crystal theories. When identical atoms are arranged on a regular lattice, the properties of the whole material can be extrapolated from the behavior of a single segment, as the translational invariance is fulfilled [1, 2]. The long-range atomic order has turned out to be a definition of the solid phase (in opposition to the liquid or gas phases).

However, in nature one can easily find a large quantity of compounds that are not ordered in a regular manner. This is due to a disorder in the lattice atoms' positions (amorphous material), or in some impurities' - atoms different than the lattice ones - positions (alloys). One cannot use the usual crystal theories to describe these compounds, as there are no long-range spatial correlations. In these systems, the matter is *ill-condensed*[1]. Some of these disordered systems are called "glasses", and have excited the curiosity of physicists.

Structural glasses (amorphous materials) are obtained by cooling down a supercooled liquid. In the liquid state, the atoms are moving and are thus in a disordered configuration. When the liquid is rapidly[2] cooled, the crystalline order may not have the time to establish. Indeed, the atoms cannot reorganize, and they are trapped in disordered positions into the solid state. This phenomenon appears below a characteristic temperature T_g, the glass temperature. Below T_g, the material is a *solid* having a structural *liquid* disorder. Such a fabrication protocol is the one used by the glass-blower who sculpts our daily objects (figure 1.1).

[1] This expression is taken from the title of a school at Les Houches.
[2] With respect to the atoms reorganization time.

Figure 1.1: *Left: a piece of obsidian, a natural volcanic glass. Right: ordinary glass being sculpted by a glass-blower before cooling.*

However the concept of glasses as a phase where disorder is frozen (quenched) is more general than that. Glasses exhibit the following properties:

1. Absence of long-range order, revealed by diffraction experiments (Xray, neutrons...).
2. Divergence of the viscosity around a critical temperature T_g, below which one enters the glassy phase.
3. The glass phase is metastable, the disorder configuration has slow dynamics, and the system relaxes on very long time scales[3].

The difficulties encountered in describing this intriguing state of matter have generated new concepts and techniques. Interestingly, the models developed are also applied to general combinatorial optimization problems, such as the "traveling salesman".

As we have already mentioned, the disorder in glasses can be of various types. In particular, it can come from magnetic impurities; this is the famous example of the spin glass that we will focus on in all the following.

1.2 Spin glasses

This work is dedicated to spin glasses [3, 4, 5, 6]. In these systems, the disorder is magnetic. It arises from the presence of magnetic impurities in a host material. Below the glass temperature T_g, the magnetic moments are competing through an interaction which is random in amplitude and sign, and leads to frustration: none of the configurations can satisfy energetically all the bonds simultaneously. This results in a state in which all the magnetic moments are frozen in random orientations. The system has a *local* magnetization, but a vanishing *global* one. In spin glasses, the source of randomness and the mechanisms behind the glassy behavior are well identified; this is why they are considered as a model glass.

[3]The thickness of stained glasses being larger at the bottom than on the top as often been attributed to the slow flowing down of the glass along centuries. This is not quantitatively true, though the disorder reorganizes slowly.

1.2.1 Disorder and frustration

As mentioned before, the two basic ingredients to obtain a spin glass phase are disorder and frustration [7]. Frustration is a situation in which all the energetic constraints of the system cannot be satisfied simultaneously. As an example, let us consider a triangular lattice of Ising spins with antiferromagnetic coupling, as shown in figure 1.2 (left panel). In this situation, one cannot satisfy the antiferromagnetic coupling for the three bonds simultaneously. If one fixes two spins satisfying antiferromagnetic coupling, the third one cannot be fixed in a way that minimizes the energy of the two other bonds. As a consequence, one of the three bonds is not satisfied, it is frustrated.

In this example, one obtains several equivalent states of lowest energy: by permuting the orientation of the spins, we change the frustrated bond, but not the energy of the system. Therefore, one has a three-fold degenerate ground state. Such a geometrical frustration due to the topology of the lattice is present, for example, in spin ice systems.

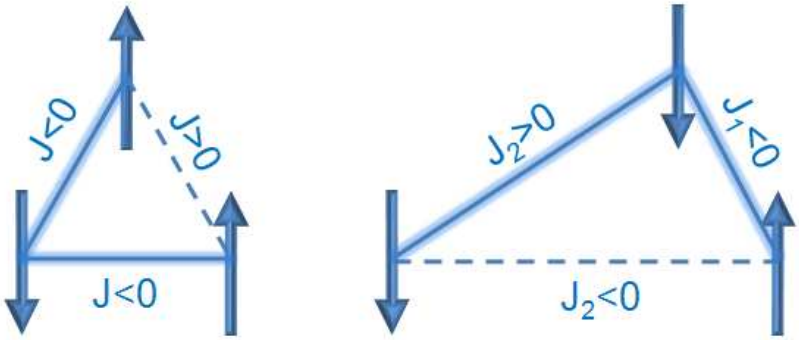

Figure 1.2: *Examples of frustration for Ising spins: the solid bonds are satisfied, and the dashed bonds are frustrated. Left: geometrical frustration of a triangular lattice, $J < 0$ is the same for all bonds. Right: disorder induced frustration, the sign of the coupling changes with the distance. At short distances, the coupling is $J_1 < 0$, whereas at long distances the coupling is $J_2 > 0$.*

In spin glasses, the impurities are randomly distributed in space. This leads to a randomness in the amplitude and the sign of the interaction between spins, as illustrated in the right panel of figure 1.2. In this situation, the coupling changes with the distance between spins; the induced frustration is due to the magnetic disorder.

Below the critical temperature T_g, the interaction becomes dominant over the temperature, and spins are frozen in a frustrated configuration. There is no long-range spatial magnetic order. The spins have a slow relaxation which is governed by the frustration. Thus, the magnetic disorder is quenched below T_g and the system has a glassy behavior.

Experimentally, such a freezing of the magnetic moments can be detected by magnetic susceptibility measurements. Like other magnetic systems presenting ordering, a signature of a phase transition in such alloys can be obtained from the temperature dependence of the susceptibility $\chi(T)$. As shown in figure 1.3, a clear cusp appears in such a measurement, and was originally observed by Canella and Mydosh [8].

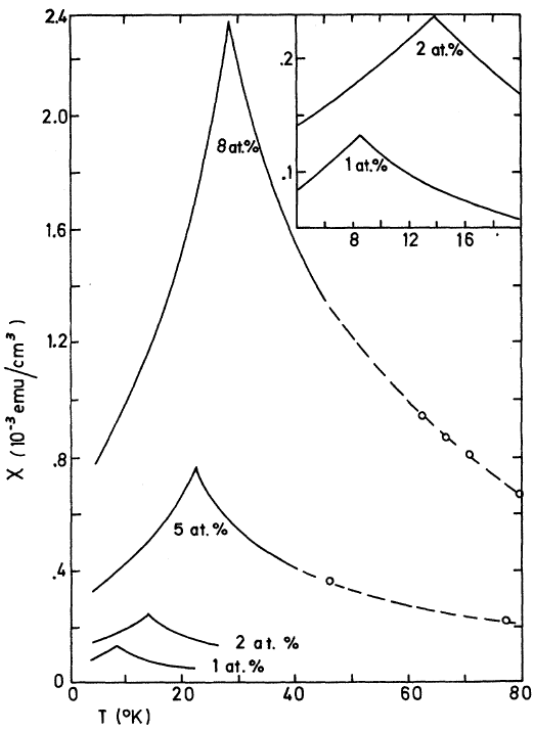

Figure 1.3: *Low-field magnetic susceptibility $\chi(T)$ of AuFe for $1 \leq x \leq 8$ at.%. From [8].*

The amplitude and the position of the cusp depend on the magnetic impurity concentration. However, the amplitude is much smaller than what is observed in ferromagnetic systems, reflecting a non uniform polarization of the spins in the sample.

A slow relaxation of the system is also observed in similar experiments [9] (not shown). It shows that the macroscopic equilibrium of the system is not reached, even on time scales up to 10^4 s.

1.2.2 Canonical spin glasses

In spin glasses that we consider in this study, the magnetic spins are coupled by the Ruderman-Kittel-Kasuya-Yosida (RKKY) interaction [10, 11, 12]. In this mechanism, a magnetic impurity polarizes the surrounding host conduction electrons with a susceptibility that oscillates with the distance [1]. These polarized electrons interact in turn with a second impurity. This leads to an oscillatory coupling between spins (see figure 1.4):

$$J(r) = J_0 \frac{\cos(2k_F r)}{(k_F r)^3} \tag{1.2.1}$$

where J_0 is the coupling constant between the electrons and the impurity.

In these alloys, the transition temperature T_g is the temperature below which the RKKY interaction prevails over temperature, leading to frustration and glassy phase. Following arguments developed by Blandin, Souletie and Tournier [13], one can show that a characteristic of the RKKY interaction is that T_g is proportional to the concentration of magnetic impurities c. The typical transition temperature expected in these alloys is about $T_g = 1$ K for a concentration $c = 1000$ ppm (part per millions).

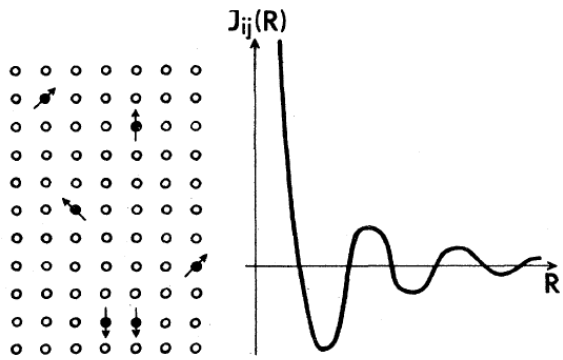

Figure 1.4: *Sketch of magnetic moments randomly diluted in a metallic matrix, and the resulting RKKY exchange plotted as a function of inter-impurity distance. Note that the coupling sign changes with the distance. Extracted from [3].*

Metallic spin glasses, *i.e.* a noble-metal host containing transition-metal impurities coupled by RKKY interaction, are called canonical spin glasses. It is worthy to note that there is a generic spin glass behavior which is independent of the details of the sample chemistry. Metallic, as well as insulating spin glasses show in three dimensions a well defined phase transition at T_g. Historically, the metallic systems such as AuFe, CuMn, AgMn, have been widely studied both theoretically and experimentally. They represent the core of what a spin glass is. We will focus on this type of spin glass in the following experimental work.

1.2.3 Spin glass phase space

Above T_g, the interaction is overcome by thermal activation and spins are paramagnetic. In this situation, each spin relaxes very fast[4], and its local magnetization is zero. In a spin glass however, the spins are frozen in random orientations below T_g, and there exists a *local* magnetization $m_i \equiv \langle S_i \rangle \neq 0$ ($\langle\rangle$ denotes the thermal averaging). However this magnetization is different for each site i, and the global averaged magnetization M is zero.

This spontaneous local magnetization suggests that the phase space is composed of energy valleys. Like in the ferromagnetic case, the free-energy landscape is transformed when the system is cooled down below the critical temperature. In spin glasses in addition, one has numerous possible states, due to the frustration. These many states correspond to the various orientations that a spin can take. One calls the ensemble of frozen spins a *configuration* of the magnetic disorder. In the spin glass state, there are many possible spin configurations, but only one is taken below T_g. Consequently, the free energy landscape appearing below T_g is viewed as a many-valley picture. Such a landscape is depicted on figure 1.5.

At any temperature below T_g, the many-valley structure appears, with valleys which are separated by barriers of different heights. The system is thus trapped into a specific valley α, β or γ. This barrier landscape disappears when one goes to $T > T_g$; the system is restored in a unique valley δ.

[4]As compared to the time scale of the experimental observation.

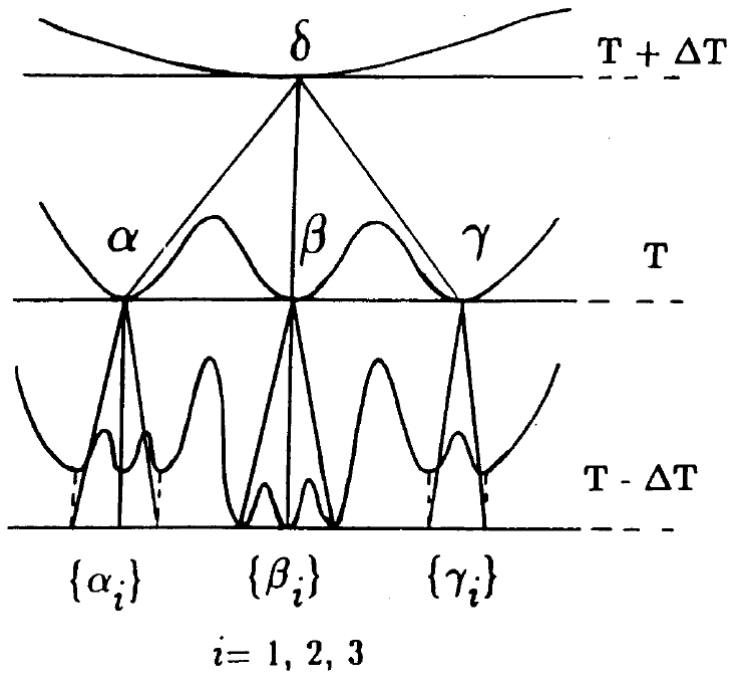

Figure 1.5: *Schematic picture of the hierarchical structure of the many-valley phase space as a function of temperature. Extracted from [14].*

1.2.4 Towards an order parameter

Generally, ordered phases can be described by an order parameter which is zero above the transition temperature, and nonzero below. In spin glasses, the order is related to the freezing of the spins. Above T_g, the spins relax very fast. Below T_g, they are frozen. A natural order parameter is thus the dynamical spin configuration. This was introduced by Edwards and Anderson [15]

$$q_{EA} = \lim_{t\to\infty} \lim_{N\to\infty} \langle S_i(t_0) S_i(t_0 + t)\rangle_i \tag{1.2.2}$$

q_{EA} is the Edwards-Anderson order parameter. The limit on N designates the thermodynamic limit, t the time and t_0 a reference time. This *correlation of the spin configurations* will clearly be zero for paramagnetic spins, and will be nonzero if the configuration is frozen.

When the spin glass is cooled down below T_g, it is trapped in a valley state. In this state, the spin configuration is frozen, and is considered independent of time. The order parameter q_{EA} thus measures the single-valley mean square local magnetization.

If one has a many-valley phase space, it is interesting to ask not only about q_{EA} in a single state but also about the correlation between states. How are they linked between them? The *overlap* $q_{\alpha\beta}$ is defined between distinct valleys α and β:

$$q_{\alpha\beta} = \frac{1}{N} \sum_i \langle S_i^\alpha S_i^\beta \rangle \tag{1.2.3}$$

Due to the complexity of the phase space, $q_{\alpha\beta}$ may take many values. Therefore one can consider its distribution $P(q)$ [16]. For a system with only two valleys (like a ferromagnet), q can only take two values: the value of the correlation of the valley α with the other valley β, or with itself α. Thus, the shape of the distribution $P(q)$ permits the investigation of the structure of the phase space.

1.3 Models for spin glass systems

Averaging in disordered systems

Randomness introduces special features into the theoretical treatment in statistical physics. As we have random parameters $\{J\}$ coming into the problem, one applies statistical physics to their distribution. Thermodynamic quantities can be derived from the free-energy that can be expressed from the partition function $\mathcal{Z}$, which depends on the disorder parameters. To recover the macroscopic behavior, the free-energy has to be averaged (noted $[\ ]_{av}$) on the distribution of $\{J\}$.

The difficulty arises in such an averaging of $F = [F\{J\}]_{av} = -k_B T[\ln \mathcal{Z}\{J\}]_{av}$, as $\ln \mathcal{Z}\{J\}$ is not an extensive quantity. The widely used *replica method* allows to overcome this difficulty. The average can be performed by decomposing the system into n identical *replicas* for a given realization of the disorder $\{J\}$, and then taking the limit $n \to 0$. In this method, the problem is symmetric under the permutation of replicas - all the replicas are equivalent.

The Sherrington-Kirkpatrick model

Phenomenologically, randomness and frustration have been identified to be the main ingredients of spin glass behavior. The model introduced by Edwards and Anderson (EA) [17] in 1975 comes from this idea. Instead of taking the randomness in the spins *position*, one takes the randomness in the *interactions* between spins lying on a regular lattice.

A mean-field version of this model was then introduced by Sherrington and Kirkpatrick (SK) [18]. It is a generalization of the EA model for infinite-range interactions and Ising spins. The Hamiltonian is

$$\mathcal{H}_{SK} = -\frac{1}{2}\sum_{i,j} J_{ij} S_i^z S_j^z + h \sum_i S_i^z \tag{1.3.1}$$

where S_i^z is the (Ising) spin at site i and h a magnetic field applied along the z axis. J_{ij} represents the random coupling between the spins i and j. The sum is performed on all the neighbors. All the randomness lies in the distribution of J_{ij}.

In mean-field models, the dimension above which mean-field theory predicts the existence of a phase transition at finite temperature is called the lower critical dimension d_l. It has been heavily debated in the past, and is still not precisely known. It may be lying between 2 and 3 for Ising systems, and about $d_l \simeq 3$ for Heisenberg systems with anisotropy [19, 20].

The SK model can be solved by using the replica method, and self-consistent equations can be derived for $q = [m_i^2]_{av}$. This solution captures well the cusp in susceptibility at T_g, the signature of the magnetic freezing of the spins.

However, this treatment leads to unphysical behaviors: the entropy at zero temperature tends to a negative value. Indeed, this solution is the *replica-symmetric* one, all the replicas are considered as undistinguishable. This is the source of the unphysical features of this mean-field solution.

Instability of the SK solution

Afterwards, de Almeida and Thouless [21] performed a detailed analysis of the SK solution and showed that it is *unstable* at low temperature, as it gives a negative susceptibility χ.

The stability condition can be calculated as a function of temperature T and in the presence of a magnetic field H. It yields a stability line in the H-T plane called the A-T line. Above the A-T line, the SK solution is stable, and the previous model describes correctly the paramagnetic phase. Below this line however, the solution is not valid anymore. One can transpose this issue of undistinguishable replicas to the complexity of the phase space. In this peculiar landscape, the valleys may not be equivalent, one has to break the symmetry of the replicas of the system. The A-T line is thus the line below which the replicas are not symmetric.

1.3.1 Replica symmetry breaking: the Parisi solution

The order parameter containing n replicas is represented as a matrix Q_{ab}, where a and b are the replicas indices. In the SK solution, all the replicas are equivalent, equal to q_0, except the diagonal terms, which are zero. This symmetry has to be broken, but how?

The solution has been proposed by Parisi [22] in 1979. We detail here a step of such a Replica Symmetry Breaking (RSB) procedure. Consider the $(n \times n)$ replica symmetric matrix filled with q_0 (for illustration we take $n = 8$ on figure 1.6). One then divides it into (n/m_1) blocks of size $(m_1 \times m_1)$. The off-diagonal blocks are left unchanged with q_0. The diagonal blocks are modified, taking the same structure as the $(n \times n)$ mother matrix, with zero diagonal value and q_1 off-diagonal value.

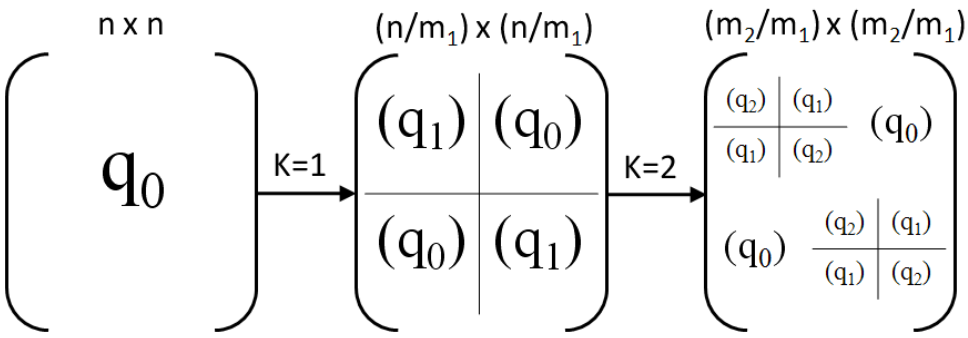

Figure 1.6: *Illustration of the Q matrix replica symmetry breaking, at steps $K = 1$ and 2.*

One can repeat this RSB procedure again (K is the number of RSB-steps performed), and the best solution will be found to be the full-step RSB [23, 24] ($K \to \infty$).

After this procedure is done, one defines $P(q)$ as the fraction of the matrix elements that are taking the value q (that is the distribution law of overlap values q).

When K is very large, one can express *continuously* the values q_i with a function

$$q_i \to q(x) \quad with \quad 0 \leq x \leq 1 \tag{1.3.2}$$

and the distribution $P(q)$ is given by

$$P(q) = \frac{dx(q)}{dq} \tag{1.3.3}$$

where $x(q)$ is defined such that $q(x(q)) = q$.

The full-step RSB Parisi solution removes the low temperature negative entropy and one recovers $S(T \to 0) = 0$. Moreover, the magnetic susceptibility can be derived from $q(x)$ [16]. The full-step RSB solution captures well the magnetic susceptibility behavior [25].

Physical interpretation of the RSB

As we have mentioned previously, the overlap between valleys gives information on the structure of the phase space. Let us consider a spin glass which is cooled down to a low-temperature state. This equilibrium state α (valley) is characterized by a spin configuration S_i^α. The sample is heated up to $T > T_g$ to change the initial spin configuration. The cooling down process can then be repeated. The many-valley picture suggests that one falls into a different state S_i^β. An interesting quantity is the overlap $q_{\alpha\beta}$, defining by how much the spin configurations are different from each other:

$$q_{\alpha\beta} = \frac{1}{N}\sum_{i=1}^{n}\langle S_i^\alpha S_i^\beta\rangle \tag{1.3.4}$$

The maximum value for $q_{\alpha\beta}$ is q_{EA} and the minimum value can be 0 if the two configurations are completely uncorrelated. The distribution of these overlaps is given by

$$P(q) = \sum_{\alpha\beta} w_\alpha w_\beta \delta(q_{\alpha\beta} - q) \tag{1.3.5}$$

where w_α and w_β are the statistical weights of the valleys.

In spin glasses, it has been shown [16] that this function $P(q)$ is indeed the one defined from the replica-symmetry breaking solution, that is, the fraction of elements of the matrix Q_{ab} taking the value q. The *replica* and the *valley* indices are, in this respect, identical. This is the physical explanation of the RSB: in the spin glass phase, the valley states are not equivalent.

Therefore, the distribution $P(q)$ gives information about the structure of the phase space of the system. Typical examples of the $P(q)$ distribution are given in figure 1.7.

As the temperature is decreased below T_g, the phase space is fragmented into sub valleys separated by energy barriers. The RSB procedure gives an insight in how this happens, leading to a hierarchical structure of the energy landscape. Above T_g, all the overlaps are equal to q_0 (unique valley). The sub-division process breaks this valley into two smaller branches q_1, which in turn are broken in branches q_2, *etc.* This hierarchical structure is called the "hierarchical tree" and is shown on figure 1.8.

In such a hierarchical space, each valley (or replica) can be labeled, and the value of the overlap $q_{\alpha\beta}$ can be obtained by tracing back their common ancestor. A distance between two states can be defined and an important feature of such a hierarchical space is *ultrametricity*: the distances d between three states α, β and γ are such that

$$d_{\alpha\beta} \leq \max\left(d_{\alpha\gamma}, d_{\beta\gamma}\right) \tag{1.3.6}$$

meaning in terms of overlaps

$$q_{\alpha\beta} \geq \min\left(q_{\alpha\gamma}, q_{\beta\gamma}\right) \tag{1.3.7}$$

This ultrametric space is a consequence of the RSB procedure and is therefore an important property of this mean-field solution for spin glasses.

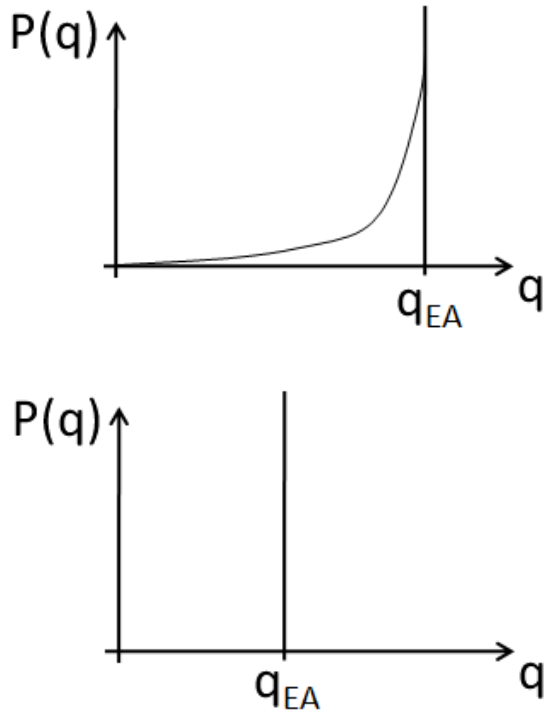

Figure 1.7: *Two typical $P(q)$ distributions. Top: the replica symmetry is broken, $P(q)$ is widely distributed up to a maximum value q_{EA}. Bottom: in the replica-symmetric case, q is single-valued.*

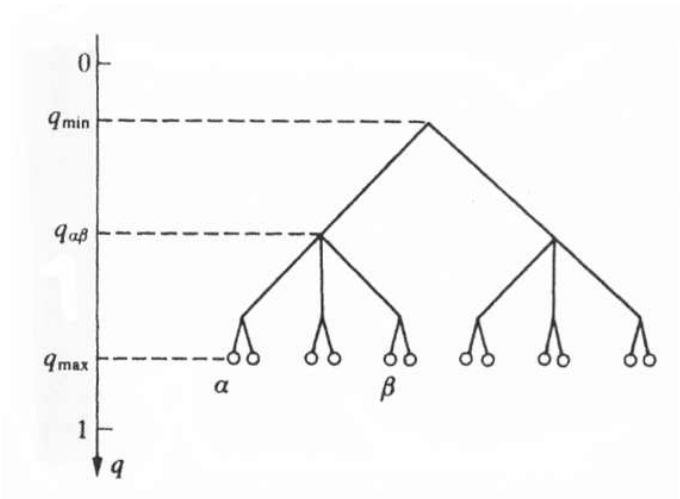

Figure 1.8: *The hierarchical tree. The overlap between a pair of states α and β (leaves of the tree) depends on how many levels one must go up to find a common ancestor. The difference between q_{max} and q_{min} depends on the temperature.*

1.3.2 Scaling theories

An alternative theory has been based on the scaling properties of domain walls. The *droplet model* is a phenomenological scaling theory introduced by Fisher and Huse [26, 27]. It is based on domain-like excitations in Ising spin glasses, with a *unique* ground state.

The basic idea is to define a droplet as the lowest energy excitation (from the ground state) of length scale L. Figure 1.9 illustrates the droplet $\bar{\Gamma}$ which consists of all the (Ising) spins in a compact region of size L oriented in opposite directions with respect to the ground state Γ.

At zero temperature, there exists a unique ground state Γ, degenerated with its symmetric $\bar{\Gamma}$. From this state, the creation of a droplet has an energy cost written as

$$F_L \propto \Upsilon(T) L^{\theta} \tag{1.3.8}$$

where F_L is the free energy cost of the droplet of size L, Υ is the stiffness constant and θ an additional exponent, which determines the stability of the droplets.

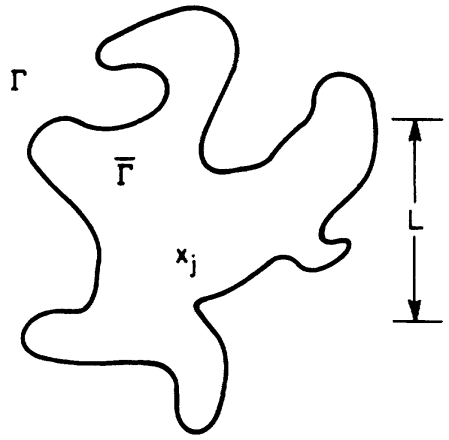

Figure 1.9: *Schematic picture of the droplet model. The surface of the droplet is fractal. Extracted from [26].*

In the ferromagnetic case, a droplet contains L^d spins, where d is the dimension. The surface contains L^{d-1} spins and the energy cost to build an interface is thus $\Delta F \sim JL^{d-1}$. If $d-1>0$, this cost is growing with L, domain walls are not favored, and the ordered phase can thus subsist. For the spin glass phase, the energy grows with L^{θ}, and due to the frustration, $\theta \leq (d-1)/2$ [26]. Numerical calculations give $\theta \simeq -0.29$ for $d=2$ and $\theta \simeq 0.19$ for $d=3$. There is therefore an ordered phase at $d=3$.

The behavior of the ordered phase is dominated by thermally active droplets, having a free energy lower than $k_B T$. Droplets of size L have a characteristic relaxation time $\tau_L \sim \tau_0\, e^{\,\beta B_L}$. $B_L \sim B_0(T) L^{\psi}$ is the height of the barriers, depending on the exponent ψ, and on B_0 the characteristic height. Equivalently, a relaxation processus on a time scale t involves droplets of size $L_t \propto [T/B_0 \ln(t/\tau_0)]^{1/\psi}$. There is a clear relation between droplet size and time relaxation that plays a major role in the slow relaxation of the system.

Under an applied magnetic field, the magnetization of the droplet grows like[5] $L^{d/2}$, and the interface energy still goes like L^{θ}. For $\theta < d/2$, the magnetic field aligns the droplets and destroys the order. This is the case at *all dimensions* d, as $\theta \leq (d-1)/2$. In the droplet model, the spin glass state *does not subsist* under a magnetic field.

Close to the transition point T_g, the characteristic relaxation time $\tau(h)$ of the domains under a magnetic field h can be evaluated through scaling arguments. If the observation time t is small compared to $\tau(h)$, the system is not in equilibrium and appears partially frozen. In other words, there exists a field $h(t)$ below which the system *appears* frozen to the observer on a time

[5] For disordered spins, the magnetization $M \propto N^{1/2}$, with N the number of spins, and $N \propto L^d$ in the droplet [28].

scale t. The droplet theory predicts an experimental transition line under magnetic field which is only a *dynamical effect*.

The droplet theory has the advantage of providing a clear picture of what happens in a spin glass. The scaling laws describe rather well the dynamics in terms of growing domain walls into the sample. In this framework, the broken symmetry is trivial, as there is a unique ground state: $P(q)$ is given by the replica symmetric example of figure 1.7.

Conclusion

Though spin glasses have been extensively studied, both theoretically and experimentally, many open questions remain. In particular, the most successful theories lead to contradictory results:

- *The phase space structure:*

  The mean-field Parisi solution predicts the existence of a hierarchical phase space composed of many states, and an order parameter that is continuously distributed. The droplet model, in opposition, suggests a unique ground state and the corresponding order parameter has only one value.

- *The magnetic field effect:*

  The droplet model suggests that there is no transition under a magnetic field, as it immediately destroys the spin glass order. In the mean-field model, the transition exists within the RSB, and thus follows the A-T line.

Even if trends have been shown experimentally towards one or the other theory, it is difficult to draw clear statements from these results.

One of the key issues in the problem of spin glasses is the overlap q. A direct measurement of q would give clear information regarding the two points discussed above. However this quantity is very difficult to measure for two reasons:

1. The system slowly relaxes towards equilibrium, and one observes the vitreous dynamics. However, the dynamical behavior can be linked to the equilibrium properties [29].

2. The overlap distribution requires a detailed microscopic observation of the configurations. This could only be achieved in numerical simulations up to now.

In the present work, we propose a method to obtain experimentally the microscopic configuration of the disorder. We will show that mesoscopic physics provides a unique tool to investigate *microscopic configuration* resulting in a *macroscopic signal*, as presented in the next chapter.

Un problème sans solution est un problème mal posé.

Albert Einstein

Chapter 2

Coherent electron transport: an original probe for disorder

Mesoscopic[1] physics [30, 31, 32] deals with systems that are in an intermediate scale between the microscopic and the macroscopic world. On the one hand, the microscopic scale is governed by the wave nature of the electrons, leading to quantum transport. On the other hand, the macroscopic world is described by collective behavior and electrons behave like classical particles. Mesoscopic effects provide a measurable signal that is strongly depending on the microscopic details of the sample. We will exploit these effects to get an insight in the microscopic structure of spin glasses. In this chapter, we introduce the mesoscopic interference effects in electron transport, in particular the universal conductance fluctuations. They are highly sensitive to the microscopic disorder configuration of the sample, and can therefore be used as a basic tool for the study of spin glasses.

2.1 Electron transport in solids

Electricity is associated to the transport of charge carriers[2] through a material. If they propagate easily, it is a good conductor (metals), otherwise it has a poor conductivity. The resistivity measured in metals is linked to the *disorder* inside the sample: this is the Drude model [1]. While crossing the sample, the electrons are scattered on centers of various types (static defects, phonons...). The motion of the electrons is thus *diffusive*.

The collisions can be taken into account through a time τ_e which represents the mean free time between two scattering events. The Boltzmann equation allows to obtain the Drude conductivity σ_0

$$\sigma_0 = \frac{1}{\rho_0} = \frac{n_e e^2 \tau_e}{m^*} \tag{2.1.1}$$

[1] From greek "mesos" meaning intermediate.

[2] Electrons also carry a spin which can be exploited as well as the charge, this is the field of spintronics.

where ρ_0 is the Drude resistivity, n_e is the electron density, e is the electron charge and m^* the effective carrier mass.

In metals, conduction electrons are very well described by the semi-classical theory [1]. The quantum nature of electrons is incorporated in the free electron approximation (the effect of the lattice is taken into account *via* the effective mass m^*). The ensemble of electrons form a quantum gas with fermionic properties: the energy is the Fermi level $E_F = \hbar^2 k_F^2/2m^*$, with $\hbar$ the Planck constant divided by 2π, and where k_F, the wave vector, takes into account the wave nature of the electrons. At temperatures T well below the Fermi temperature $T_F \sim 10^4$ K in metals, the electron gas is strongly degenerated and exhibits quantum properties. The characteristic length $\lambda_F = 2\pi/k_F$ is the Fermi wavelength and represents the spatial extension of the electron wave packet.

The value of this wavelength is related to the electron density in the system

$$n_e \propto \left(\frac{1}{\lambda_F}\right)^d \tag{2.1.2}$$

where d is the dimension. In metals $d = 3$, and $d = 2$ in semiconducting heterostructures. In a sample, one can decompose the electron transport into one-dimensional channels, corresponding to the transverse quantization of the wave vector. In three dimensions, for a section S, the number of channels is $N_c = S/\lambda_F^2$. In metals, λ_F is typically about 0.5 nm and is the smallest length of the problem. The number of channels in our samples of section 100×100 nm^2 is about $N_c \approx 4.10^4$.

In metallic systems, the free electron approximation holds very well, the plane electron waves are propagating freely between scatterers, within a renormalisation of the carrier mass m^*. Scattering induced by the *static* disorder changes the orientation of the electron wave vector $\vec{k}$, but not its modulus. It does not imply a loss of energy, the diffusion is *elastic*. Between two collisions, the electron motion is ballistic at a speed v_F which is the Fermi velocity ($v_F = (\hbar/m^*)k_F \simeq 1.4\ 10^6$ m/s in metals). One can define the elastic mean-free-path l_e as the distance traveled between two elastic scattering events

$$l_e = v_F \tau_e \tag{2.1.3}$$

where τ_e is the time associated with elastic scattering, that is the Drude time.

As the global motion of electrons is diffusive in the sample, it can be characterized by a diffusion coefficient D which represents the area explored per time unit.

$$D = \frac{1}{d} v_F l_e \tag{2.1.4}$$

with d the dimension of the system. In clean metals, $l_e \simeq 30$ nm and $D \simeq 150$ cm^2/s.

Coherent regime

The Drude model gives the classical resistivity of the material. The conductance of the system is quantifying the ease for the electrons to traverse the sample diffusively. The larger the disorder, the more difficult the electron propagation. In the Drude model, the total conductance

is given by the sum of the diffusion probabilities for the electrons. However, the quantum nature of the electrons is responsible for deviations to this classical resistivity. In the regime where the electrons can *interfere*, the conductance has an additional component. This correction arises from the quantum interference between electron trajectories.

As the propagating electron waves have the same energy E_F, they can interfere. However, among the diffusion processes, there are some that change the energy of the scattered electron, the phase of the wave associated is randomized and the electron wave cannot interfere anymore. The coherence of the electrons is thus limited by *inelastic* scattering. The length over which an electron has lost its phase coherence is L_Φ, the phase coherence length.

This length depends strongly on temperature, as electron-phonon inelastic processes are dominant at high temperature. By cooling down, these processes are weakened, and in clean metals, L_Φ can reach up to 20 μm. Thus, if one wants to observe the deviations to Drude resistivity due to the quantum nature of electrons, one has to measure a sample of size $L < L_\Phi$. This explains both why these effects are not important for macroscopic samples at room temperature, and the late emergence of mesoscopic physics which needs low-temperature techniques ($T < 1$ K) and samples of micrometer size.

The phase coherence length is related to the phase coherence time τ_Φ by

$$L_\Phi = \sqrt{D\tau_\Phi} \tag{2.1.5}$$

2.2 Universal Conductance Fluctuations

Mesoscopic interferences arise between electron trajectories diffusing on a length scale of L_Φ. The detail of these interferences is thus depending on the microscopic disorder of the sample, in a block of size L_Φ. For large samples, ($L \gg L_\Phi$), the interference figure is different for each block, and the resulting signal is canceled on average. But if the sample has a length $L < L_\Phi$, the *quantum corrections* to the conductance depend precisely on the microscopic realization of the disorder. In that sense, they give a *fingerprint* of the disorder configuration.

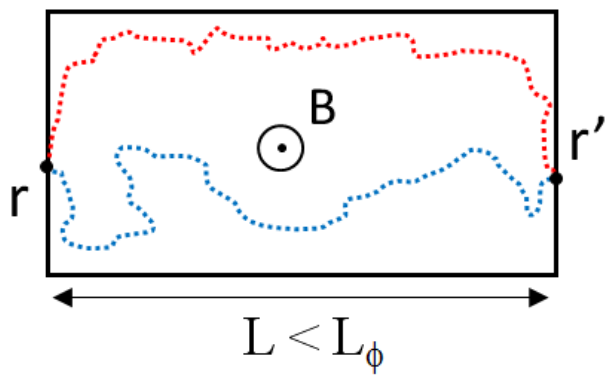

Figure 2.1: *In a sample of length $L < L_\Phi$, diffusive electron trajectories going from r to r' interfere. A mean to modulate the phase difference between the paths is the use of a magnetic field.*

In the schematic of figure 2.1, the electron paths are interfering ($L < L_\Phi$). The diffusion of the electrons on the static disorder yields a probability $P(r, r')$ to cross the sample, and the related macroscopic conductance. $P(r, r')$ does not change as long as the static disorder

remains the same. If one changes the sample, one changes the disorder configuration, and the conductance changes, due to the quantum corrections [33]. A first way to observe such effects is thus to measure sample-to-sample conductance fluctuations [34].

A magnetic vector potential couples to the electron charge[3] and changes the phase of the electron wave [35]. Therefore, a magnetic flux dephases the electron trajectories. Applying a magnetic field does not change the disorder configuration, but changes smoothly the phase of each electron path, in an unknown, but deterministic way. The resulting probability $P(r, r')$ will fluctuate as we dephase the trajectories. Importantly, for a given realization of the disorder, the dephasing of the paths is fixed for a given field: as a result, the fluctuations are *aperiodic* but *reproducible* with respect to the magnetic field.

These fluctuations have been interpreted as Universal Conductance Fluctuations (UCF) by Lee and Stone in 1985 [36]. They are:

Aperiodic: the conductance fluctuations are aperiodic. Sample-to-sample fluctuation occur randomly.

Reproducible: with respect to the dephasing parameter, the fluctuations are reproducible for a given realization of the disorder.

Universal: the amplitude of the fluctuation is of the order of e^2/h, independently of the degree of disorder.

As an example of the universality, conductance fluctuations of three different systems are shown on figure 2.2. While the background conductance varies on three orders of magnitude, the conductance fluctuations remain of order e^2/h.

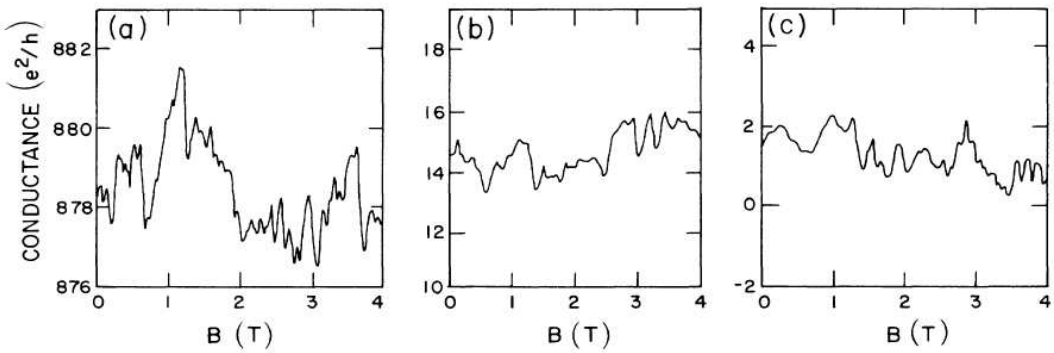

Figure 2.2: *Comparison of aperiodic magnetoconductance fluctuations in three different systems. (a) $g(B)$ in a 0.8 μm diameter gold ring. (b) $g(B)$ for a quasi 1d silicon MOSFET. (c) numerical calculation of $g(B)$ for an Anderson model. Conductance is measured in units of e^2/h, magnetic field in Tesla. Note the three orders of magnitude variation in the background conductance while the fluctuations remain of order unity. Extracted from [37].*

Indeed, it can be shown that the conductance of a channel is e^2/h, the *quantum of conductance*. Thus the conductance g can be expressed in units of e^2/h, and directly reflects the number of channels N_c [31] in the sample. The amplitude of mesoscopic corrections is of the order of one channel (out of the total number of channels).

[3]The vector potential acts on the electron phase even in the absence of magnetic forces on the particles.

The important feature of these conductance fluctuations that we exploit in the following work, is that they represent a *fingerprint of the microscopic disorder configuration.* In this work, we develop this original approach as a tool to study the disorder in spin glasses.

2.2.1 Quantitative description

Amplitude of the fluctuations

The amplitude of these conductance fluctuations $\overline{\delta g^2}$ (in units of $(e^2/h)^2$) can be calculated from the Kubo formula [30, 33]. At zero temperature and for a length $L \ll L_\Phi$ one obtains

$$\overline{\delta g^2} = \frac{12s^2}{\beta} \sum_q \left(\frac{1}{q^2 L^2} \right)^2 \tag{2.2.1}$$

where q is the wave vector associated with the propagation mode of the electrons and s is the spin degeneracy. The term β is a known numerical factor depending on the time-reversal symmetry of the problem. Note that this result does not depend on l_e that is on the strength of the disorder: the fluctuations are universal.

In our experiments, we study samples in the quasi $1d$ geometry, that is only one dimension L exceeds L_Φ. In this case, the sum in the above equation equals $\pi^4/90$, thus

$$\overline{\delta G^2} = \frac{2}{15\beta} G_0^2 \tag{2.2.2}$$

where $G_0 = se^2/h$ is the (spin-dependent) quantum of conductance. This formula sets the amplitude of the universal conductance fluctuations in fully coherent systems at zero temperature.

Aperiodicity of the fluctuations

As we have mentioned above, the UCF are aperiodic. If the dependence of g on B is really random, the following correlation function should decay to zero over some range in ΔB [36]:

$$F(\Delta B) = \langle g(B) g(B + \Delta B) \rangle - \langle g(B) \rangle^2 \tag{2.2.3}$$

where the angular brackets $\langle\ \rangle$ denote the average on the magnetic field span. In order to have reliable results, the field span has to be much larger than the typical decay ΔB.

This function can be calculated, and for $\Delta B = 0$, zero temperature, and large L_Φ, it yields the same result as equation 2.2.2 for the amplitude of the fluctuations.

In addition, this calculation allows to obtain the typical spacing between the aperiodic peaks of the fluctuations. One can estimate a field correlation range B_c defined by $F(B_c) = F(0)/2$. One obtains in the quasi $1d$ case

$$B_c \simeq \frac{\Phi_0}{w L_\Phi} \tag{2.2.4}$$

where w is the width of the sample, and $\Phi_0 = h/e$ is the *flux quantum.* In the quasi $1d$ regime, the typical field scale between the fluctuations of the conductance is given by a quantum flux threaded through a sample area of wL_Φ, as sketched on figure 2.3.

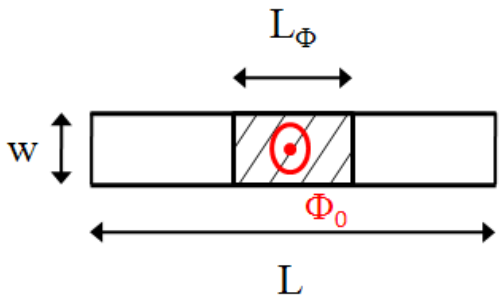

Figure 2.3: *A magnetic flux Φ_0 is threaded through the coherent surface of the sample. In the quasi 1d regime, this area is delimited by the width w and the phase coherence length L_Φ.*

2.2.2 Effect of the temperature

Thermal diffusion length

The boundary conditions are important in coherent diffusion, as the electron can escape the sample after its path. By doing so, it couples to the environment and loses its phase memory. The length L of the sample over which the electrons propagate is linked to a characteristic diffusion time

$$\tau_D = \frac{L^2}{D} \tag{2.2.5}$$

τ_D is the Thouless time [38], and represents the time it takes to go diffusively across the sample. For times larger than τ_D, the boundaries of the sample are felt by the electrons.

The Thouless energy is associated with this time

$$E_c = \frac{\hbar}{\tau_D} \tag{2.2.6}$$

When an electron crosses the sample, it acquires a phase proportional to $\tau_D/\hbar$. There are constructive interferences between two electron trajectories if their relative phase difference is less than 2π, that is if their energy difference $\Delta\epsilon \leq E_c$. Thus, only the electrons lying in an energy band of width E_c around the Fermi level can participate to interference effects.

This has to be compared to the total number of electrons participating to the transport that are lying in an energy interval of width k_BT, k_B being the Boltzmann constant. The ratio between these quantities gives rise to the thermal diffusion length:

$$L_T = L\sqrt{\frac{E_c}{k_BT}} = \sqrt{\frac{\hbar D}{k_BT}} \tag{2.2.7}$$

As a result, the temperature weakens coherence effects when $E_c < k_BT$, that is $L > L_T$.

Temperature-dependence of the conductance fluctuations amplitude

The universal conductance fluctuations amplitude is strongly depending on temperature. The effect of temperature is two-fold: it changes the thermal broadening of the energy levels (L_T), but it also modifies the coherent scattering rate ($L_\Phi(T)$). At low temperature, these two lengths are large, and we recover large conductance fluctuations. When temperature increases, the fluctuations are progressively suppressed. The characteristic lengths L, L_Φ and L_T have to

be compared to determine precisely the amplitude. In the asymptotic regimes for these lengths, the temperature-dependence of the UCF amplitude is given by known analytic laws [30].

2.3 Onsager symmetries

Note that the theoretical descriptions set above have been calculated in a two-point geometry, that is when current I and voltage V are contacted on the same leads. In experimental mesoscopic physics, one often uses four-point measurements (different contacts to drive the current and to measure the voltage). In this situation, one really performs a *local* measurement (see figure 2.4). In such geometry, special symmetries apply to the coherent magnetoconductance of a sample [39]. These symmetries will be useful in our experiment, in order to separate out conductance fluctuations due to orbital effects from fluctuations attributed to the magnetic atoms.

Starting with a two-point setup having leads i and j, the current conservation and time-reversal invariance in the presence of a flux Φ imposes relations on the transmission T and reflection R coefficients between i and j

$$T_{ij}(\Phi) = T_{ji}(-\Phi), \quad R_{ii}(\Phi) = R_{ii}(-\Phi) \tag{2.3.1}$$

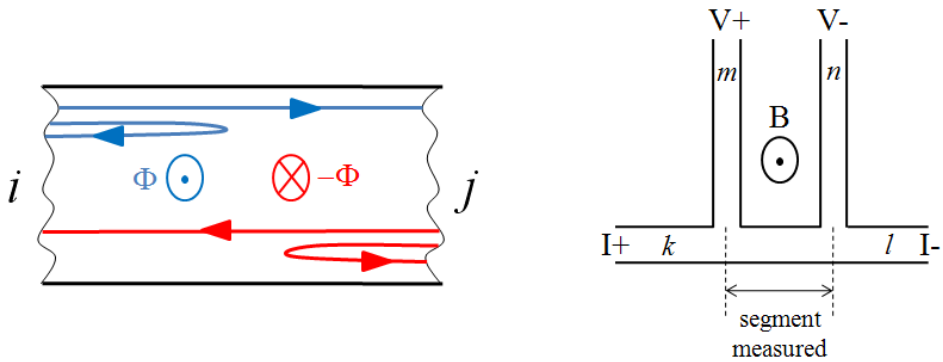

Figure 2.4: *Left: two-probe measurement. The blue lines for $T_{ij}(\Phi)$ and $R_{ii}(\Phi)$ are equivalent to the red lines $T_{ji}(-\Phi)$ and $R_{jj}(-\Phi)$. Right: four-probe local measurement. k, l, m, n are the leads, I and V designate current and voltage probes respectively.*

In a common four-point measurement, two leads drive the current and the two others are used to measure the voltage. In these conditions, where the leads are k, l, m and n the resistance is given by

$$\mathcal{R}_{mn,kl} = (h/e^2)(T_{km}T_{ln} - T_{kn}T_{lm})/D \tag{2.3.2}$$

where D is a determinant of the currents matrix, independent of the indices $klmn$. Using the previous reciprocity equations, we obtain the Onsager relation

$$\mathcal{R}_{mn,kl}(\Phi) = \mathcal{R}_{kl,mn}(-\Phi) \tag{2.3.3}$$

This symmetry applies also to the conductance, and to the conductance fluctuations. Using our experimental scheme of figure 2.4, one can derive from the above equation useful relations.

We designate by I the pair of current leads and by V the pair of voltage probes. As an example, one can symmetrize our conductance fluctuations with respect to the field:

$$\delta G_S = \frac{\delta G_{IV}(B) + \delta G_{IV}(-B)}{2} \tag{2.3.4}$$

$$\delta G_A = \frac{\delta G_{IV}(B) - \delta G_{IV}(-B)}{2} \tag{2.3.5}$$

where B is the magnetic field. δG_S and δG_A are respectively the symmetric and the antisymmetric components with respect to the field.

As the Onsager relation is relying on the time-reversal invariance hypothesis, one can build quantities that depend on this symmetry

$$\delta G_M = \frac{\delta G_{IV}(B) - \delta G_{VI}(-B)}{2} \tag{2.3.6}$$

$$\delta G_O = \frac{\delta G_{IV}(B) + \delta G_{VI}(-B)}{2} \tag{2.3.7}$$

One symmetrizes here with respect to the $I - V$ leads permutation. We call the magnetic component δG_M, as it is a vanishing quantity when time-reversal invariance is verified. Thus, it is sensitive to magnetic degrees of freedom that we have in a spin glass. We call the orbital component δG_O the complementary term so that the decomposition is complete. When performing a four-probe measurement, one can refer to such symmetries in order to extract particular magnetic contributions [40].

Conclusion

In this chapter, we have described the quantum corrections to the conductance of a small metallic sample, that are observable at low temperature. In particular, the interferences between electron trajectories yield universal conductance fluctuations that are accurately representing a fingerprint of the microscopic disorder. This kind of phenomena thus provides an original probe to study disordered systems, like spin glasses. In such magnetic systems, we can use special symmetries of the conductance fluctuations in order to investigate specifically the magnetic features of the sample. In the next chapter, we describe the few studies that have been performed with this approach.

Les hommes construisent trop de murs
et pas assez de ponts.
Isaac Newton

Chapter 3
Universal conductance fluctuations and spin glasses

The idea that universal conductance fluctuations (UCF) can be used as a probe of the disorder in a spin glass was suggested in 1985 by Altshuler and Spivak [41]. But the link between the UCF signal and reliable information on spin glasses is not straightforward. Several ideas have been developed in this purpose. First, one can measure the low-frequency noise resulting from UCF, and thus reflecting the microscopic reorganizations of the disorder. Second, another approach consists in measuring the fluctuations as a function of the magnetic field - the magnetofingerprint - and to extract the component that is directly due to the spin disorder configuration.

More recently, the correlations between magnetofingerprints have been theoretically linked to the spin overlap Q, the order parameter of the spin glass transition. In this chapter, we present these approaches that have motivated our study.

3.1 A first attempt, noise experiments

One of the promising ways to exploit the sensitivity of UCF is the measurement of $1/f$ noise [42]. In glassy systems, the disorder configuration is slowly relaxing. Therefore, the universal conductance fluctuations are affected. Such a local reorganization of the disorder leads to an additional noise in the conductance of the sample. Consequently, measurements of low-frequency noise in spin glasses are sensitive to the microscopic disorder reorganizations.

These ideas have been implemented experimentally, as the noise can leave direct information on the nature of the spin glass phase [43]. The authors measured the temperature dependence of $1/f$ noise in the electrical resistance of films of CuMn alloys at several concentrations [44], as presented on figure 3.1.

One observes a sharp step in the temperature dependence of the noise, which increases by more than one order of magnitude at the spin glass freezing temperature. This is confirmed by

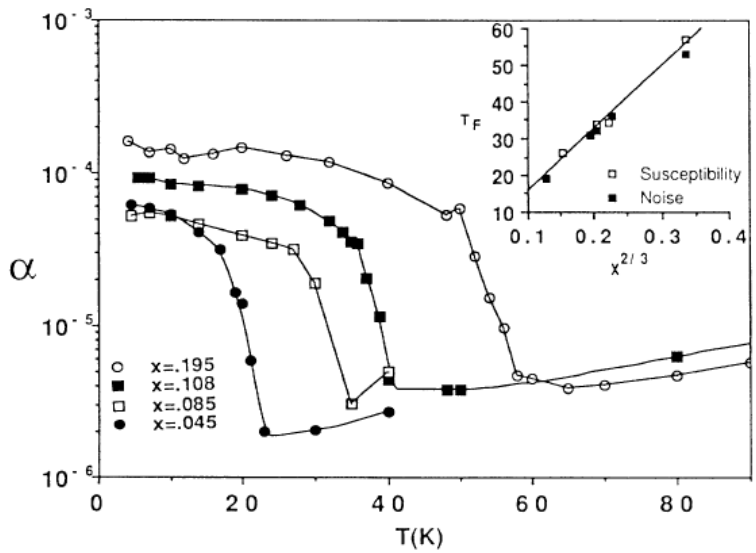

Figure 3.1: *Normalized resistance low-frequency noise α (0.08 − 17 Hz) as a function of temperature T for $Cu_{1-x}Mn_x$ films at several concentrations x of magnetic impurities. In inset, the spin glass freezing temperature ($T_F \equiv T_g$ in the text) determined from magnetic susceptibility and noise measurements versus $x^{2/3}$. Extracted from [44].*

comparing the characteristic temperature of the noise increase to independent estimation of T_g with susceptibility measurements, presented in the inset of figure 3.1.

As a conclusion, these measurements show that the noise signal attributed to the universal conductance fluctuations is observable in spin glasses. However, the amplitude of the UCF alone does not give information on the detailed microscopic configuration of the disorder in the sample. To achieve such a probe, one has to study the *reproducibility* of the fingerprints. Surprisingly, this way of investigation was less explored in the past.

3.2 Pioneering work on universal conductance fluctuations

The first measurements of universal conductance fluctuations as a function of the magnetic field in spin glasses have been performed by de Vegvar, Levy and Fulton in 1991 [45]. This article is the foundation of the work presented in this manuscript. In their experiment, the authors are exploiting the ideas of Altshuler and Spivak [41], by measuring the magnetoresistance of a spin glass sample at low temperature. Several samples of a 1000 ppm CuMn alloy have been fabricated ($T_g \approx 1$ K expected), and show clear quantum fluctuations in the magnetoresistance. From the amplitude of the effects, the phase coherence length is estimated to be about 1 μm. This value is rather large, and proves that quantum interference effects can be observed experimentally in low concentration spin glasses.

As discussed in chapter 2, it is possible to separate the magnetic and orbital contributions to the UCF by using the Onsager relations. In this experiment, the magnetic contribution, which is only sensitive to the magnetic disorder, has been extracted. The results are presented on figure 3.2. As the magnetofingerprints are reproducible at low temperatures, the data suggest that the spin configuration is indeed frozen in the spin glass sample.

The most striking result of this work is the reproducibility of the magnetofingerprint: when

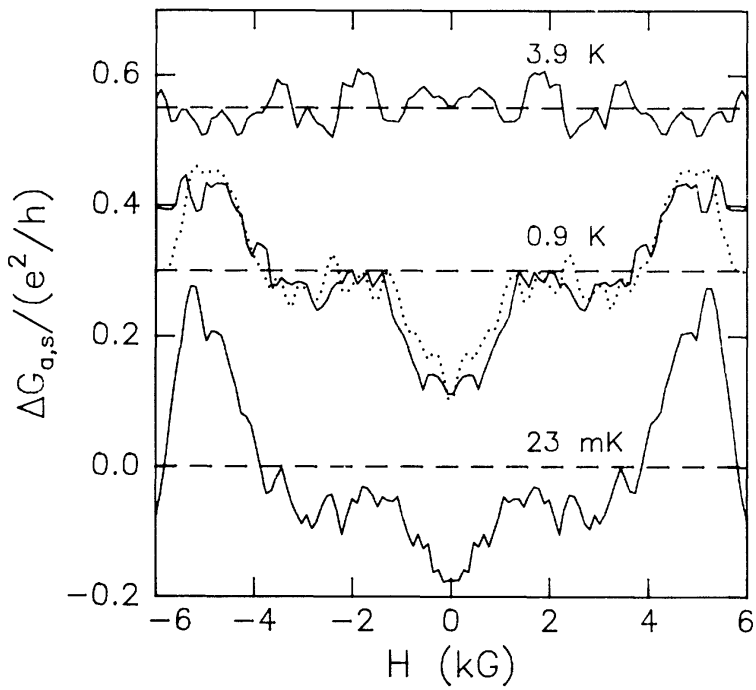

Figure 3.2: *The symmetric magnetic contribution to the UCF extracted from a wire of length* $L = 0.65\ \mu m$. *The sample was field cooled from* 4 *K to* 12 *mK under* 0.7 *T and subsequently warmed to the indicated temperatures. The curves are shifted for clarity. The two traces at* 0.9 *K indicate the experimental reproducibility. From [45].*

cycling the field up to 9 times the exchange field H_g (defined as $g\mu H_g = k_B T_g$), the traces remain highly identical. This is indeed surprising and suggests that the spin configuration is not affected by such a large magnetic field.

This pioneering work clearly demonstrates that quantum fluctuations are measurable in spin glasses. However, the magnetofingerprints are not clearly randomized when heating the sample above T_g. This can be interpreted by the presence of clusters in the sample, resulting in a freezing of the spin configuration which is only partial [46]. Therefore, it is rather difficult to draw quantitative conclusions from this measurement. To go further, we aim a deeper understanding of the UCF in the spin glass regime, and a clear strategy to extract properly and precisely relevant microscopic information on spin glasses.

3.3 A recent renewal

To tackle the above mentioned issues, we have started a collaborative effort between theoreticians and experimentalists. The idea that the UCF are sensitive to the spin glass configuration has been revisited in 2008 [47], and has motivated our experimental work.

In the spin glass problem, the important quantity is the *spin overlap* Q_{12}, the order parameter of the transition. As presented in chapter 1, it is given by the correlation between the microscopic spin configurations in the system. It can be written

$$Q_{12} = \frac{1}{N_{imp}\langle S^2\rangle} \sum_{i=1}^{N_{imp}} \langle \vec{S}_i^{(1)} \cdot \vec{S}_i^{(2)} \rangle \tag{3.3.1}$$

where N_{imp} is the number of magnetic impurities of spin S. Q_{12} is thus the spin overlap between the spin configurations $\{\vec{S}_i^{(1)}\}$ and $\{\vec{S}_i^{(2)}\}$. This overlap represents roughly the fraction of spins that have changed between configurations (1) and (2).

Conductance fluctuations are sensitive to a change in the spin configuration of the sample. On the one hand, a change in the spin configuration is characterized by the overlap Q. On the other hand, the modification of the magnetofingerprints can be evaluated by the *correlations*. The idea is thus to link quantitatively the correlations of the magnetofingerprints to the spin overlap.

One considers the correlations between conductance fingerprints obtained for two different spin configurations $\{\vec{S}_i^{(1)}\}$ and $\{\vec{S}_i^{(2)}\}$

$$(\Delta G)^2_{S^{(1)}S^{(2)}} = \langle \delta G\left(V, \{\vec{S}_i^{(1)}\}\right) \delta G\left(V, \{\vec{S}_i^{(2)}\}\right)\rangle_V \tag{3.3.2}$$

where the average is taken over the disorder potential V. This conductances correlation is shown to depend directly on the spin configurations correlation, that is on the spin overlap Q_{12}

$$(\Delta G)^2_{S^{(1)}S^{(2)}} = F(L/L_m, Q_{12}) \tag{3.3.3}$$

where L is the sample length and L_m is called the magnetic length. This length is defined as the length that an electron travels before it scatters elastically on a magnetic impurity. It is the analogue of the elastic mean free path l_e, but between magnetic impurities. The appropriate function F is known in mesoscopic physics theory[1]. This theoretical link between the fingerprints correlation and the spin overlap Q_{12} is displayed on figure 3.3.

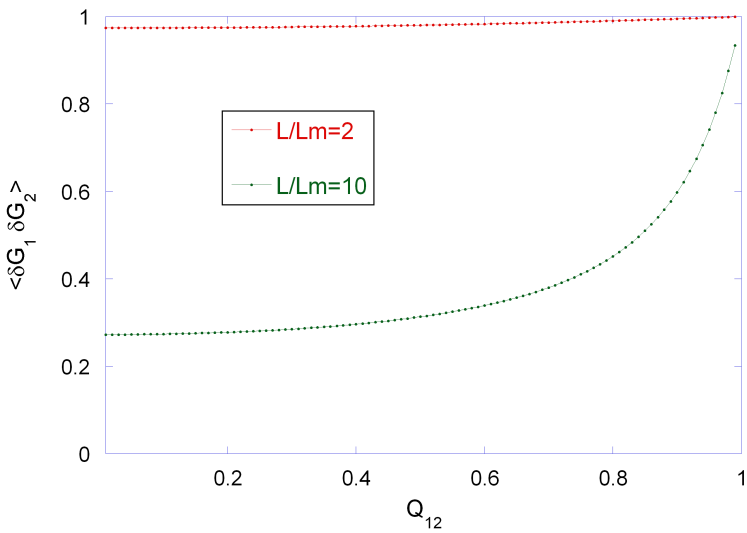

Figure 3.3: *Typical theoretical variation of the conductance correlation $\langle \delta G_1 \delta G_2 \rangle$ as a function of the spin overlap Q_{12}. A low value $L/L_m = 2$ and a large value $L/L_m = 10$ are represented.*

Notice that theory predicts a resulting correlation at zero overlap $\langle \delta G_1 \delta G_2 \rangle (Q_{12} = 0)$ which is finite. It means that even for zero overlap, that is *all* the spins orientations have changed, *the correlation between traces is not zero*. Indeed, the shape of the curve and the

[1] $F(x) = 3x^{-4}\left(x^2 csch^2(x/\sqrt{2}) + \sqrt{2}x \coth(x/\sqrt{2}) - 4\right)$ where the argument x is depending both on L/L_m and Q_{12}.

value $\langle \delta G_1 \delta G_2 \rangle (Q_{12} = 0)$ strongly depends on the ratio L/L_m. The magnetic length L_m plays a very important role in the sensitivity of the UCF to the magnetic disorder : in order to "feel" the difference between magnetic configurations and get appreciably uncorrelated fingerprints, the electrons have to encounter a large number of magnetic impurities. This is quantified by the ratio L/L_m, the longer the sample, the more sensitive the UCF. For short L/L_m, the correlation $\langle \delta G_1 \delta G_2 \rangle$ is predicted to be close to 1, whatever the value of Q_{12}. On the contrary, for large L/L_m, the correlation is very sensitive to Q_{12}, the spin overlap.

This has been confirmed by the PhD work of Guillaume Paulin [48]. Using a numerical Landauer method, with a tight-binding Anderson model, they were able to numerically evaluate the conductance fluctuations correlations $\langle \delta G_1 \delta G_2 \rangle$, and recovered these analytical results [49], which have also been confirmed by other theoretical works [50].

These results provide a quantitative way to measure the spin overlap Q_{12} using the correlation between conductance fluctuations. In theory, magnetofingerprints are taken by averaging over a large number of disorder configurations. Experimentally, such averaging is difficult to achieve. Thus, in the measurements, one performs an average over the magnetic field in order to get a fingerprint of the configuration. Using the ergodic hypothesis, the average over disorder V can be equivalently taken by averaging over magnetic field B. Finally, an experimental protocol is proposed to give a *direct measurement of the spin glass order parameter* Q_{12}, as depicted on figure 3.4.

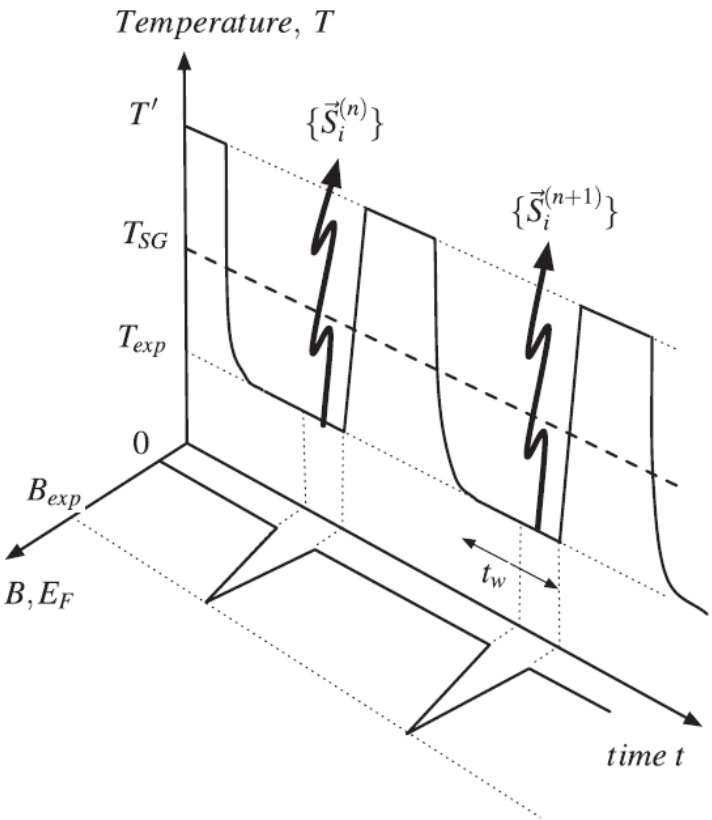

Figure 3.4: *Temperature cycles through T_g. Different measurements at temperature T_{exp} correspond to different spin configurations $\{\vec{S}_i^{(n)}\}$. Extracted from [47].*

The main protocol suggested in figure 3.4 is the following: the system is cooled through T_g down to T_{exp}, so that the spin configuration is frozen. The magnetic field is then applied, in order to record the magnetofingerprint of the configuration $\{\vec{S}_i^{(n)}\}$. The sample is heated up to the paramagnetic regime, the spin configuration is randomized. The operation is repeated, giving a second magnetofingerprint $\{\vec{S}_i^{(n+1)}\}$ at T_{exp}. The correlation between two traces $(m) \equiv (n+1)$ and (n) gives Q_{mn}, the spin overlap. Repeating this process many times should yield the statistical distribution of overlap $P(Q)$ that is the fundamental quantity in the theory of spin glasses. This tool can further serve to study aging effects, through the dependence on the waiting time t_w, and also memory effects.

Conclusion

The use of universal conductance fluctuations to study the microscopic configurations of spin glasses is a well-established idea. However, it is difficult to draw definitive conclusions from the existing experimental works. The new approach proposed in this work is to investigate directly the reproducibility of the magnetofingerprints. The correlation between conductance fluctuations traces can be experimentally measured, and allow to extract the spin overlap. We present, in the next part, the experimental implementation of these ideas.

Part II

Experimental implementation

Je n'ai pas échoué. J'ai simplement trouvé dix mille solutions qui ne fonctionnent pas.

Thomas Edison

Chapter 4
Experimental implementation

4.1 Experimental setup

In order to study mesoscopic effects in the spin glass regime, several requirements have to be fulfilled. Low-temperature measurements are required ($T \ll 1$ K) in order to reach the quantum regime ($L_T, L_\Phi \simeq L$), but also samples in the micron range, large magnetic fields, as well as very low noise electronic detection as the signals to be measured are very small. In addition, the concentration of the magnetic spins (impurities) has to be well controlled. In the following, we detail the experimental techniques that we have implemented for the measurement of universal conductance fluctuations in spin glasses.

4.1.1 Samples fabrication

Electron beam lithography

In order to make samples below the micrometer size, we use standard electron beam lithography techniques. A sensitive resist is insolated by a focused electron beam, following a pattern defined by the user. The beam affects the resist, and the insolated part is removed in a chemical solution (the developer). This is followed by a metal evaporation on the whole substrate. The last step consists in removing the resist layer, the so-called "lift-off". A schematic of the whole lithography procedure is shown on figure 4.1.

The best suited geometry to study experimentally mesoscopic interference effects is the quasi $1d$ geometry: only one dimension of the sample is larger than L_Φ. Indeed, in this geometry the resistance is larger and the number of channels N_c is reduced. As the quantum fluctuations are of one channel, the relative resistance correction is thus larger.

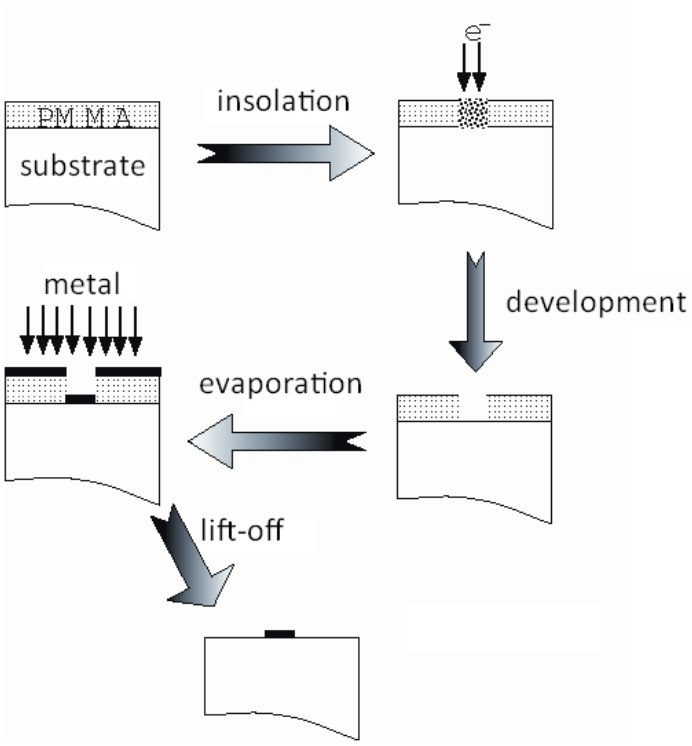

Figure 4.1: *Schematic of the several steps of the lithography procedure.*

There are also experimental constraints coming from the signal detection: as a very low current is required to perform a measurement at equilibrium, we have calculated that the resistance of the sample has to be $R > 10\ \Omega$ in order to be able to measure the UCF signal at $T = 30$ mK. The length L of the sample has to be of the order of L_Φ. Using the resistivity of pure noble metals, we thus have to design the sample very narrow and thin.

However, we have chosen transverse dimensions that are larger than the elastic mean free path, in order to have three-dimensional diffusive properties for the sample. We finally designed a sample of length $L = 3\ \mu$m with several intermediate probes, of width $w = 50$ nm and thickness $t = 40$ nm. For these dimensions, we can estimate that for a concentration of magnetic spins $c = 1000$ ppm, there are about 300 spins in the transverse section of the wire. An Atomic Force Microscope (AFM) picture of a typical sample is shown on figure 4.2. The large reservoirs aim at having a good thermalization of the wire.

Choice of the materials

Canonical spin glasses that we want to study are AuFe, AgMn or CuMn alloys, in the 1000 ppm concentration regime. There are two ways to make them: we can evaporate directly the alloy, or we can evaporate the noble metal host alone, and implant the magnetic impurities afterwards. In such noble metals, there subsist small concentrations of magnetic impurities [1] in the sample after evaporation. These give rise to a Kondo effect [51]. In this situation, the phase coherence length is reduced [52], around the typical Kondo temperature T_K. Consequently, if T_K is in the Kelvin range, the presence of residual magnetic impurities dramatically affects the

[1] These may come from the evaporator.

phase coherence properties of the sample. It is thus very important to have a good control on the metal evaporation in order to avoid parasite magnetic impurities effects. For this reason, we elaborate our sample from a very high purity source of host material (samples were prepared in the Quantronics group for Ag[2], and in the Orsay group for Au), and we implant the magnetic impurities afterwards.

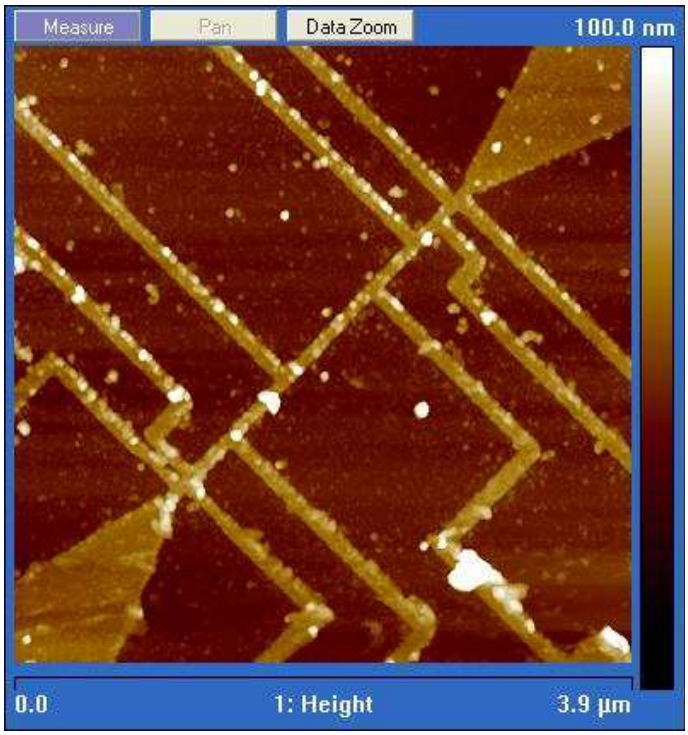

Figure 4.2: *AFM picture of a typical sample designed for the measurement of UCF. The current is driven between the large reservoirs, and several voltage probes are available for measurement.*

Implantation of the magnetic impurities

The implantation strategy has several advantages. As all samples are fabricated from the same metal source in a single evaporation run, it allows for a direct comparison between the non implanted metal and the spin glass samples. Moreover, the implantation technique ensures a uniform spatial distribution of the spins. This is important, as a clustering of magnetic impurities may lead to ambiguous results, due to inhomogeneities of the concentration.

The implantation has been performed in the Institut de Physique Nucléaire de Lyon (IPNL), in a collaboration with Christophe Peaucelle and Angela Perrat-Mabillon[3]. The principle of the technique is to accelerate ions in an electric field, in order to give them sufficient energy to penetrate into the target sample. The advantages of this technique are an accurate isotopic selection, and well controlled fluence (the number of impurities implanted per surface unit) and penetration depth. The main drawback is that the high energy implantation creates defects in the sample. These can however be erased by an annealing process.

[2] This source has been characterized in reference [53], giving typically $L_\Phi \simeq 10\ \mu$m at the lowest temperatures.
[3] See http://www.ipnl.in2p3.fr/spip.php?article212 for more information.

In our samples, we will keep the defects for two reasons. One the one hand, the annealing process can induce clustering of the spins, that we want to avoid. On the other hand, the static defects created by the implantation lead to an increase of the resistance of the sample[4] which helps for the conductance fluctuations measurement. In addition, it has been shown that the presence of defects created during implantation do not lead to additional inelastic scattering in the sample [54].

Figure 4.3: *Photograph of the IMIO400 implantation equipment in IPNL.*

The implantation has been performed with an IMIO400 which is represented on figure 4.3. The energy of the accelerated ions is in the range $E = 60$ to 400 keV. The ion current ranges from few μA to hundreds of μA. During the implantation, the beam is scanning the surface of the sample, leading to fluences ranging between 10^{12} at/cm^2 and 10^{17} at/cm^2.

In canonical spin glasses, T_g is proportional to the concentration c. The corresponding fluence required is calculated from numerical simulations of the implantation process, using the software SRIM[5] (the Stopping and Range of Ions in Matter). Giving the information on the source and target, we obtain from the simulation a profile of the ions distribution in the material, as shown on figure 4.4.

From the profile, we estimate[6] the mean value of the gaussian $\langle c \rangle$, which is half of the maximum value. The fluence is given by

$$f_c = \frac{c_{imp} n_{at}}{\langle c \rangle} \tag{4.1.1}$$

f_c is the fluence needed to obtain a concentration c_{imp}, and n_{at} is the atomic density of the host material.

As an example, table 4.1 gives the fluences for the implantation of ^{55}Mn into Ag (40 nm layer). For information, $n_{at} = 5.86$ at/cm^3 and the simulation ($E = 70$ keV) yields $\langle c \rangle = 12.5\ 10^4$ $(at/cm^3)/(at/cm^2)$.

[4]For one serie of our samples, we have observed a surprising increase of the resistivity by a factor 5 between pure Ag and implanted AgMn samples. In reference [54], implantation at equivalent energies lead to an enhancement factor of 1.5. For the other series of samples, we have recovered the same enhancement factor of 1.5.

[5]Software in free access http://www.srim.org/.

[6]We take into account in the estimation the proportion of ions that are propagating out of the sample. They represent in our samples about 10 % of the ions.

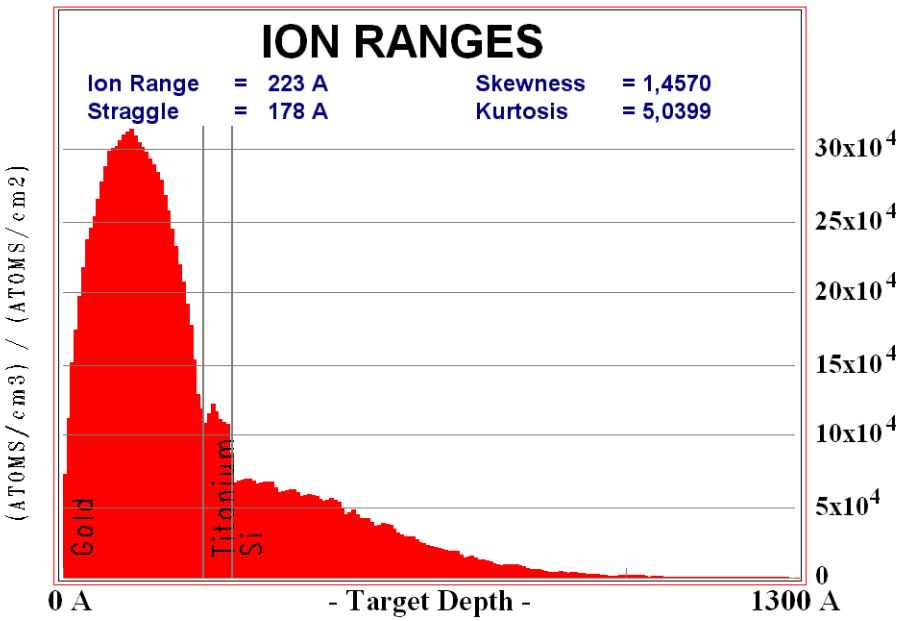

Figure 4.4: *Ion distribution profile as a function of target depth, as numerically computed with SRIM. In this example, two layers of 40 nm Au + 5 nm Ti and the Si substrate constitute the target. The profile is given in units of $(at/cm^3)/(at/cm^2)$.*

AgMn samples	c_{imp} (ppm)	fluence f_c $(ions/cm^2)$	Purpose
SG-Ag1/Ons-Ag1	150	7.03 10^{13}	Probe $T > T_g$
SG-Ag2/Ons-Ag2	400	1.87 10^{14}	UCF for $T \sim T_g$
SG-Ag3/Ons-Ag3	700	3.28 10^{14}	UCF for $T \sim T_g$
SG-Ag4/Ons-Ag4	1000	4.69 10^{14}	Probe UCF for $T < T_g$
SG-Ag5/Ons-Ag5	1500	7.03 10^{14}	Probe UCF for $T \ll T_g$
SG-Ag6/Ons-Ag6	2000	9.37 10^{14}	Probe UCF for $T \ll T_g$

Table 4.1: *Table of implantation values used for ^{55}Mn into Ag.*

We have chosen the AgMn alloy for its low Kondo temperature, $T_K \ll T_g$ for all the samples fabricated. This ensures that we can neglect the influence of Kondo effect, so that we are mainly probing the spin glass phase. As T_g is determined by the concentration ($c_{imp} \approx 1000$ ppm gives $T_g \approx 1$ K), samples of different concentrations have been elaborated, in order to study various physical regimes regarding T/T_g.

Another set of implanted samples have been prepared with AuFe alloys. In this system, the Kondo temperature is higher $T_K \approx 1$ K, and we have access to a regime where $T_g \approx T_K$.

4.1.2 Experimental setup

Dilution refrigerator

In order to cool the sample down to the quantum regime ($T \leq 1$ K), we use a standard commercial dilution refrigerator. This equipment was acquired at my arrival in the team. The specifications are a base temperature of $T \approx 11$ mK and a cooling power of 250 μW at 100 mK. In order to bring the sample into the magnetic coil, we have built a cold finger which was carefully adapted to the refrigerator.

Magnetic fields

A magnetic field perpendicular to the sample, called the Z field, is produced with a solenoidal superconducting coil. The maximum field is about $B_z = 8$ T. In addition, we can produce a magnetic field in the plane of the sample, the X-Y field. This is achieved by two Helmoltz coils, and the maximum field obtainable is $B_{xy} = 1.3$ T. The sample has to be well aligned with the Helmoltz coils, so that the X-Y field is accurately produced in the plane of the sample. We have calibrated the experimental misalignment by using a standard Aharonov-Bohm measurement: the magnetoconductance of a mesoscopic ring is sensitive to a small perpendicular component of the field. We have found that in our setup, the application of the X-Y field induces a component in Z of about $B_z = 1.5\ 10^{-3} B_{xy}$, which is a quite acceptable value.

Wiring

The wiring of the dilution refrigerator has been realized with particular precautions: first, to filter the external high-frequency noise and second, not to bring additional thermal noise to the sample.

In our experiment, the signals are very low, thus we need a very low noise set of Direct Coupling (DC) lines. For the wiring, we have taken special care of the high temperature intrinsic noise of the lines, which are cabled from room temperature down to the sample. The Johnson-Nyquist [55, 56] intrinsic voltage noise amplitude is given by $\Delta V = \sqrt{4k_B T R}$, where k_B is the Boltzmann constant, T the temperature and R the resistance. Thus, for cables having a resistance of about 100 Ω, the resulting noise at 300 K is about 1 nV. In order to have an experimental noise limited by the amplifiers ($0.4\ \mathrm{nV}/\sqrt{Hz}$), we have wired the fridge from room temperature 300 K to 4 K with low-resistance coaxial shielded cables[7].

Moreover, in this type of experiments, the low temperature noise can be attributed to extrinsic high-frequency electromagnetic radiation in the GHz range [57]. To circumvent this problem, we use *Thermocoax* cables that act as very good radio-frequency filters [58]. For a length of about 2 m, the electromagnetic signal is attenuated enough to ensure that the sample is not affected by the external radiation. At 4 K, a connection is thus made between the high temperature coaxial cables and the thermocoax cables. We paid attention to the thermalization of the wires at each stage of the dilution refrigerator, and the length of the wires between stages has been maximized in order the reduce the thermal flow. The detailed schemes of the wiring are shown in appendix A.

After wiring, the refrigerator has been cooled down to a base temperature of $T = 15$ mK. This means that the wiring does not significantly degrade the cooling properties. With this setup, we have verified that the electrons are cooled down to 40 mK, by measuring the temperature dependence of the resistance in a long wire. As a conclusion, the refrigerator has been prepared to allow measurements below the nV noise level, down to 40 mK.

An ultra-low noise detection

The samples we want to study are metallic. The resulting resistance of a typical quasi $1d$ Ag wire is about 10 Ω. As the resistance of the system is small, the best suited setup for the measurement is a current bias, and we measure the *voltage* of the sample.

[7] An alloy of Cu and Be with resistance $R \approx 4\Omega/m$.

In order to perform a measurement at equilibrium for the electrons, the condition $eV_{sample} \leq k_B T$ has to be fulfilled. e is the electron charge, and V_{sample} the voltage across the sample. In the temperature range of interest, the bias current ranges from the nA to the μA. The relative resistance fluctuations amplitude is of the order of one channel, that is $\Delta R/R \approx 10^{-4}$ in our samples ($R = 10\ \Omega$ corresponds to $N_c = 2500$).

In this setup, we use a standard Lock-In technique. The sample voltage probes are connected to a home-made amplifier "EPC1-A". This amplifier has a gain up to 10^4 and a noise level of 0.4 nV/$\sqrt{Hz}$. In addition, as we want to measure small relative corrections to the resistance, we use a bridge configuration.

Additional filtering of the signal is realized at room temperature with low-pass filters at the MHz level, and band-pass filters at the Lock-In frequency.

As the whole circuit contains several inductive or capacitive components, we have optimized the detection noise level with respect to the frequency of the Lock-In. The $1/f$ noise of the amplifiers increases below 1 Hz. We have measured the noise level of the whole setup as a function of the frequency f around 10 Hz at room temperature. The results are presented on figure 4.5, and show that for the optimum frequency of $f \approx 11$ Hz, the noise is minimum. The increase at larger frequencies is attributed to a parasitic noise that we could not remove. At $f \approx 11$ Hz, and at 4 K, the sample noise level has been regularly measured at $\Delta V \approx 0.36$ nV/$\sqrt{Hz}$. This confirms that our experimental setup is limited by the amplifier noise level.

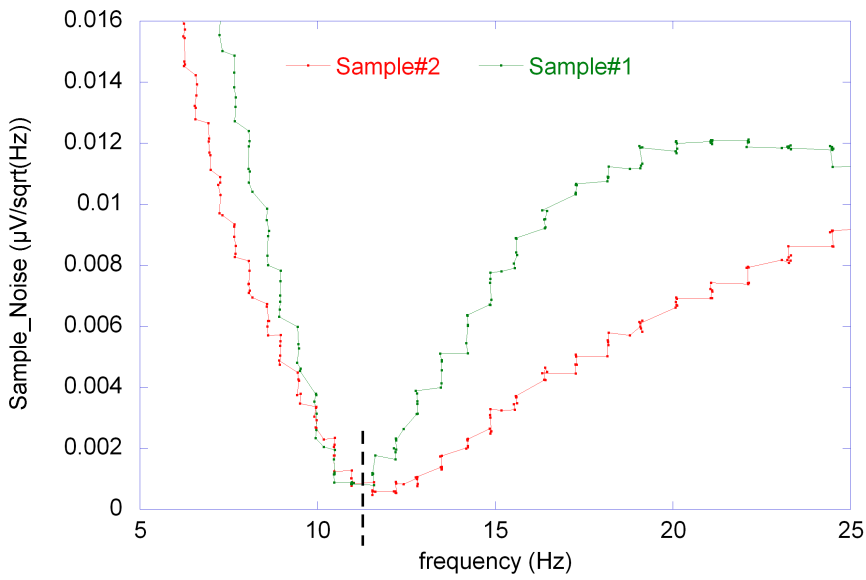

Figure 4.5: *Noise level measured for two samples as a function of frequency at room temperature. It is minimum for a frequency of about* 11 *Hz.*

The signal measured is sent to a 16 bits Analog to Digital Converter, and recorded on a computer with a dedicated acquisition program, built using the software LabView. Output voltages (Digital to Analog Converter) are used to sweep the magnetic field. The thermometry of the fridge is monitored independently with a temperature controller "TRMC2". The scheme of the electronic measurement setup is summarized on figure 4.6.

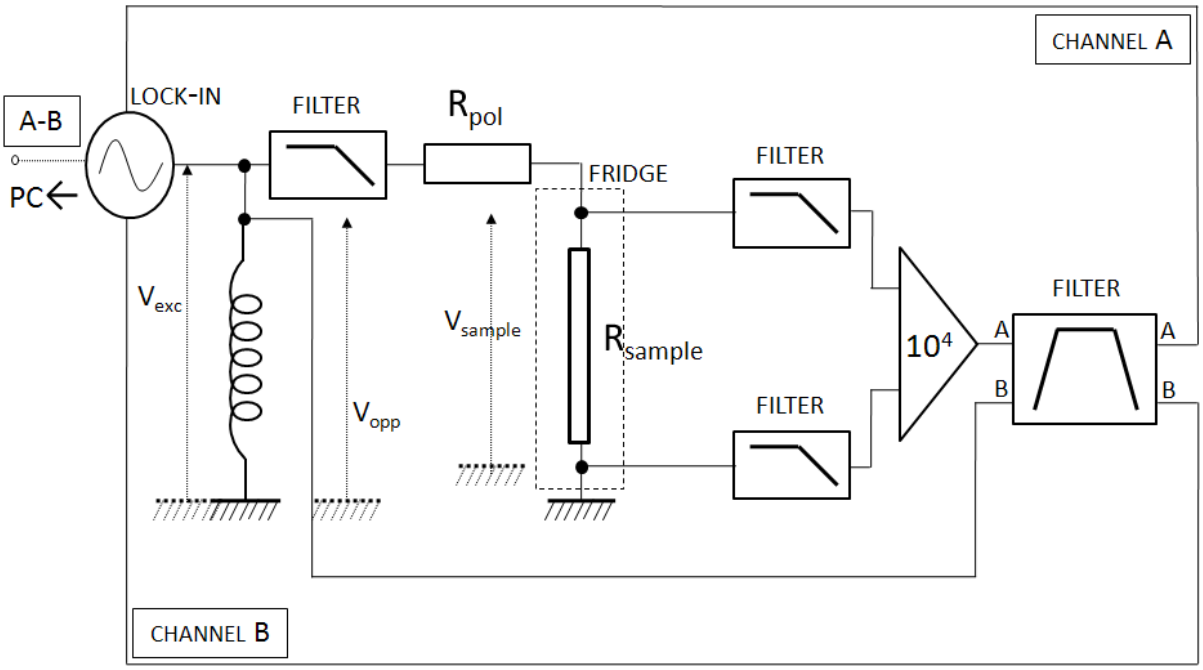

Figure 4.6: *Scheme of the electronic measurement setup. The Lock-In delivers an excitation voltage V_{exc} through a resistance R_{pol} and measures the input channels A (sample) and B (opposition). The subtracted signal A-B is sent to the computer for recording.*

4.2 Measurement implementation

In this section, we present the experimental quenching strategy and the analysis tools that we have developed in order to obtain a reliable measurement of the correlations between magnetofingerprints.

4.2.1 Rapid quench strategy

A crucial point in the physics of spin glasses is to know whether there exist in the ground state a unique spin configuration, or many of them. One protocol to test this is to compare spin configurations resulting from several thermal cycles above T_g. The thermal cycle is realized by heating the sample above T_g, so that the spin configuration is randomized, and then cooling down the sample, so that the spin configuration is frozen. In order for the magnetofingerprints to be comparable, the sample has to be quenched rapidly from $T_1 > T_g$ to $T_2 < T_g$. That is, it has to be cooled down fast enough to prevent any reorganization of the spins at an intermediate temperature between T_1 and T_2. This type of quench is not achievable by heating the whole refrigerator, as it takes several hours to heat it up to 4 K and cool it down again to 50 mK.

We have thus developed a strategy to heat locally the sample and quench it in a controlled manner. This can be realized by injecting a large electrical current I into the sample, which acts as a Joule heater. This allows to change the temperature rapidly. Such heating effect has been previously studied in the context of decoherence at very low temperature [59, 60, 61].

In order to control the effective temperature of the sample, we have calibrated our method. On the one hand, the (weak) temperature dependence of the resistance $\Delta R(T)$ is measured while cooling down the whole fridge, and represents the reference curve. On the other hand, we

measure the resistance variation when applying a large heating current $\Delta R_d(I)$. When applying a large heating current I, the effective temperature T_{eff} of the sample is locally higher than the temperature of the refrigerator. The comparison between the resistance variation $\Delta R_d(I)$ obtained and the reference curve $\Delta R(T)$ allows to convert the applied heating current into the effective temperature of the sample.

Experimentally, the $\Delta R(T)$ curve is obtained by using the detection described in 4.6. The resistance variation induced by the heating current I^{DC} is measured *via* the Lock-In detection by superposing an additional current i^{AC}. As an example, we present measurements performed in a pure Ag sample. The quasi $1d$ wire probed is shown on figure 4.7, and the results are presented on figure 4.8.

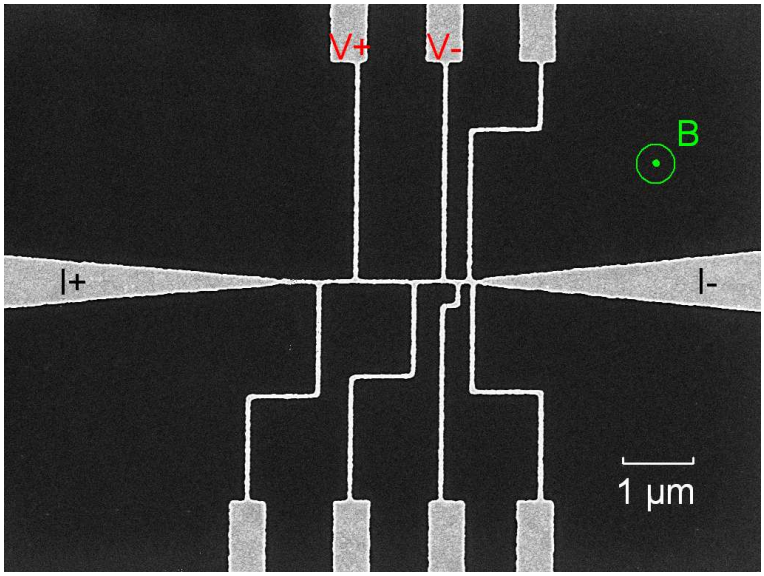

Figure 4.7: *Scanning electron microscope picture of the sample. The current is driven from $I+$ to $I-$, and the voltage measured between $V+$ and $V-$.*

In this experiment, the heating current has been applied to the sample at a refrigerator temperature $T_0 = 40$ mK. By comparing $\Delta R_d(I)$ with the reference $\Delta R(T)$, the observed increase shows that we are able to reach $T_{eff} \approx 17$ K for a current of $I = 100$ μA. We can graphically determine the heating current needed to reach an effective temperature on demand. It is worthy to discuss the homogeneity of the temperature in the wire. At high temperatures, typically above 1 K, the electron-phonon interaction dominates the electron energy relaxation. In this regime, the temperature profile is constant in the wire, all the energy is dissipated in the reservoirs [61]. At low temperatures (below 1 K), the electron-electron interaction dominates and the temperature is inhomogeneous in the sample. When we heat the system above 1 K, we can thus consider that the temperature is homogeneous in our sample.

As a conclusion, this heating technique allows to access a range of temperatures lying well above T_g. In addition, when we cut the heating current, the sample is cooled down very rapidly. In our situation, the overheat in the metallic wire is dissipated in the substrate, and is limited by the Kapitza resistance. The time it takes for a wire to be cooled down to the fridge temperature has thus been estimated to be about 10 μs at 100 mK [62]. Consequently, we estimate that our samples are cooled down faster than 1 ms, and this technique can be used to perform an experimental quench of the high temperature spin configuration in a calibrated way.

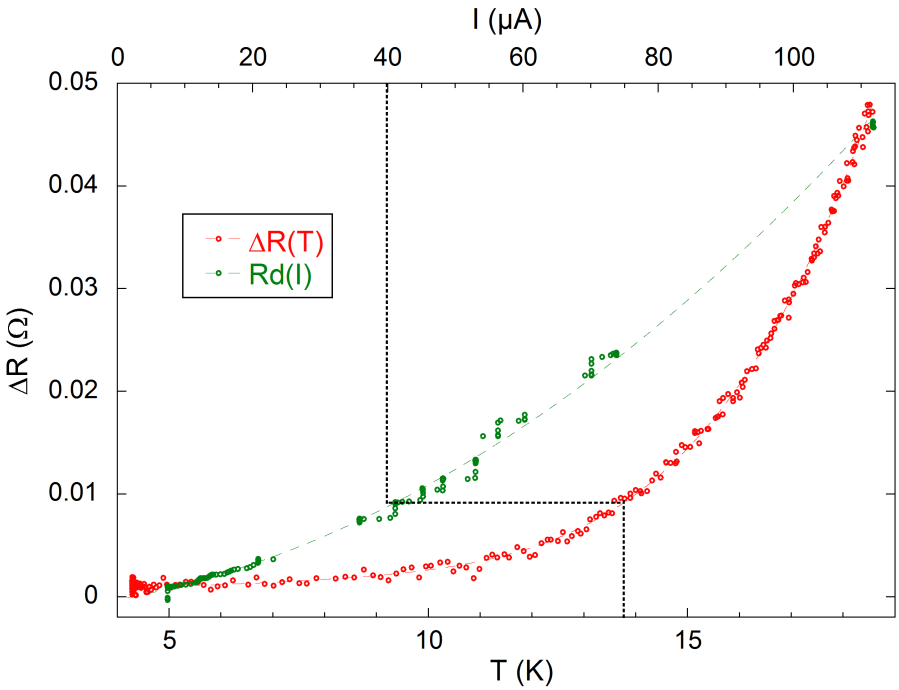

Figure 4.8: *Resistance variation of an Ag sample as a function of temperature T (bottom axis) and as a function of current I (top axis). The conversion is graphically determined, for $I = 40\ \mu A$, the resistance variation corresponds to $T \approx 14\ K$.*

4.2.2 Correlations

Correlations are a tool which allows to evaluate quantitatively the similarity of data. The measurement of a magnetofingerprint yields an array of values of the conductance variation ΔG as a function of the magnetic field. A natural tool to compare such traces is the linear (or Pearson) correlation coefficient C defined for two sets of data $X \equiv \{x_i\}$ and $Y \equiv \{y_i\}$

$$C(X,Y) = \frac{\sum_i^N (x_i - \bar{x}).(y_i - \bar{y})}{\sqrt{\sum_i^N (x_i - \bar{x})^2}.\sqrt{\sum_i^N (y_i - \bar{y})^2}} \tag{4.2.1}$$

where the notation $(^{-})$ denotes the mean of the ensemble, and N the number of points. The denominator normalizes the correlation C to 1.

This coefficient gives a quantitative measurement of the similarity of two magnetofingerprints, that is of two spin configurations. Let us consider two magnetofingerprints taken on the same sample at different times. If the disorder is completely frozen, the spin configuration does not change, and the two traces are strictly identical. The correlation is $C = 1$. On the contrary, if the disorder has been completely randomized, after a time spent in the paramagnetic regime for instance, the correlation $C \to 0$. The correlation coefficient can be negative when the magnetofingerprints are exactly symmetric with respect to the mean, $C = -1$. Note that having an anti-correlation $C = -1$ is giving as strong information on the spin configuration than $C = 1$.

In order to implement these correlations, we have measured several magnetofingerprints in a pure Ag sample, as a function of time. The sample is the same as the one shown in figure 4.7.

At low temperature, the disorder in the Ag sample is frozen, as thermal activation does not permit the motion of atoms. Therefore, we can test the stability of the magnetofingerprints in Ag as a function of time. We have performed this experiment for 4 days, with more than 40 traces taken. The results are shown on figure 4.9.

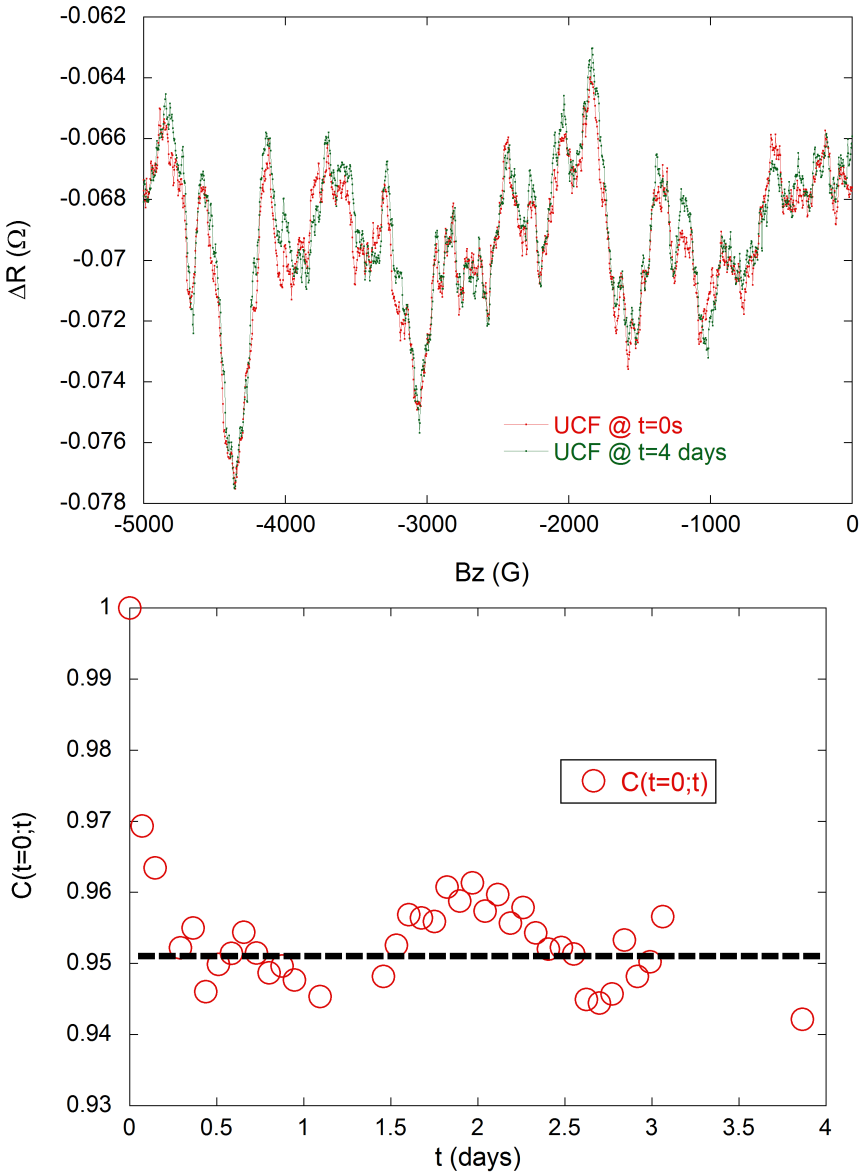

Figure 4.9: *Top: two experimental magnetofingerprints taken at a time interval of four days. Bottom: correlation coefficient of two magnetofingerprints taken at different times. Each point shows the correlation of a trace taken at time t with the trace taken at $t = 0$.*

The correlation coefficient $C(t = 0; t)$ is calculated between magnetofingerprints taken at time $t = 0$ and an arbitrary time t. This correlation is roughly constant as a function of time, around a mean value of $C \approx 0.95$. This coefficient is not reaching the ideal value of 1, due to the noise on the magentofingerprint signal. This point is discussed in the next section. The fluctuations around the mean value evaluates the uncertainty of the measurement: $C = 0.95 \pm 0.01$. As a conclusion, during this four days experiment, the traces remain highly correlated, we can consider that the static disorder is unchanged or in other words, that *the atoms do not move.*

4.2.3 Calibration of the reproducibility

The correlation coefficient between two experimental magnetofingerprints can be strongly affected by the noise of the measurement. Indeed, for each experimental curve, there is a white noise superimposed to the UCF signal, determined by the noise floor of the electronic setup. As the signal is small, the signal to noise ratio can be quite poor. Therefore, the quantitative comparison between the curves is sensitive to this noise.

In our experiment, this noise issue is very important, as the correlation between magnetofingerprints has to be determined reliably. In addition, the uncertainty on such a measurement has to be properly calibrated, so that we can draw clear conclusions on the spin configuration changes. For this purpose, we have studied both experimental and numerically simulated magnetofingerprints.

In particular, we have studied how the correlation coefficient is affected by the noise floor of the detection. We calculate the correlation coefficient between two identical simulated magnetofingerprints on each of which we add different random noises. Because of this noise, the resulting correlation coefficient is smaller than 1. The coefficient C is calculated as a function of the inverse of the signal to noise ratio called h, and is presented on figure 4.10.

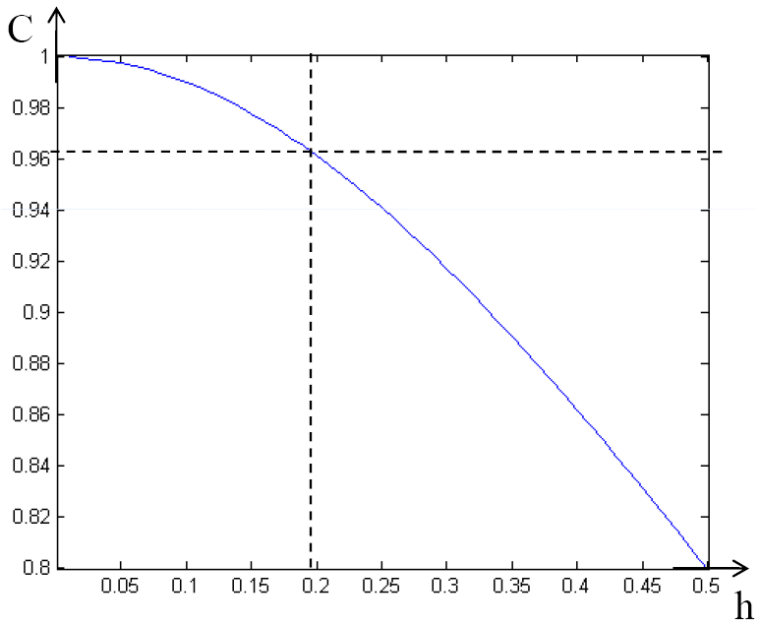

Figure 4.10: *Correlation coefficient calculated between two identical simulated magnetofingerprints, as a function of the inverse of the signal to noise ratio h.*

In our experimental situations, the signal to noise ratio yields typically $h \approx 0.2$, and this leads to a correlation coefficient $C = 0.96$ determined from the simulated curves, which is in very good agreement with experimental observations.

In addition, we have investigated how the correlation coefficient C evolves with the size of the experimental field span ΔB over which we calculate the correlation. Thus, we have evaluated the correlation coefficient between magnetofingerprints as a function of the field interval ΔB. Results obtained from experimental data are presented on figure 4.11.

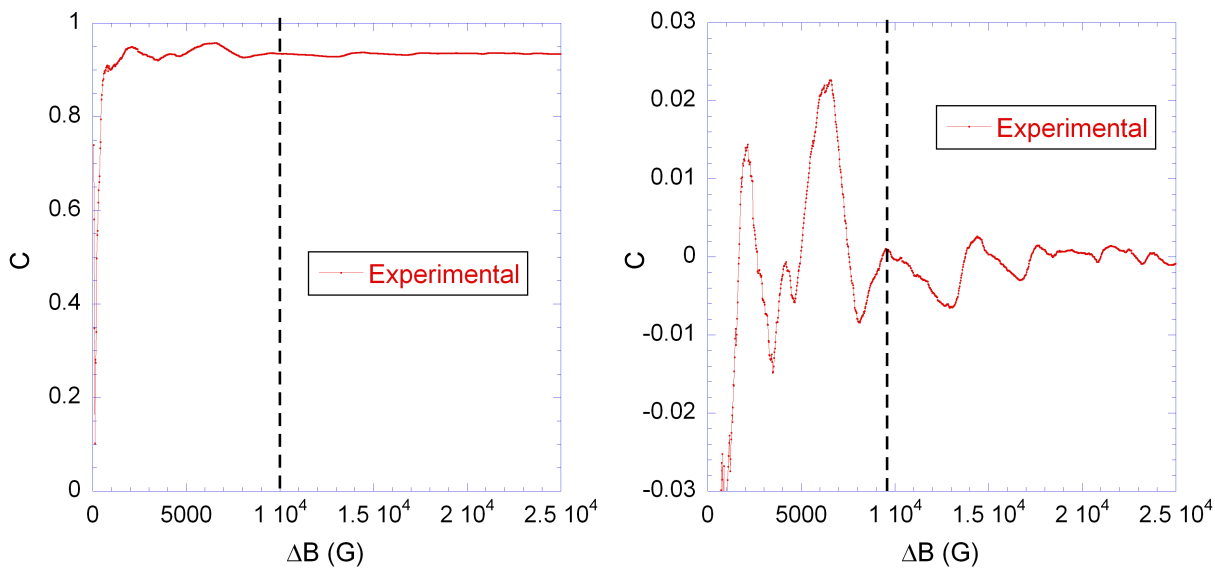

Figure 4.11: *Left: correlation as a function of the field span ΔB obtained experimentally. The data converges rapidly to a constant value. Right: correlation deviation to the constant value $C - \langle C \rangle$ as a function of ΔB. Above $\Delta B = 10000$ G, the error is negligible.*

We observe that the correlation coefficient C is converging rapidly when the field interval increases. For this sample, if the field span $\Delta B \geq 10000$ G, C is obtained with an uncertainty below ± 0.01.

Conclusion

In order to implement UCF measurements in spin glasses, we have elaborated suitable nanostructures of spin glasses by using standard e-beam lithography and implantation techniques. We have prepared an experimental setup capable of ultra low-noise measurements (0.4 nV$/\sqrt{Hz}$) of magnetofingerprints (up to $\Delta B = 8$ T) at temperatures down to $T = 40$ mK. In addition, we have developed and calibrated a quenching method for cooling our samples, which is necessary to obtain different spin configurations of the sample in a reliable way. Finally we have established the experimental conditions required for a proper and quantitative determination of the correlation coefficient C.

Part III

Experimental study of spin glasses

Si faire était aussi aisé que savoir ce qu'il est bon de faire, les chapelles seraient des églises, et les chaumières des pauvres gens des palais de princes.

William Shakespeare, Le marchand de Venise

Chapter 5
Experimental calibration on pure Ag

In order to calibrate the experiment, we have implemented Universal Conductance Fluctuations (UCF) measurements of a pure Ag sample which will serve as a reference in the analysis of spin glasses. First, we have characterized the coherence properties of a Ag sample by standard weak-localization measurement. Second, we have performed UCF measurements. Their behavior is in good agreement with theoretical predictions.

5.1 Weak-localization measurements

We want to characterize the phase coherence in our Ag samples, by measuring the amplitude of L_Φ. For this purpose, we use a well-established procedure consisting in performing a weak-localization measurement. Weak-localization is a quantum correction to the conductance arising from interferences between time-reversed electron paths. This interference leads to an increase of the resistance, which is suppressed by applying a perpendicular magnetic field. The magnetic field for which this correction is eliminated depends directly on L_Φ [63]. Therefore, a low-temperature magnetoresistance measurement allows to determine L_Φ. This method has been extensively used for the determination of the phase coherence length in various materials (as an example, see [64]).

We have prepared the samples from a high purity silver source (99.9999 %, prepared in the Quantronics group). We have fabricated in the same evaporation run long wires allowing for the measurement of weak-localization[1] and short wires for the measurement of universal conductance fluctuations. A picture of the long wire sample is presented on figure 5.1.

Using the experimental setup described in chapter 4, we have measured the low-field magnetoresistance of such a long Ag wire at low temperatures. In Ag, spin-orbit effects lead to a weak-antilocalization: the resistance is increasing as we apply the magnetic field. The method

[1]For short samples $L \sim L_\Phi$ the signal is dominated by UCF. For long wires $L \gg L_\Phi$, the UCF signal is canceled on average, only the weak-localization signal subsists.

used for the determination of L_Φ however remains the same. The experimental magnetoresistance data is fitted with the quasi $1d$ theoretical formula [65], a method previously reported by our group [54]. Such a measurement is repeated at several temperatures, and the resulting temperature dependence of L_Φ is presented on figure 5.1.

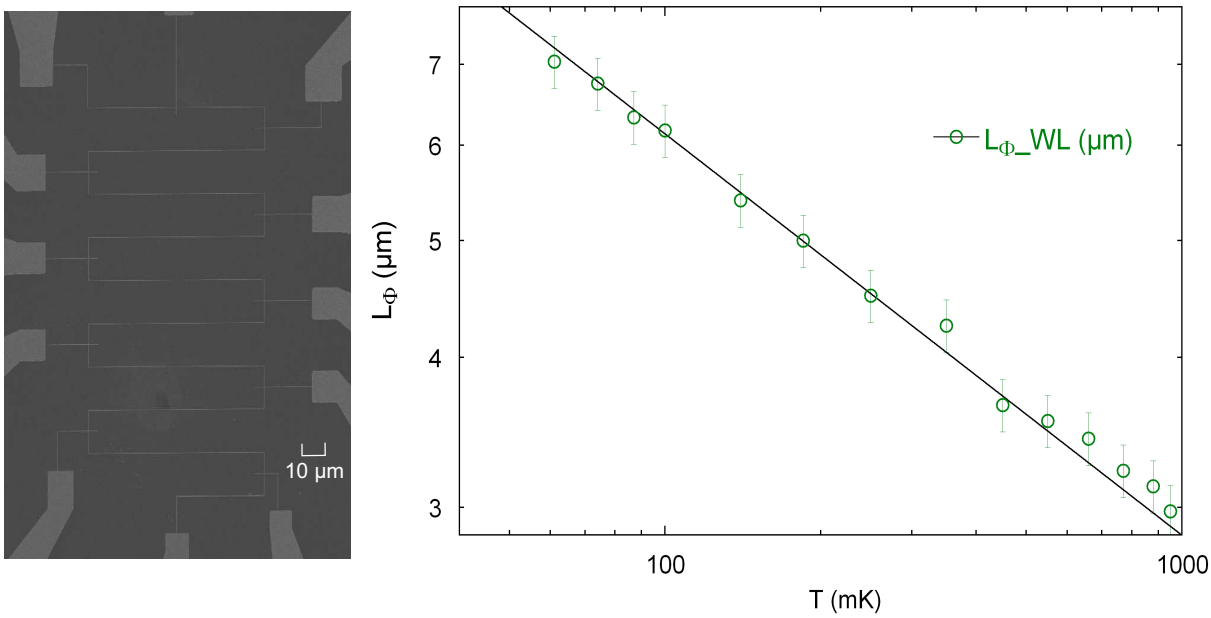

Figure 5.1: *Left: scanning electron microscope (SEM) picture of the sample used to measure the weak localization. The wire has dimensions $L = 86$ μm, $w = 110$ nm and $t = 40$ nm. Right: experimental phase coherence length L_Φ as a function of temperature. The solid line is a fit to the power law $T^{-1/3}$ predicted by the AAK theory.*

The temperature dependence obtained is in good agreement with the power law $L_\Phi \propto T^{-1/3}$ predicted by Aronov, Altshuler and Khmelnitsky (AAK) [66] in these systems. The experimental coefficient of this power law is lower than the one predicted by AAK, as it is frequently observed in such metallic samples [52]. The absolute value of L_Φ reaches about 7 μm at 60 mK. This is indeed the order of magnitude expected for a very clean metal. This measurement thus confirms that there are no important quantities of magnetic impurities having a Kondo temperature $T_K > 60$ mK. This sample is thus suitable for being the pure Ag reference for our experiment.

5.2 Universal conductance fluctuations

We have measured the universal conductance fluctuations in a quasi $1d$ sample of length $L \geq L_\Phi$ which is presented on figure 5.2. The multiple voltage probes allow to choose experimentally the length of the probed section of the wire.

The magnetoconductance measurements have been performed by using the experimental protocol described in chapter 4. At the lowest temperature $T = 40$ mK, the conductance fluctuations are clearly visible, as shown on figure 5.3. For comparison, the noise level is also shown on this figure. We have measured two traces, separated by a time interval of a few hours, and they are highly reproducible: the correlation coefficient is $C = 0.98$. As expected, the conductance fluctuations have an amplitude of (e^2/h).

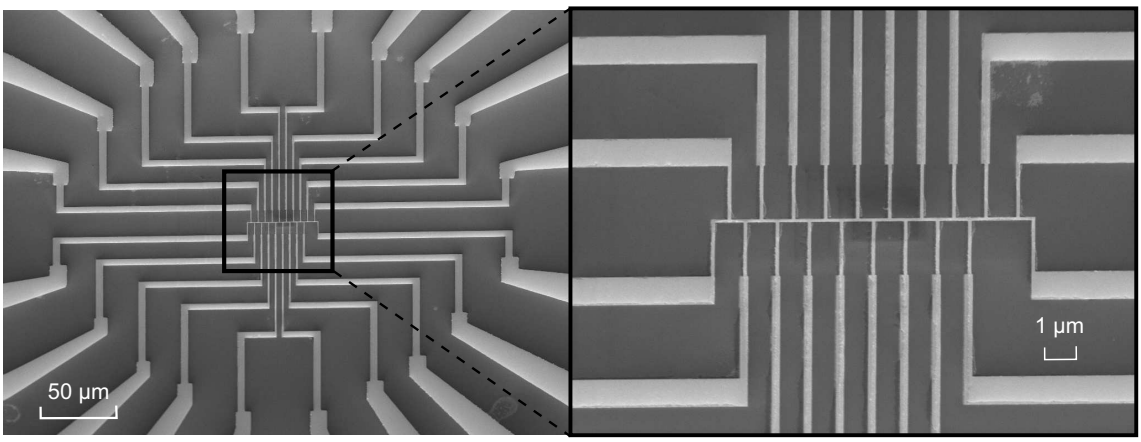

Figure 5.2: *SEM picture of the sample used to measure the UCF. The left image shows a large view, and the right is a zoom on the center part. The wire has dimensions $L = 20$ μm, $w = 100$ nm and $t = 40$ nm, with voltage probes arranged every μm.*

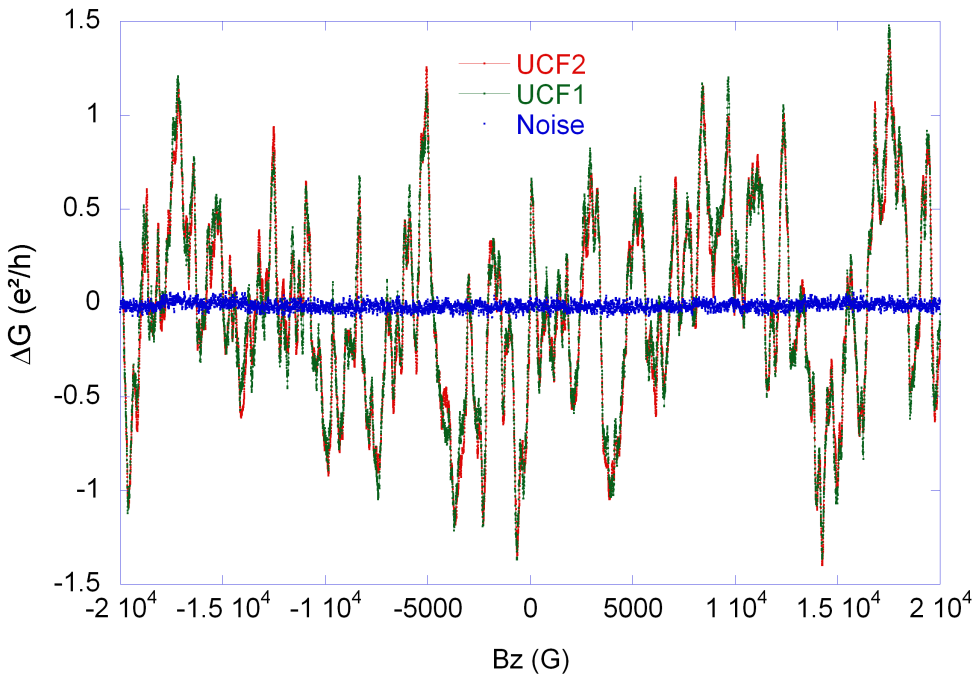

Figure 5.3: *Universal conductance fluctuations measured as a function of the magnetic field B in a range of ± 2 T at $T = 40$ mK. The noise level of the measurement is shown by the blue trace. The two traces in green and red have been taken successively, separated by a time interval of few hours, and show high reproducibility.*

Magnetoresistance of the sample have been further measured on a large field span at several temperatures between 40 mK and 1 K. Two raw curves are shown on figure 5.4. One can clearly see the decrease of the fluctuations when the temperature is raised.

In order to check that we can quantitatively extract L_Φ from the UCF measurements, we have compared the results obtained using this technique with those obtained using weak-localization measurements. In the case of the UCF, the phase coherence length is extracted by analyzing the amplitude of the conductance fluctuations.

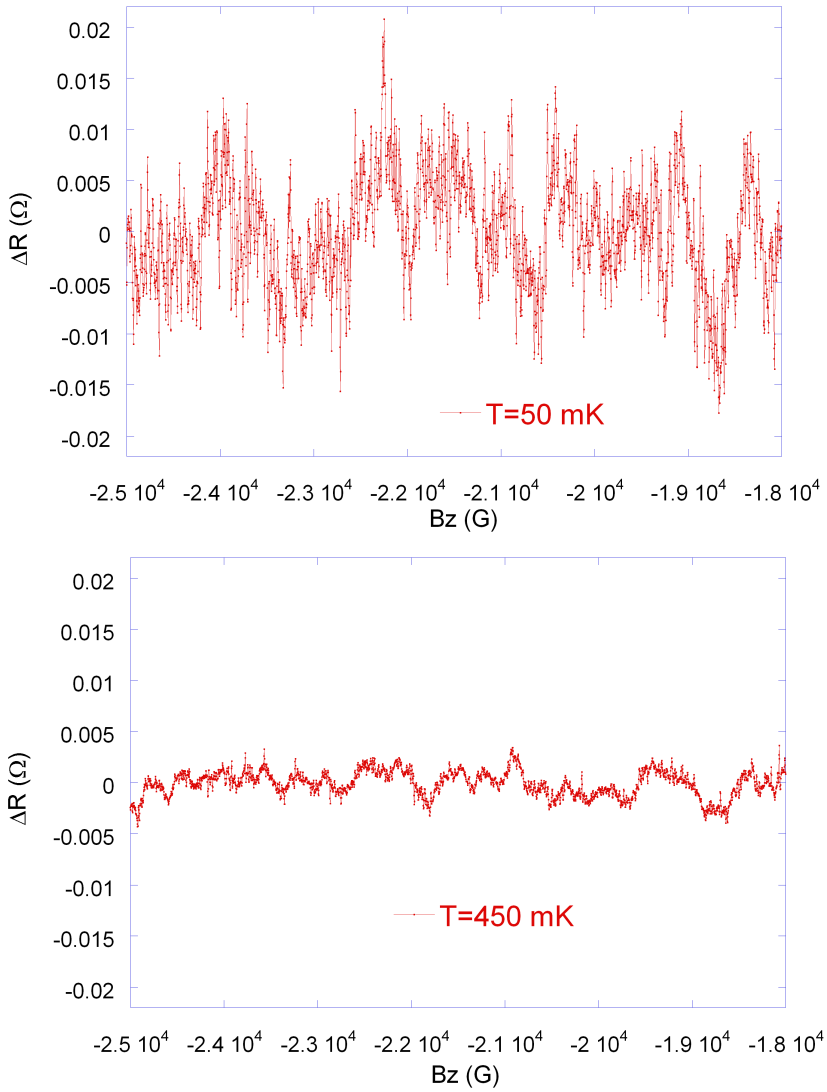

Figure 5.4: *Universal resistance fluctuations as a function of the magnetic field (plotted on an interval of* 0.7 *T), measured on a sample of length* $L \approx 8$ *μm. Top: at* $T = 50$ *mK. Bottom: at* $T = 450$ *mK.*

Amplitude analysis

As presented in chapter 2, the amplitude of UCF depends on the quantities L, L_Φ and L_T. In our experiment, the sample has a length $L = 8.4$ μm. The thermal length is given by $L_T = \sqrt{\frac{\hbar D}{k_B T}}$. The diffusion coefficient D is obtained from the resistivity of the sample: $D = 210$ cm^2/s. In these conditions, the amplitude of the UCF is given by [30]

$$\Delta G^2(T) = E\frac{L_T^2 L_\Phi(T)}{L^3} \tag{5.2.1}$$

where E is a constant of proportionality which has a theoretical value $E_{theo} \approx 0.28$.

At each temperature, the amplitude of the conductance fluctuations ΔG is obtained by taking the standard deviation of the magnetoconductance fluctuations on the whole field range. The comparison between the resulting value $L_\Phi^{\Delta G}$ and the value obtained from weak-localization L_Φ^{WL} is presented on figure 5.5.

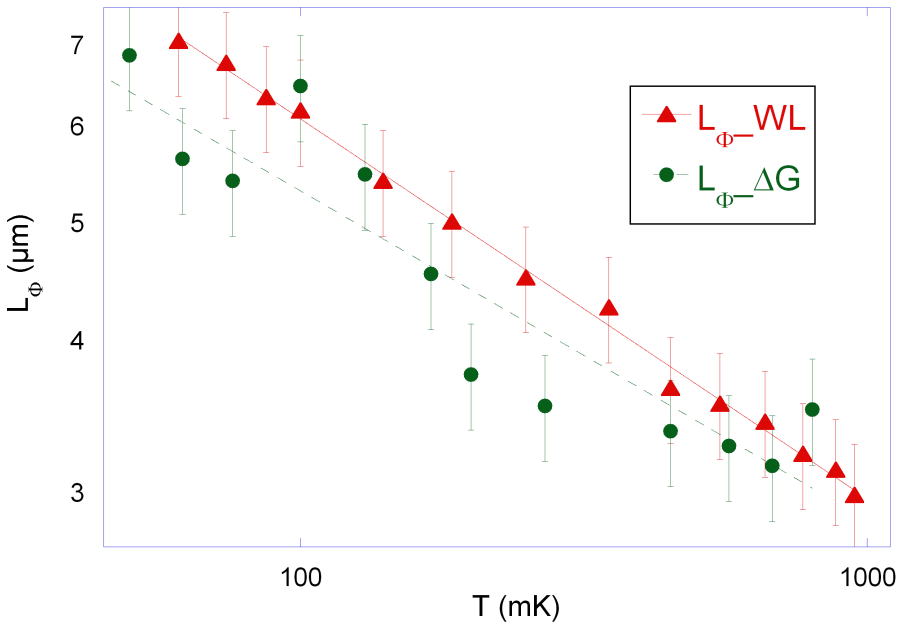

Figure 5.5: *Phase coherence length L_Φ extracted from the weak-localization (red triangles) and the UCF (green dots), as a function of temperature. The dashed lines show a fit to a power law dependence close to the $T^{-1/3}$ predicted by AAK.*

The phase coherence lengths extracted from the two methods are in good agreement, in both temperature dependence and absolute value. In this experiment, L_Φ is very sensitive to the amplitude of the conductance fluctuations, and this explains the dispersion of the values. Though this determination is not as accurate, it gives the same trend for L_Φ as the weak-localization measurement. As a conclusion, the phase coherence length determined by UCF measurement or by weak-localization measurement is the same. This proves that the UCF can lead to a reliable determination of L_Φ [67], which can be applied at non zero magnetic field.

5.3 Onsager relations

As presented in chapter 2, by using the Onsager symmetries one can extract the magnetic contribution ΔG_M to the UCF. In the following, we calibrate the amplitude of ΔG_M in a non magnetic Ag sample.

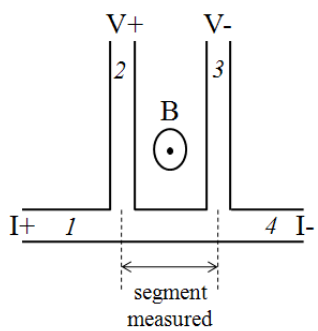

Figure 5.6: *Scheme of a four-probe measurement. Contacts $1, 2, 3, 4$ can be used as current leads or voltage probes in order to extract the different contributions to the UCF.*

We have measured the magnetoconductance fluctuations of the sample described previously, in a four probe configuration. As presented on figure 5.6, contact numbers (1,4) are connected as current leads I, and contacts (2,3) as voltage probes V. We thus obtain a set of data G_{1423} called $G_{IV}(B)$. After permutation of voltage probes, now connected to (1,4), and current leads connected to (2,3), we repeat the measurement in the same conditions. It gives a second set of data G_{2314} called $G_{VI}(B)$. For a non magnetic system, the Onsager symmetry holds: $G_{VI}(B) = G_{IV}(-B)$. We present the experimental curves obtained on figure 5.7.

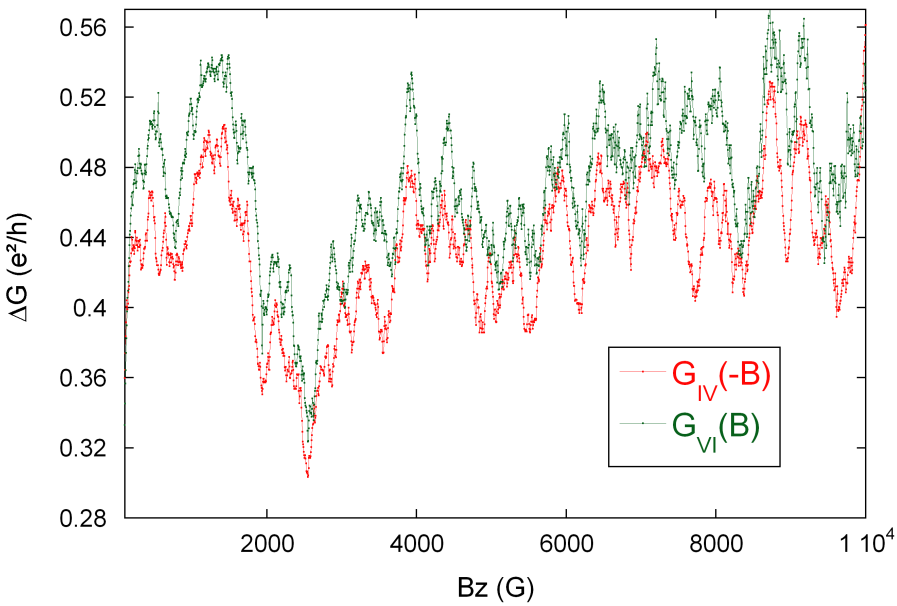

Figure 5.7: *Conductance fluctuations as a function of the magnetic field, at $T = 400$ mK for a Ag sample. The two different measurements $G_{IV}(-B)$ and $G_{VI}(B)$ are compared. They visually look similar, and the calculated correlation coefficient between the curves is $C = 0.87$.*

The pair of curves $(G_{IV}(-B), G_{VI}(B))$ has a high correlation coefficient of $C = 0.87$. Experimentally, we observe a small deviation to the ideal value $C \approx 1$ which we believe is not significative, and probably due to a possible asymmetry between the probe configurations. Indeed, for comparison, the correlation between $G_{IV}(B)$ and $G_{IV}(-B)$ is $C = 0.2$.

Amplitude of the different contributions

From the experimental magnetoresistance traces we can extract

$$\Delta R_M = \frac{\Delta R_{IV}(B) - \Delta R_{VI}(-B)}{2} \tag{5.3.1}$$

$$\Delta R_O = \frac{\Delta R_{IV}(B) + \Delta R_{VI}(-B)}{2} \tag{5.3.2}$$

where ΔR_M is the magnetic component and ΔR_O the orbital component. In a non magnetic system, like the Ag sample we are studying, the magnetic component should be zero as time-reversal invariance is fulfilled. The obtained traces for magnetic and orbital components are shown on figure 5.8. In this experiment, the amplitude of the magnetic component extracted is $\Delta R_M \approx 0.9$ mΩ, whereas the amplitude of the orbital component is $\Delta R_O \approx 2.2$ mΩ. The magnetic component amplitude is slightly higher than the noise level ($\Delta R_{noise} \approx 0.4$ mΩ), but is clearly smaller than the orbital one.

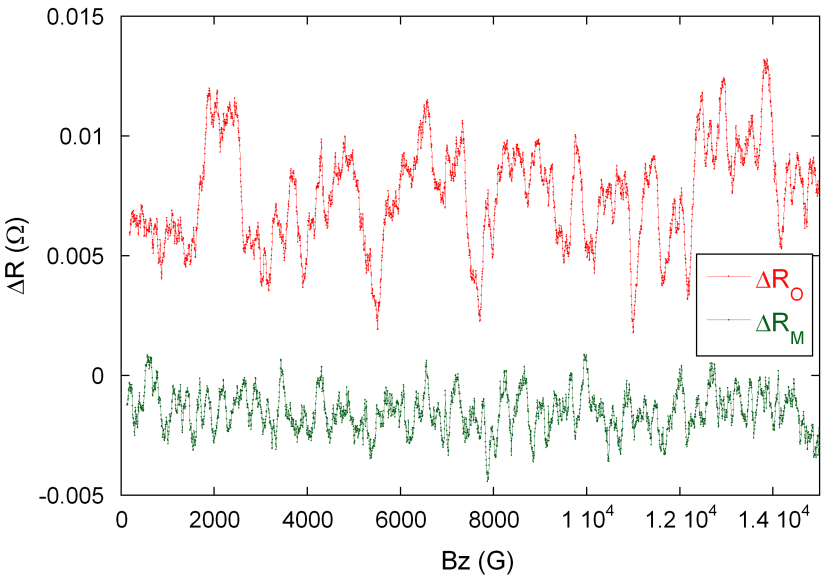

Figure 5.8: *Resistance fluctuations as a function of the magnetic field in a pure Ag wire. Top trace: orbital component ΔR_O, bottom trace: magnetic component ΔR_M. The curves have been shifted for clarity.*

In spin glasses, we have local random fields that break the time-reversal symmetry of the system. In order to understand how this affects the different components, we use an additional parallel field B_{xy} which breaks the time-reversal invariance in the sample. Magnetoresistance traces are recorded by sweeping B_z, but under several stationary values of B_{xy}. For each set of curves, we extract the magnetic and orbital components. The measured amplitudes are presented on figure 5.9.

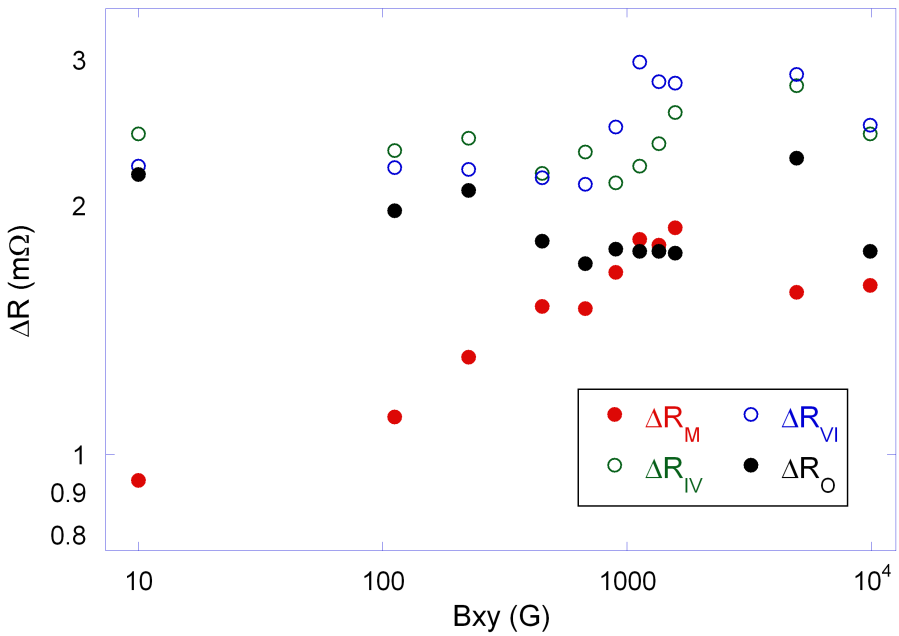

Figure 5.9: *Various resistance fluctuations amplitudes as a function of the parallel field B_{xy}, taken at $T = 200$ mK. The open symbols show ΔR_{IV} (green) and ΔR_{VI} (blue). The solid symbols represent ΔR_M (red) and ΔR_O (black).*

We observe that the experimental amplitudes ΔR_{IV} and ΔR_{VI} are roughly constant as a function of B_{xy}, up to 1 T. At $B_{xy} = 0$ G, $\Delta R_M \ll \Delta R_O$ as the time-reversal invariance is fulfilled. By applying the additional field B_{xy}, we break progressively the time-reversal invariance, and the amplitude of the magnetic component ΔR_M increases. Above a value of the order of $B_{xy} \approx 500$ G, the amplitudes of ΔR_M and ΔR_O are about the same.

The field scale $B_{xy} \approx 500$ G is compatible with the amount of field required to produce a flux quantum Φ_0 in the side area of the sample, which is indeed the field scale needed to dephase time-reversed paths in the sample. Figure 5.9 thus shows an experimental signature of the breaking of time-reversal symmetry in a non magnetic system, due to an external magnetic field.

Conclusion

In this chapter, we have presented the experimental results obtained in a non magnetic Ag sample, which will serve as a reference for the measurements in spin glasses. We have shown that our Ag samples have good coherence properties before implantation, with a phase coherence length L_Φ of 7 μm. The universal conductance fluctuations can be measured, and used to quantitatively extract L_Φ. In addition, we have validated the method for the extraction of ΔR_M, the component of the fluctuations which is linked to the magnetic properties of the sample.

Le doute est père de la création.

Galilée

Chapter 6

Remanence in the resistivity of AgMn spin glass

We characterize the low temperature properties of AgMn spin glass mesoscopic samples. An important point is to be able to evaluate T_g: our small samples do not provide enough volume to allow for usual magnetic susceptibility measurements. In this chapter, we present the results obtained on the resistivity of AgMn samples.

6.1 Size effects in spin glasses

In usual thermodynamic phase transitions, size effects are important. There exist a critical dimensionality range in which the transition exists. In spin glasses, the lower critical dimension has been heavily debated and investigated, and is thought to be between $d = 2$ and $d = 3$. As we reduce the dimensions of the system to observe coherent effects, the question of the existence of a spin glass phase in such samples is thus relevant.

To answer this question experimentally, the main difficulty arises from the fact that magnetic susceptibility measurements cannot be performed in low-dimensional systems. There are however two experiments that have circumvented this issue.

A first investigation has been realized in thin AuFe films [68], by measuring the anomalous Hall resistivity which gives a signal directly proportional to the magnetic susceptibility. Therefore, they could observe the cusp as a function of temperature, characteristic of the spin glass behavior. The transition temperature as determined was not modified down to a thickness of about 15 nm.

Another study was performed on multi-layer samples of CuMn and AgMn, the stacking of thin layers allowing for direct magnetic susceptibility measurements [69]. Here also, the transition temperature was not affected down to thicknesses of 15 nm. As a conclusion, in our mesoscopic samples of dimensions $L > l_e > 15$ nm, we can estimate that the spin glass transition is still three dimensional.

6.2 Experimental signatures of the spin glass phase

6.2.1 Temperature dependence of the resistivity

Bulk properties

Unlike magnetic susceptibility, the resistivity does not offer sharp features around T_g in spin glasses. However, the additional magnetic scattering of the electrons in these systems is expected to affect the resistivity ρ. The effect of the magnetic spins is two-fold. On the one hand, there is a Kondo effect: the resistance is increasing with decreasing temperature below the Kondo temperature T_K. On the other hand, the spin glass phase appears below T_g, and the resistance is decreasing with decreasing temperature, due to the spins freezing. In low-concentration canonical spin glasses, the interplay between the two contributions leads to a non-monotonic behavior of the temperature-dependence of the resistivity [70, 71].

A maximum appears at a temperature T_m which has been theoretically linked to the two characteristic temperature scales [72, 73]:

$$T_m \propto T_g \ln\left(\frac{T_g}{T_K}\right) \qquad (T_g \gg T_K) \tag{6.2.1}$$

This maximum in resistivity has been previously observed in various bulk metallic spin glasses as shown on figure 6.1.

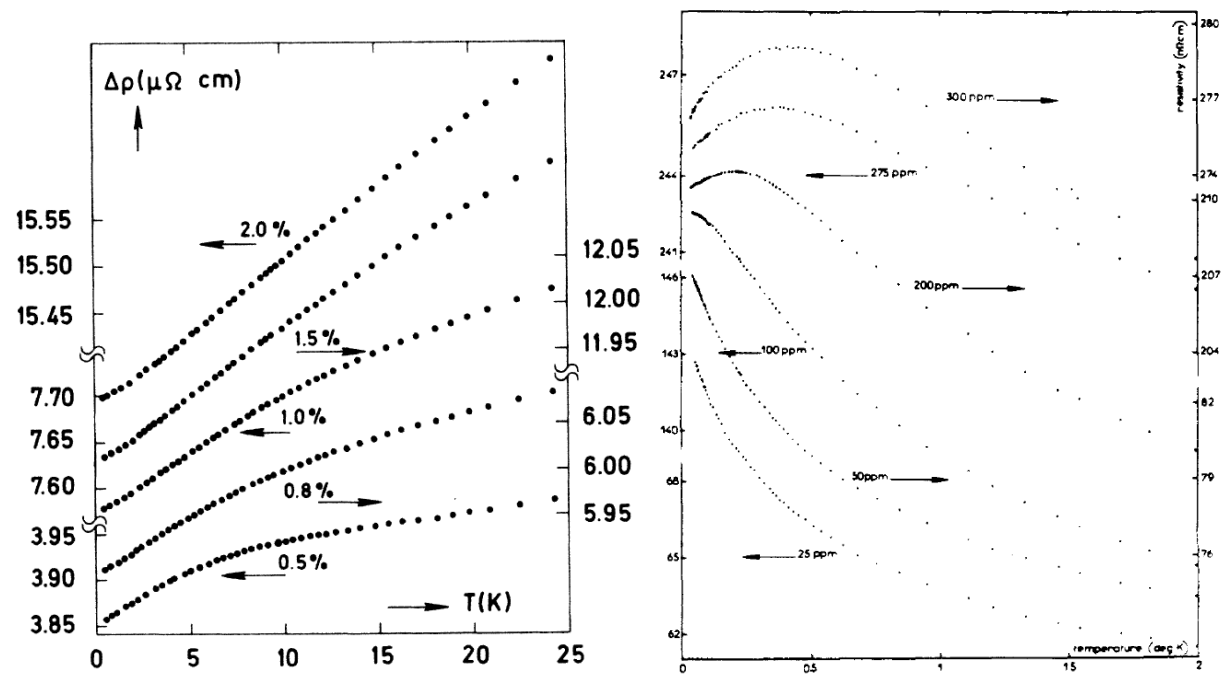

Figure 6.1: *Resistivity variation as a function of temperature for several concentrations in a AuFe alloy ($T_K \approx 1$ K). Left: for high concentrations ($T_g > T_K$), the spin glass contribution prevails, from [71]. Right: in the diluted regime ($T_g \leq T_K$), the Kondo contribution is important, from [70].*

Experimental study of AgMn wires

We investigate the low-temperature resistivity behavior of AgMn wires. The quasi $1d$ samples have been elaborated from a very well controlled source of Ag 6N, and further implanted

with Mn ions, at a concentration $c = 700$ ppm. For this alloy, we thus expect $T_g \approx 700$ mK and $T_K = 40$ mK [74]. The wire is shown on figure 6.2, and has a total length $L = 3$ μm, width $w = 50$ nm and thickness $t = 40$ nm, with several voltage probes available along the wire.

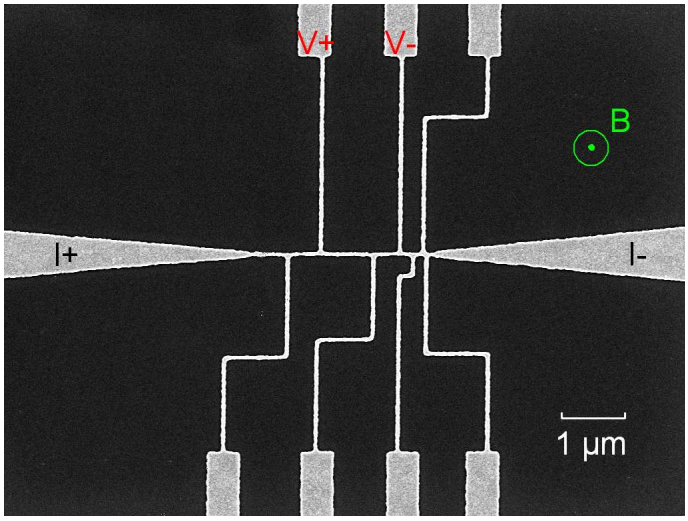

Figure 6.2: *Scanning electron microscope picture of the sample. The current is driven from $I+$ to $I-$, and the voltage measured between $V+$ and $V-$, that can be chosen along the wire. A perpendicular magnetic field B_z can be applied.*

We measure a AgMn wire of length $L = 2$ μm, using the experimental measurement scheme described in chapter 4. The resistance measured at 4 K is $R = 105$ Ω. This yields a resistivity of $\rho = 1.10^{-7}$ Ω.m, and a diffusion constant $D = 42$ cm^2/s. For comparison, the resistivity of the pure Ag sample is $\rho_{Ag} = 2.10^{-8}$ Ω.m, and $D = 210$ cm^2/s. The resistance variation is recorded while cooling down the sample, as presented on figure 6.3.

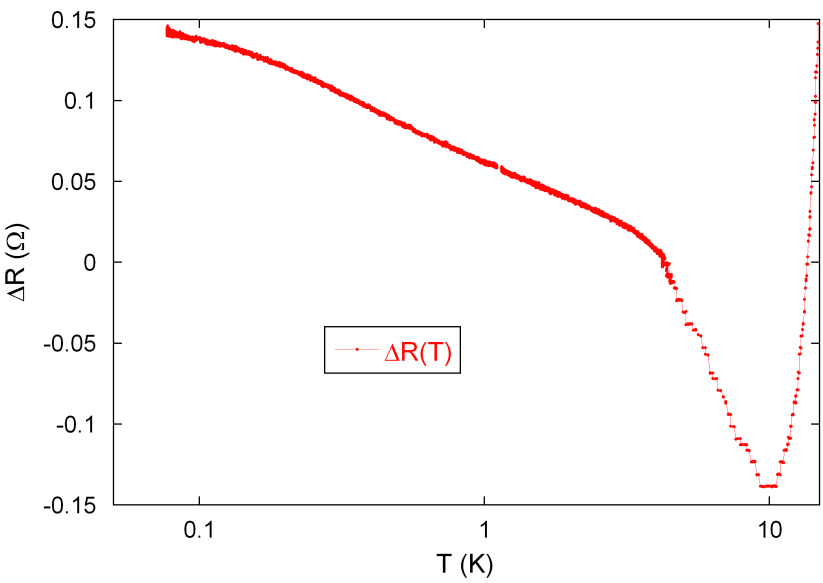

Figure 6.3: *Variation of the resistance $\Delta R = R - R_0$ in Ω as a function of the temperature T in K (log scale). At high temperature (above 10 K), the electron-phonon scattering processes are dominating. At low temperature (below 3 K) the electron-electron interaction prevails.*

The total low temperature resistance can be written as the sum of different contributions

$$R = R_0 + \Delta R_{e-ph} + \Delta R_{e-e} + \Delta R_{SG} \tag{6.2.2}$$

where R_0 is the residual resistance due to static impurities, ΔR_{e-ph} is due to the electron-phonon scattering, ΔR_{e-e} the term due to electron-electron scattering, and we add ΔR_{SG} to take into account the magnetic scattering. When temperature decreases from room temperature, the phonon contribution becomes weaker, and the resistance decreases as a known power law T^5 which is experimentally observed above 10 K. At lower temperatures, the resistance variation is attributed to electron-electron scattering and a spin glass contribution. In order to extract the spin glass contribution, the electron-electron contribution has to be known.

This electron-electron contribution can be determined by measuring the low temperature resistance in a pure Ag sample. In metals, the electron-electron interaction leads to a correction at low temperature, which can be written for quasi $1d$ wires [75]

$$\Delta R_{e-e} = 0.782\lambda_\sigma \frac{R^2}{R_K}\frac{L_T}{L} \tag{6.2.3}$$

where R_K is the quantum of resistance h/e^2, and $L_T = \sqrt{\hbar D/k_B T}$ the thermal length. λ_σ is a parameter representing the strength of electron-electron interactions in the sample. We have measured the low-temperature resistance of a pure Ag sample which is plotted on figure 6.4 as a function of $T^{-1/2}$.

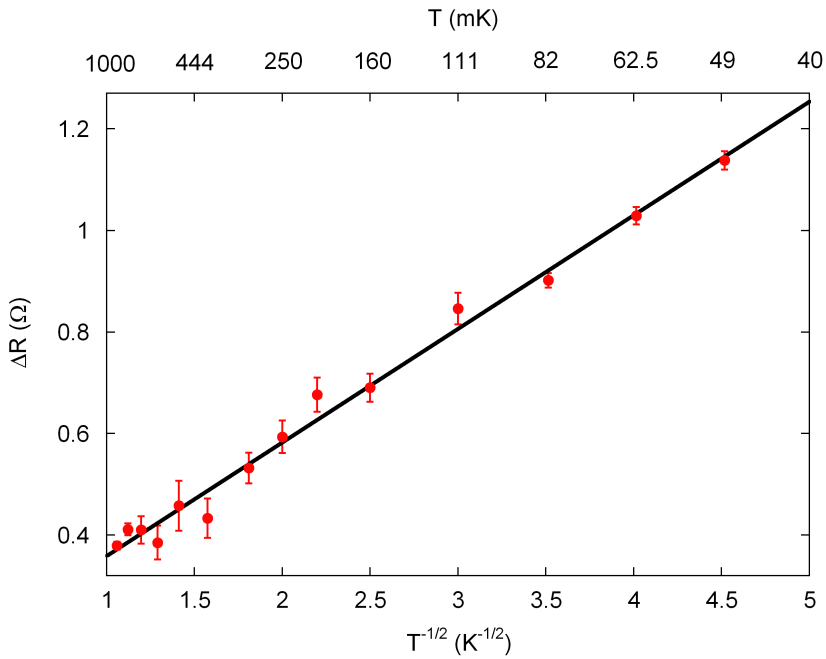

Figure 6.4: *Resistance variation in a pure Ag sample as a function of $T^{-1/2}$ in $K^{-1/2}$. Data points follow the expected power law. The slope of the solid line yields the value of λ_σ.*

The experimental data follow very well the expected power law. All the other parameters being known, the slope of the fitted line yields a value of $\lambda_\sigma \approx 3.1$ which is in excellent agreement with previous measurements [54, 76] in Ag[1].

[1]In reference [54], λ_σ is found to be the same for the unimplanted AgAg1 and the 30 ppm implanted AgAg3 samples. We can thus assume that the implantation does not affect λ_σ.

Let us go back to our spin glass sample AgMn 700 ppm. The low-temperature resistance variation is plotted on figure 6.5 in the same way as the previous Ag sample. One clearly sees the deviation between the experimental AgMn data and the theoretical electron-electron contribution, which is indicated by the solid green line.

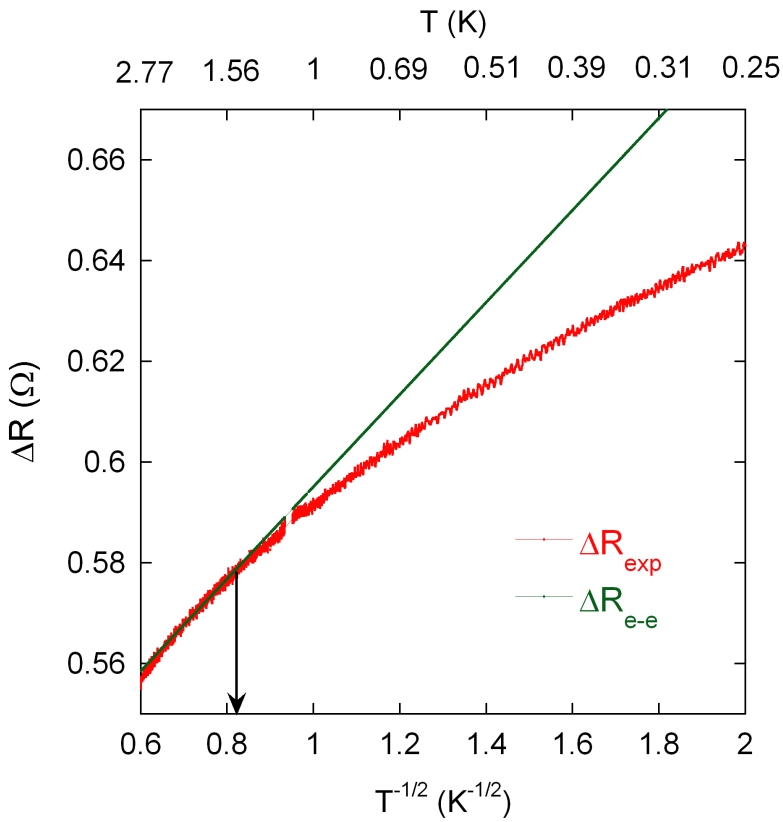

Figure 6.5: *Resistance variation in AgMn 700 ppm as a function of $T^{-1/2}$. The experimental data ΔR_{exp} (in red) deviate from the theoretical ΔR_{e-e} (in green) below a temperature $T \approx 1.5$ K.*

We observe a clear deviation between the AgMn data and the expected electron-electron contribution below a temperature $T \approx 1.5$ K. Therefore, this deviation is interpreted as a signature of the presence of magnetic impurities in the sample. At high temperature (above 1.5 K), the data follow well the theoretical electron-electron contribution ΔR_{e-e} (in green on figure 6.5). In order to extract the resistance contribution attributed to the influence of the magnetic spins ΔR_{SG}, we subtract the theoretical electron-electron contribution ΔR_{e-e} from the experimental data. The resulting temperature dependence $\Delta R_{SG}(T)$ is presented on figure 6.6.

The experimental spin glass contribution obtained is decreasing below a temperature $T_m \approx 2$ K. As the Kondo temperature of the alloy is very low ($T_g \gg T_K$), the interplay between Kondo and spin glass is unbalanced, the Kondo influence is negligible. Such a decrease in the resistance confirms a spin glass-like behavior of the AgMn wire and is consistent with previous bulk measurements [77, 78, 71].

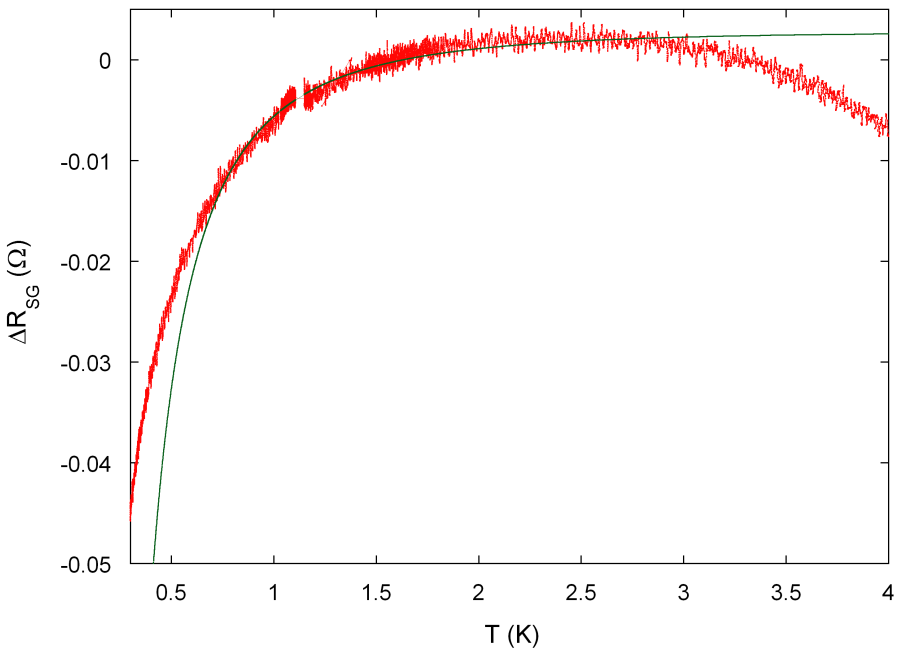

Figure 6.6: *Spin glass resistance contribution ΔR_{SG} extracted as described in the text, as a function of temperature. The experimental data are in red, and a fit to equation 6.2.4 with $T_g = 0.7$ K is shown in green.*

This interplay between Kondo effect and spin glass freezing has been theoretically studied by Vavilov *et al.* [73]. They propose an analytical description of the resistance in the regime $T_g \gg T_K$:

$$\Delta R_{SG}(T) = \frac{A}{\ln^2(T/T_K)}\left(1 - \alpha_S \frac{T_g}{T}\right) \tag{6.2.4}$$

where A is a numerical prefactor and α_S is taking into account the impurity spin S. For a spin $S = 5/2$ that is the case of Mn in Ag, $\alpha_S = 2.33$. The fitting of the data with this equation is shown on figure 6.6. For $T_K = 40$ mK fixed, the best agreement with the data is obtained for a prefactor value $A = 0.06$ and for $T_g \approx 0.7 \pm 0.1$ K. Below T_g, the theoretical calculation is not valid anymore. The data is very well described by the formula in the temperature range between T_g and T_m. Therefore, the experimental data show that $T_g \approx 0.7$ K in our AgMn wire, in agreement with what is usually observed for such alloys at this concentration.

6.2.2 Magnetic irreversibilities

Irreversibilities in the magnetic susceptibility

Spin glasses are sensitive to very small magnetic fields. In particular, a small field applied above T_g before cooling down strongly influences the low-temperature properties of the spin glass. Let us distinguish two cooling down protocols used for the measurement of the magnetic susceptibility χ:

- *Zero-field-cooled (ZFC):* The system is cooled down below T_g without applying a magnetic field. In the low temperature phase, a small field is applied to measure the susceptibility.
- *Field-cooled (FC):* The system is cooled down under a given weak magnetic field B. The susceptibility can be recorded at the same time.

Striking differences between the two protocols have been experimentally observed, as shown on figure 6.7.

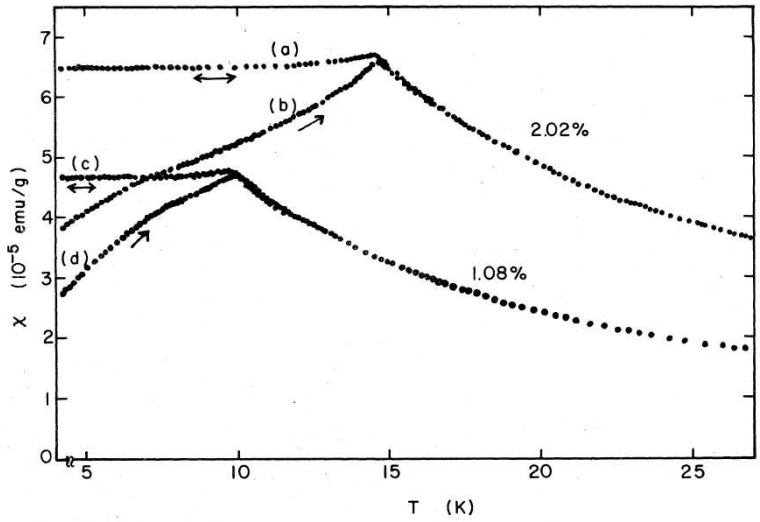

Figure 6.7: *Static susceptibility of CuMn vs temperature for* 1.08 *and* 2.02 *at.% Mn. Field-cooled [(a),(c)] and zero-field cooled ($H < 0.05$ G) [(b),(d)] measurements have been done in an external field $H = 5.9$ G. Extracted from [79].*

One observes a clear deviation between the field-cooled χ_{FC} and the zero-field-cooled χ_{ZFC} susceptibilities, appearing below T_g, and which is called magnetic irreversibility. Moreover, the FC curve is reversible, as shown with the double-arrow: the FC susceptibility is the same when going down or up in temperature. As a conclusion, the transition temperature T_g can also be defined by the onset of strong irreversibilities in quantities measured by a ZFC and a low-field FC protocols.

Experimental study of AgMn

As mentioned previously, there is no abrupt change of the resistivity ρ around T_g. Another signature linked to T_g is the appearance of magnetic irreversibilities, which can be detected by a direct comparison between FC and ZFC experiments. The idea is thus to look for these magnetic irreversibilities in the resistivity of our spin glass samples.

Using the same AgMn sample as previously, we record the resistivity variation $\Delta\rho$ as a function of temperature while cooling down from 900 mK to 200 mK. As a reference curve, we use the ZFC protocol, cooling down the sample without magnetic field. We repeat the procedure after applying above T_g a small magnetic field B_z kept constant during the cooling (FC protocol). The results of this experiment are presented on figure 6.8.

We have measured the resistivity variation for $B_z = 0$, $B_z = 5$, $B_z = 10$ and $B_z = 35$ G applied at $T = 900$ mK. While the curves are superimposed at high temperature, we observe small deviations between ZFC and FC curves at low temperature. As the deviation is very small, we have taken great care for the measurement. We have used a long integration time (50 s) so that the noise level is reduced to ≈ 120 pV (corresponding to 0.24 pΩ.m). Thus, the temperature ramp must be very slow, we have taken a cooling rate $\dot{T} = 5$ mK/min, that yields a measurement resolution of 20 mK. To make the curves comparable, it is very important that the cooling down procedures are strictly the same.

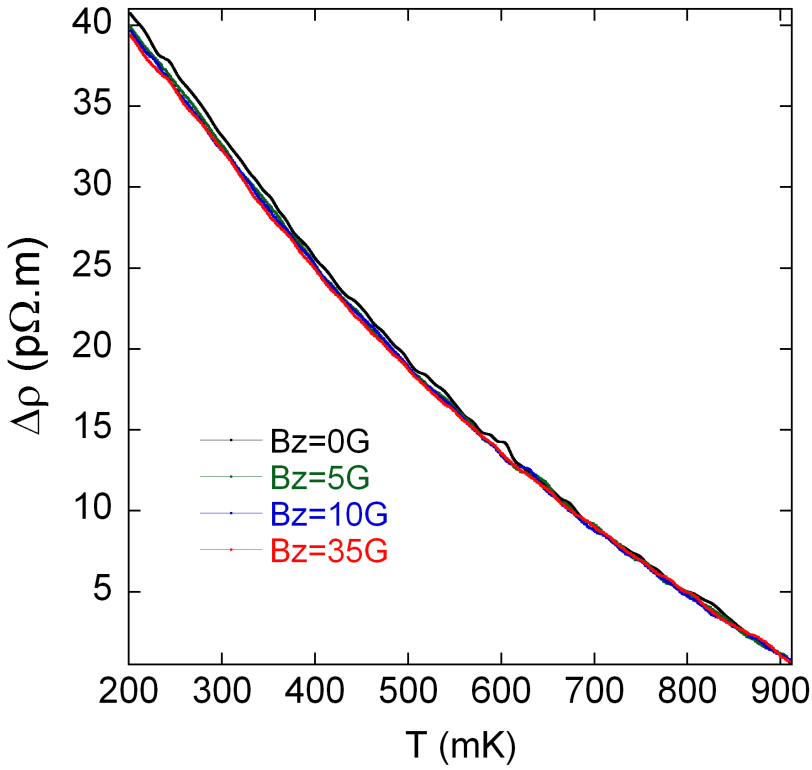

Figure 6.8: *Resistivity variation as a function of temperature from* 900 *to* 200 *mK under several fields* B_z*. Low fields of* $B_z = 5$*,* $B_z = 10$ *and* $B_z = 35$ *G applied above* $T = 0.9$ *K make the data deviating from the* $B_z = 0$ *G curve.*

The observed deviation is of the order of 1 pΩ.m at $T = 200$ mK. We have checked that the magnetoresistance of the sample cannot account for this deviation. First, the applied field is much smaller than the typical decorrelation field $B \ll B_c \approx 1000$ G, so that the effect cannot be attributed to quantum magnetoresistance (UCF or weak-localization). More precisely, we have measured the low temperature magnetoresistance at low fields: at $T = 300$ mK constant, we sweep slowly the field up to $B = 100$ G. The resistance does not change more than 0.075 pΩ.m in this field range. As a result, the observed deviations are more than one order of magnitude larger, and magnetoresistance contribution can be ruled out.

It is also important to characterize accurately the drift of the experiment. This has been quantified by repeating twice exactly the same cooling down experiment. We obtain two curves taken at different times $R(T, t_1)$ and $R(T, t_2)$. The difference between the two curves $\Delta R_{12} = R(T, t_1) - R(T, t_2)$ depends only on $R(t_2 - t_1)$ the drift of the experiment during one cooling procedure. The resulting data (not shown) displays a drift $\Delta \leq 0.11$ pΩ.m.

We have also estimated the drift directly by measuring the resistance as a function of time. Within the time of the cooling down procedure, we obtain a drift of $\Delta \leq 0.15$ pΩ.m in good agreement with the previous estimate. Therefore, the drift of the experiment is also one order of magnitude smaller than the measured deviations.

In order to highlight these irreversibilities, we subtract the ZFC reference data from the FC curve, as presented on figure 6.9. For each set of data (including the drift), we have averaged the experimental points in order to reduce the noise, so that the trend is clearly visible. The averaged drift is also shown for comparison.

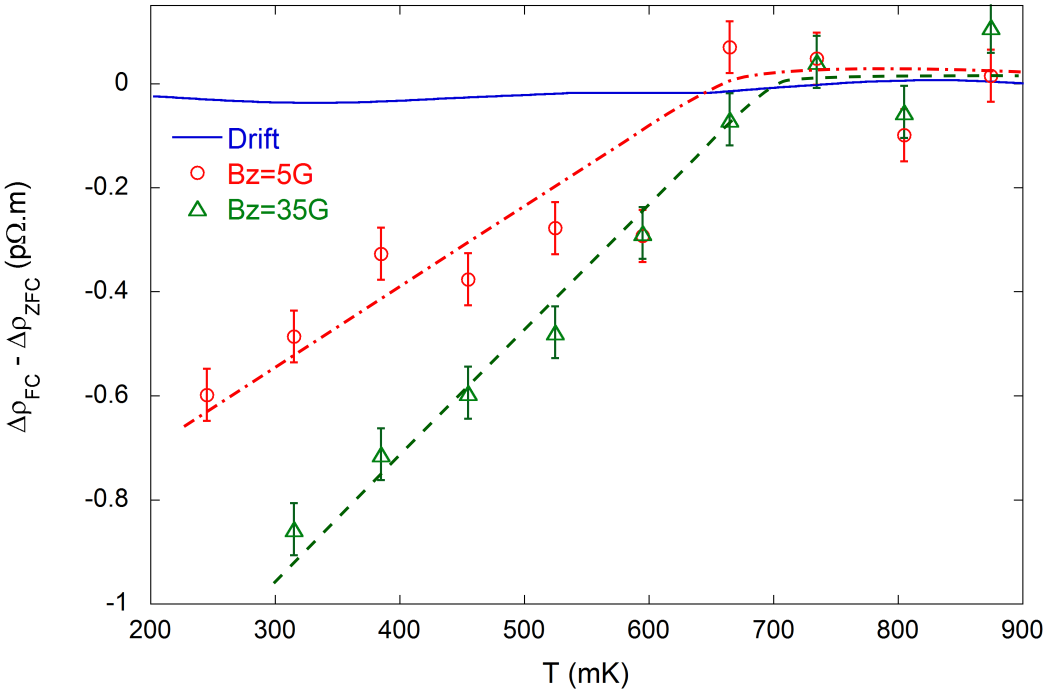

Figure 6.9: *Difference between FC and ZFC resistivity curves, as a function of temperature, for $B_z = 5$ G and $B_z = 35$ G. The drift is shown for comparison. The data have been averaged, and the curve $B_z = 10$ G has been removed for clarity. Dashed lines are a guide to the eye.*

Though the deviation is small, it becomes clearly visible below 670 mK. Note that the ZFC curve is not taken after application of the magnetic field *in* the spin glass phase, as usually done in magnetic susceptibility measurements. However, we have checked that the application of the field at low temperature does not change significantly $\Delta\rho_{ZFC}$, which indicate that the results should be the same. As the deviation is not attributed to magnetoresistance effects, we can assert that it is due to the magnetic response of the sample, similarly to what is observed for the magnetic susceptibility.

In addition, our data suggest that the amplitude of the effect depends on the applied field, which is consistent with recent measurements of the irreversibility in the magnetic susceptibility of spin glasses [80, 81]. We have also checked that the FC curve is reversible: the $\Delta\rho_{FC}(T)$ data follow closely the same trace when cooling down or when heating up. The important point is that the difference between FC and ZFC curves appears exactly at the transition temperature T_g which is in good agreement with the one determined independently from the temperature dependence of the resistance. We therefore conclude that we can determine $T_g \approx 670$ mK from the onset of irreversibilities in the resistivity of AgMn.

Conclusion

We have confirmed that our mesoscopic AgMn wire has a spin glass-like behavior in the temperature dependence of the resistance. From this measurement, we are also able to obtain an estimate of T_g which is consistent with previous bulk measurements. In addition, we have observed remanence, due to a small magnetic field, in the resistivity of our sample which appears below T_g. Consequently, this remanence effect and the temperature dependence of the spin glass resistance can be combined to determine T_g *directly* in a mesoscopic wire, for which magnetic susceptibility measurements are not possible.

La simplicité est la sophistication suprême.

Léonard de Vinci

Chapter 7
Universal conductance fluctuations in AgMn spin glass

As the phase coherence length L_Φ is limited by the inelastic processes, its measurement gives information on the underlying electron energy relaxation mechanisms. As an example, a low-temperature measurement yielding $L_\Phi \propto T^{-1/3}$ is characteristic of a quasi $1d$ system in which the electron-electron interaction is the main scattering mechanism. This is known as the AAK theory, as mentioned in chapter 5.

However, such a technique has been only poorly used in the study of magnetic systems. One reason is that the weak-localization correction is not an well adapted tool to extract L_Φ in magnetic systems[1]. Therefore we will evaluate L_Φ from Universal Conductance Fluctuations (UCF) measurements.

For such measurements, there are theoretical predictions concerning *paramagnetic* systems: when applying a magnetic field, the spins are polarized and it is predicted that the phase coherence length L_Φ increases [82, 83]. This behavior has been qualitatively observed in low concentration magnetic alloys: at large fields, the amplitude of Aharonov-Bohm oscillations or UCF increases, and this has been used as a test of the presence of magnetic impurities in a metal [84, 85, 86]. Very little is known in the case of spin glass samples.

In this chapter, we present the UCF measurements that we have performed in a AgMn:700 ppm spin glass wire. The phase coherence length in the system can be quantitatively extracted from the data. The resulting L_Φ is shown to be sensitive to the magnetic field.

7.1 Measurement of universal conductance fluctuations

We have measured the magnetoresistance of a AgMn:700 ppm wire shown on figure 7.1.

[1] In magnetic systems, time-reversal symmetry is broken and therefore time-reversed paths giving rise to weak-localization are destroyed.

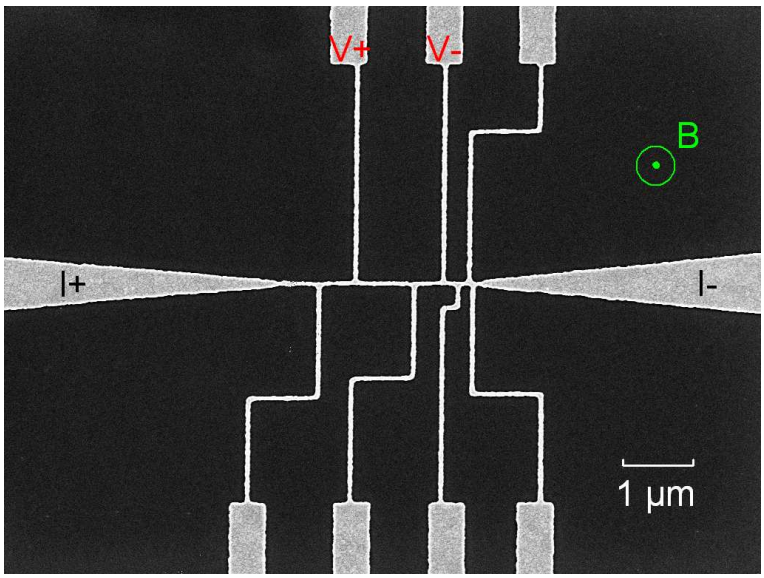

Figure 7.1: *Scanning electron microscope picture of the sample. The current is driven from $I+$ to $I-$, and the voltage measured between $V+$ and $V-$. Resistance fluctuations are recorded while sweeping the perpendicular magnetic field B_z.*

We probe a sample of length $L = 2$ μm, width $w = 50$ nm and thickness $t = 40$ nm. The perpendicular magnetic field B_z is swept from 0 to 8 T and the resistance fluctuations are recorded by using the experimental setup described in chapter 4, at several temperatures from $T = 60$ mK to $T = 1$ K. As an example, two typical curves are presented on figure 7.2.

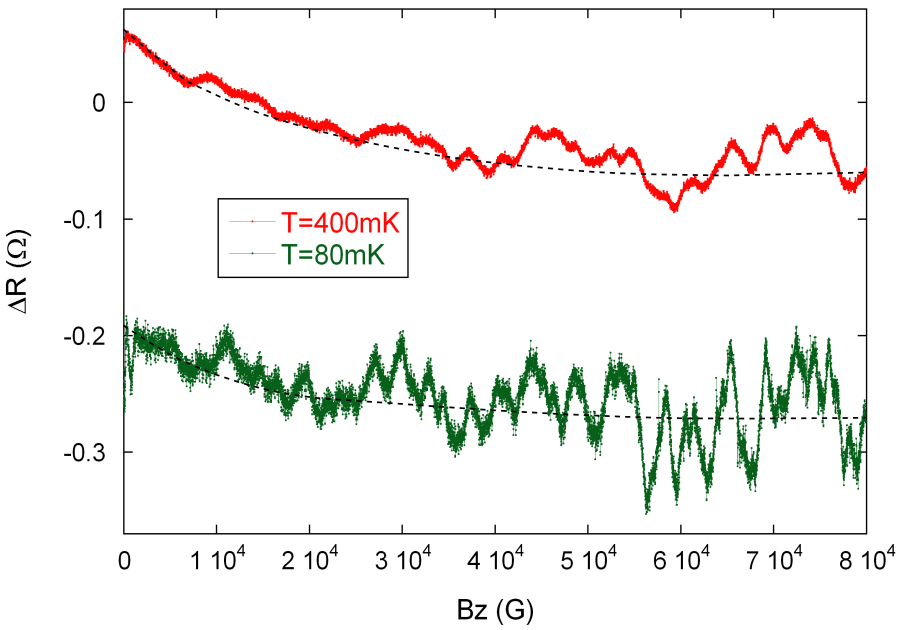

Figure 7.2: *Resistance variation of a AgMn:700 ppm wire as a function of the magnetic field from 0 to 8 T at high ($T = 400$ mK, red) and low ($T = 80$ mK, green) temperature. Dashed lines are a guide to the eye.*

The signal observed is composed of a classical magnetoresistance on which the universal conductance fluctuations are superimposed. Such a shape of the classical magnetoresistance

has been previously observed in similar experiments [45]. As it is not present in the pure Ag sample, we conclude that this is a feature of the spin glass phase. It may be attributed to a polarization of the magnetic spins with the field, which results in a decrease of the resistance and deserves further investigations. Note that for higher concentration alloys (and higher temperatures), a different magnetoresistance varying as B^2 has been reported [87].

To continue our study, we subtract this overall magnetoresistance to our data, so that only the universal resistance fluctuations are left, as presented on figure 7.3.

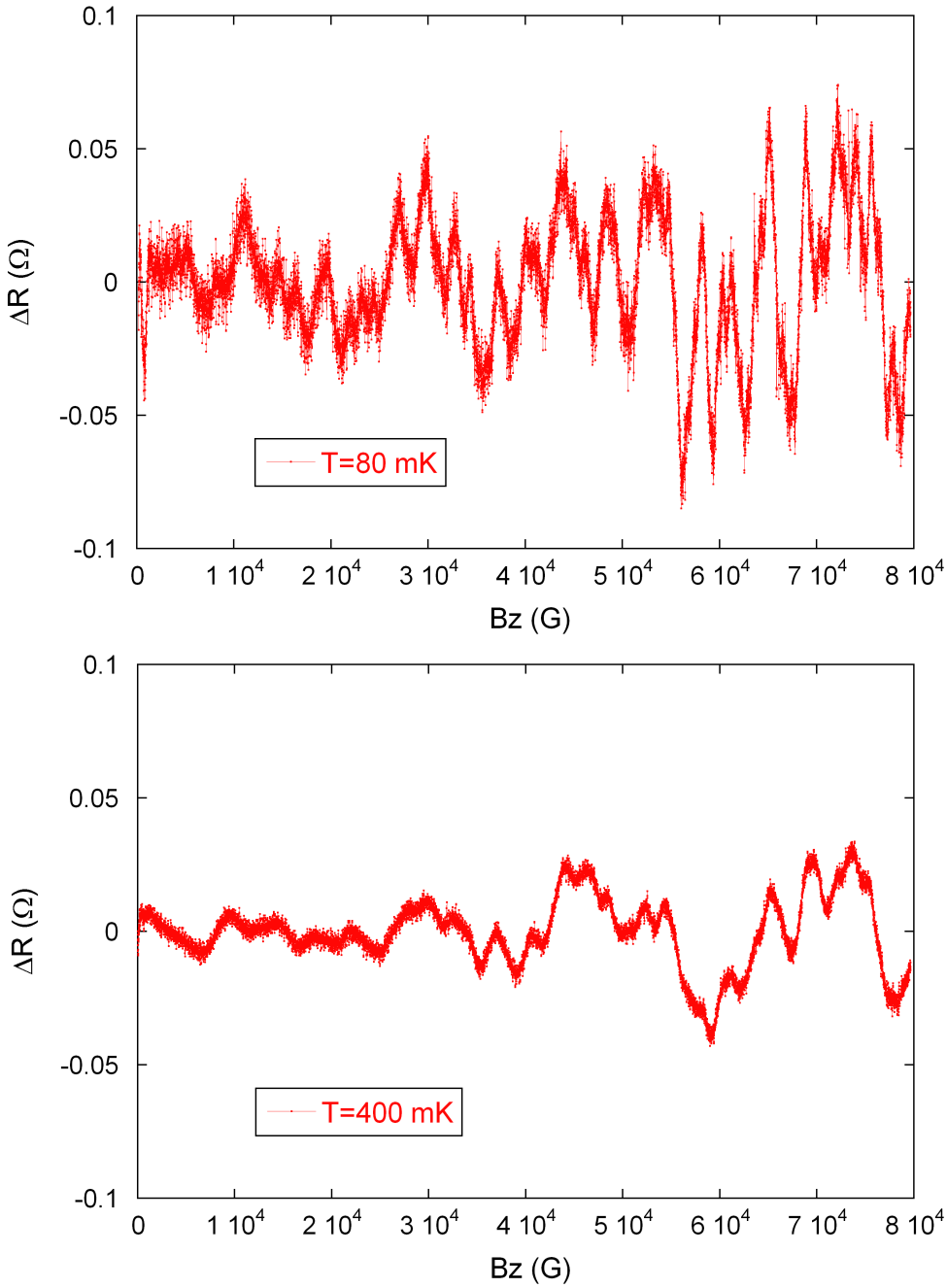

Figure 7.3: *Resistance fluctuations as a function of magnetic field B_z in a range between 0 and 8 T. Top: at $T = 80$ mK. Bottom: at $T = 400$ mK.*

7.2 Magnetic excitations

At all temperatures, we observe that the amplitude of the fluctuations ΔR enhances when increasing the magnetic field. As mentioned previously, this could be attributed to the presence of magnetic impurities being polarized by the magnetic field. Qualitatively, we observe two regimes for the amplitude of the fluctuations: a low-field regime $B_z < 4$ T and a high-field regime $B_z > 4$ T.

In order to characterize this enhancement with the magnetic field, we calculate the amplitude of the UCF averaged on a large interval (typically 2 T), and we slide this interval along B_z. We can thus compute the amplitude of the UCF as a function of the magnetic field, as presented on figure 7.4.

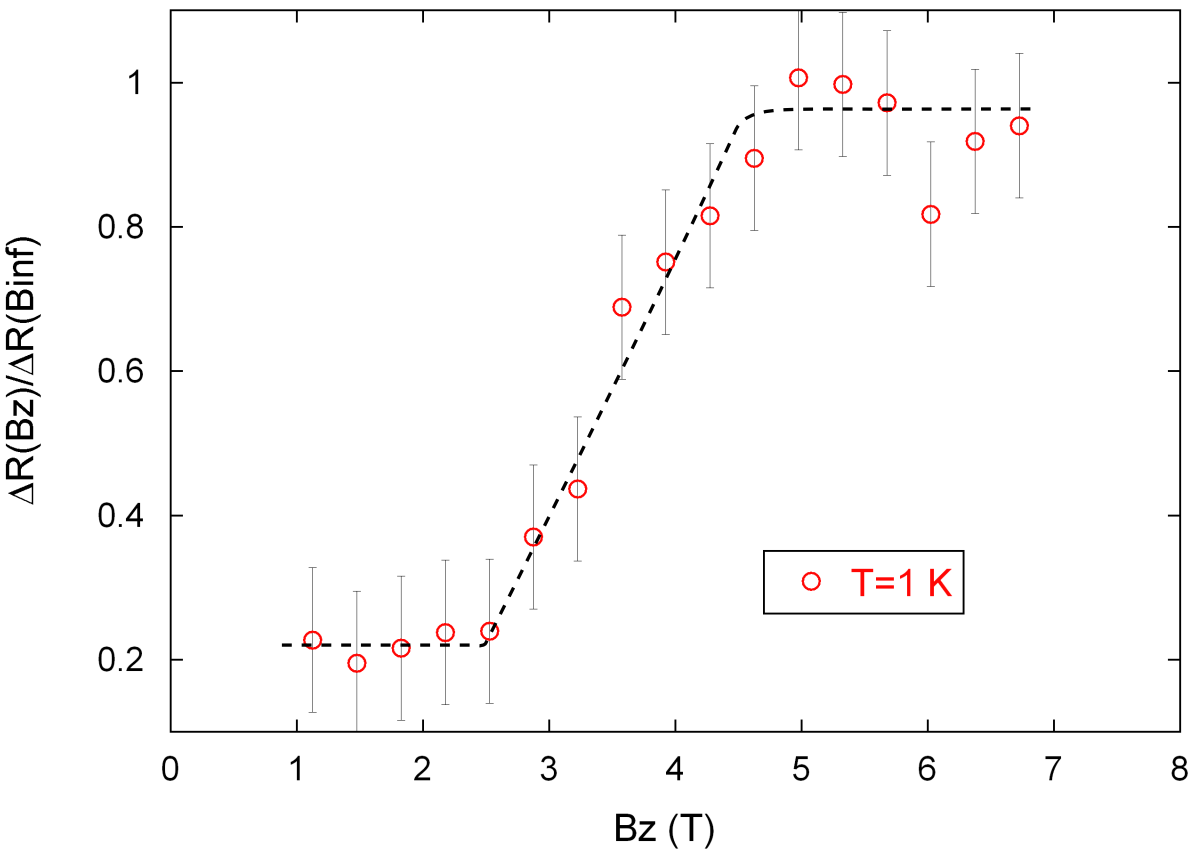

Figure 7.4: *Normalized averaged amplitude of the UCF as a function of the magnetic field at $T = 1$ K. The crossover field is about 4 T. The dashed line is a guide to the eye.*

Enhancement of L_Φ

This analysis confirms the two regimes for the amplitude of the UCF, with a crossover field around 4 T. Such an increase of the amplitude can be attributed to an enhancement of the phase coherence length $L_\Phi(B_z)$ in the sample. Qualitatively, when the magnetic field gets larger than 4 T, the sample evolves from a non-polarized situation to a regime where the spins are polarized. When scattering, the electrons can exchange energy with non-polarized spins, whereas polarized impurities act as static. The inelastic magnetic scattering degree of freedom is thus weakened

when a magnetic field $B_z > 4$ T is applied, and this leads to an enhancement of L_Φ. Such an experimental behavior is qualitatively in agreement with theoretical predictions [83].

We can estimate the value of the phase coherence length from the UCF amplitude ΔR (the procedure is described later in details). We obtain $L_\Phi(B_z < 4\ T) \approx 0.067\ \mu$m and $L_\Phi(B_z > 4\ T) \approx 1.65\ \mu$m at $T = 1$ K. The enhancement factor is about 25. Such a large factor is not surprising, as we have a quite large concentration of magnetic impurities ($c = 700\ ppm$) in the sample, which should lead to a high magnetic scattering rate.

Freezing magnetic excitations

At high temperatures $T > T_g$, we expect that the magnetic field is polarizing "free" magnetic impurities. However at low temperatures $T < T_g$, the sample is in a spin glass state. In this regime, we observe a similar enhancement of L_Φ, but in two steps. The averaged amplitude of the UCF as a function of magnetic field for the two temperature regimes is presented on figure 7.5.

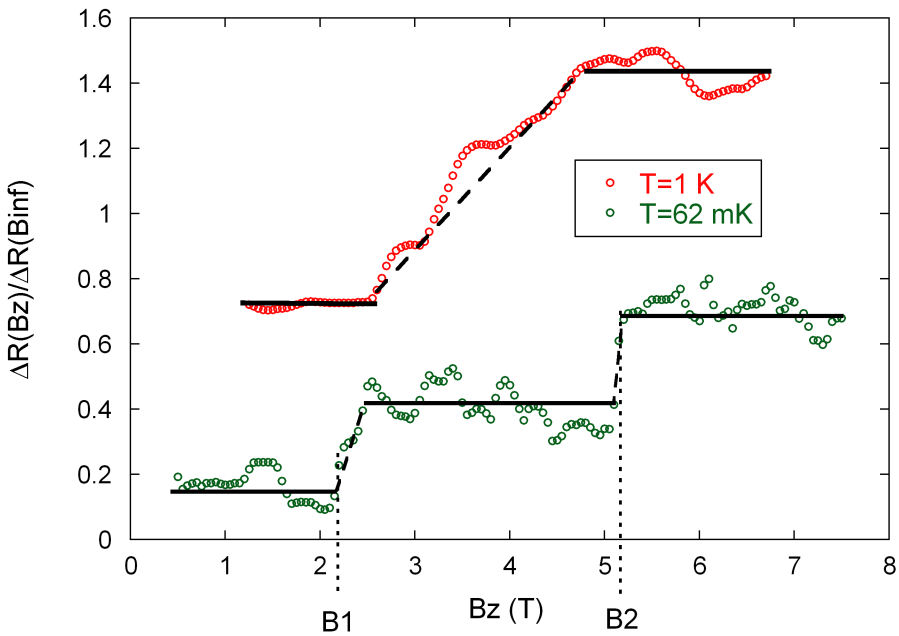

Figure 7.5: *Normalized averaged amplitude of the UCF as a function of the magnetic field at $T = 1$ K ($T > T_g$) and $T = 62$ mK ($T < T_g$). The high temperature curve shows two plateaus, whereas the low temperature curve shows three plateaus. The curves have been shifted for clarity. The field values B_1 (B_2) represent the end (beginning) of first (last) plateau.*

We observe an enhancement of L_Φ with the magnetic field even below T_g. This is still attributed to a weakening of the magnetic scattering with increasing magnetic field. However the shape of this enhancement suggests that some magnetic excitations of the spin glass sample are suppressed stepwise.

We notice that the typical field scale for which the amplitude increases is roughly the same at low and high temperatures. In order to investigate this in detail, we determine experimentally the field B_1 for which the amplitude starts to increase (end of first plateau), and the field B_2

for which it becomes constant again (beginning of last plateau), in all the temperature range. The results are presented on figure 7.6.

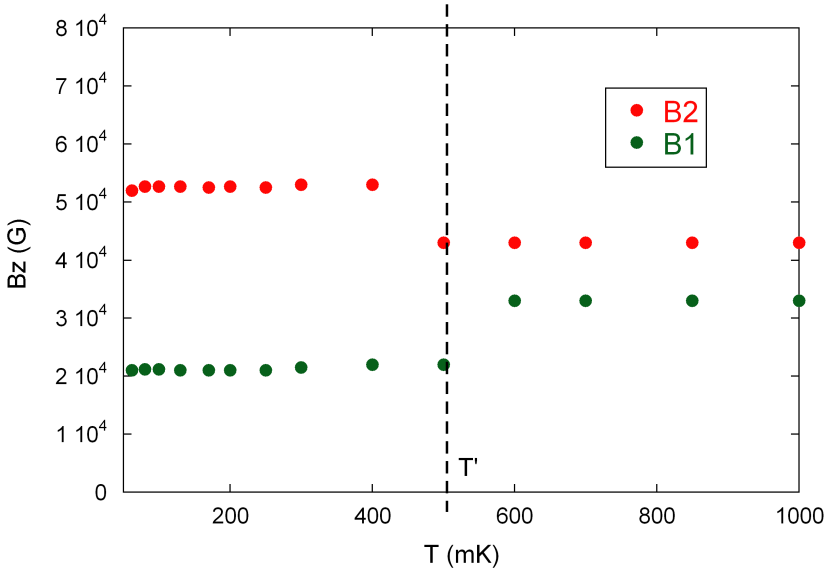

Figure 7.6: *Magnetic field values B_1 and B_2 determined as presented in the text, as a function of temperature. They are constant above and below a value T' for which they seem to join together.*

The two field values B_1 and B_2 obtained are roughly constant up to a temperature of $T' \approx 500$ mK. Above this temperature, the two values seem to merge. The low temperature UCF "plateau" between B_1 and B_2 observed in figure 7.5 disappears for $T > T'$. Above T', B_1 and B_2 delimit the region for which the UCF amplitude increases.

Note that the temperature T' for which the behavior changes is different than the characteristic temperature of the system $T_g \approx 700$ mK, though these temperatures are quite close. In addition, the order of magnitude of the field for which L_Φ increases $B_m \approx 4$ T is much larger than the typical spin glass field scale $B_g \approx 0.1$ T, defined as $g\mu B_g = k_B T_g$ with $g = 2$ the Landé factor, $\mu = 5\mu_B$ the magnetic moment of Mn in units of Bohr's magneton and k_B the Boltzmann constant.

In this experiment, the large value of B_m could be attributed to the rigidity of the spin glass phase to an external magnetic field. In CuMn alloys, such robustness can be attributed to random anisotropy [88], that affects the phase diagram of spin glasses [89]. In AgMn alloys, we can expect the same type of anisotropy, that could prevent the spins from fully rotating in the presence of a magnetic field.

As a conclusion, we can use the field-dependence of phase coherence length as a tool to study unexpected magnetic features of the sample. The observed behavior in our spin glass AgMn sample may be attributed to magnetic excitations (droplets, spin waves...), or an intermediate phase of the system... It leads to questions on the effect of a magnetic field in spin glasses that clearly deserve further investigations.

7.3 Temperature dependence of the phase coherence length

We now turn to the analysis of the temperature-dependence of the phase coherence length in the AgMn sample. From the above study, we define two distinct regimes for the behavior of the UCF amplitude: the low-field regime for $B < B_1 < 2$ T and the high-field regime for $B > B_2 > 6$ T. We extract the average amplitude of the UCF in the two regimes, at all temperatures. The resulting data are presented on figure 7.7.

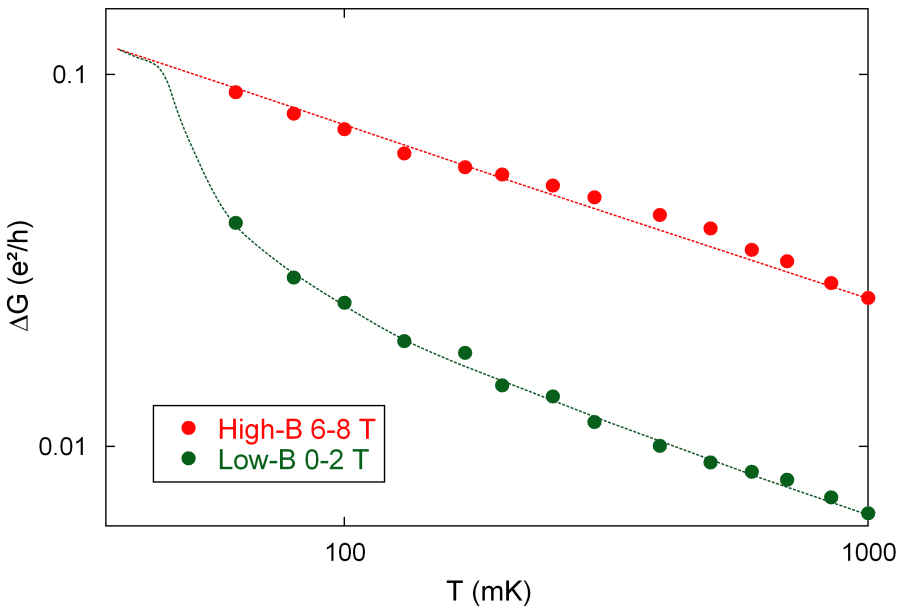

Figure 7.7: *Amplitude of the UCF as a function of temperature, in the low-field (green) and high-field (red) intervals. The two curves seem to join together at low temperatures (dashed lines are a guide to the eye).*

The enhancement of the UCF amplitude with the magnetic field is clearly visible at all temperatures. In the high-field regime, we may consider that the spins are polarized, and that the resulting UCF amplitude reaches the value one should obtain in presence of static magnetic impurities. At low field, we observe that the UCF amplitude increases faster with decreasing temperature than the high-field data. In order to highlight this effect, we calculate the ratio $r = \Delta R(low\ B)/\Delta R(high\ B)$ as a function of temperature, as presented on figure 7.8.

Above $T' \approx 400$ mK, the ratio is roughly constant, the UCF amplitude has the same temperature dependence at low and high field. However below T', the amplitude of the UCF at low field is increasing towards the amplitude of the high-field regime ($r \to 1$). Indeed, this is a signature of the freezing of the magnetic moments in the spin glass phase: as temperature decreases, spins are freezing, becoming similar to static impurities for the electrons. In this experiment, with respect to L_Φ, the effect of reducing the temperature is thus equivalent to the effect of applying a large magnetic field. As a result, the fluctuations amplitude at low field tends towards the high-field value representing a full freezing of the spins.

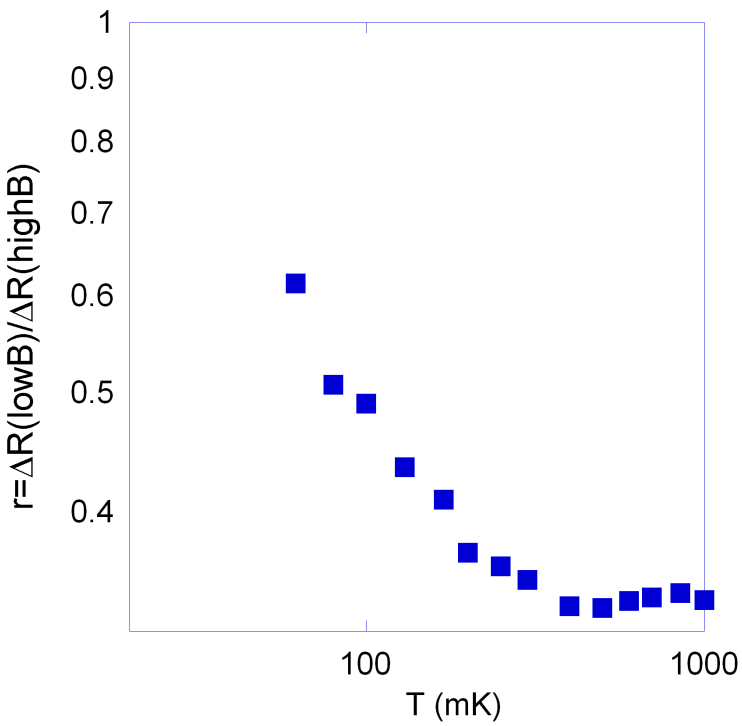

Figure 7.8: *Ratio r of the amplitudes at high and low field as a function of temperature. Above $T' \approx 400$ mK, the ratio is constant. Below this temperature, it increases.*

High-field behavior

In the high-field regime, L_Φ is greatly enhanced (a factor 25). In this situation, $L \leq L_\Phi$ and the amplitude of the UCF is only weakly depending on L_Φ. Therefore, we cannot extract precisely the phase coherence length in this regime.

Extraction of the phase coherence length

In our spin glass, we write the phase coherence scattering rate as the sum of the inelastic scattering rates mechanisms at low temperature[2] (below 1 K)

$$\frac{1}{L_\Phi^2} = \frac{1}{L_s^2} + \frac{1}{L_{e-e}^2} \tag{7.3.1}$$

where L_s designates the inelastic magnetic scattering, and L_{e-e} the electron-electron scattering. The electron-electron term is well known as it is given by the AAK [66] theory. In clean metals this scattering mechanism is dominant at low temperature (see chapter 5). In a spin glass however, we expect that the magnetic scattering prevails, so that the phase coherence length is essentially limited by $L_\Phi = L_s$ (as $L_s \ll L_{e-e}$). At larger fields, due to the polarization of the impurities, the magnetic scattering length increases, and the phase coherence length is thought to be dominated by the residual electron-electron interaction $L_\Phi(B \to \infty) = L_{e-e}$ [83]. The resulting phase coherence length at low field is presented as a function of temperature on figure 7.9.

[2]Below 1 K, the electron-phonons interaction term is negligible.

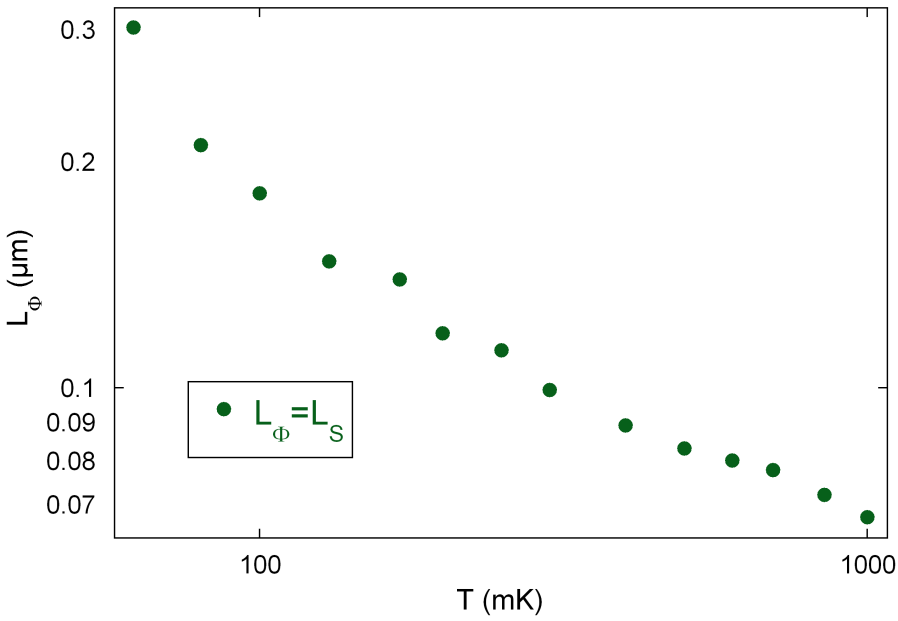

Figure 7.9: *$L_\Phi = L_s$ as a function of temperature extracted from the amplitude of the low-field UCF.*

The phase coherence length in the sample is quite short: it ranges from 67 nm at $T = 1$ K to 300 nm at $T = 62$ mK. Such a low absolute value of L_Φ can be attributed to the strong magnetic scattering off the spins (the spin concentration in the sample is $c \approx 700$ ppm). When decreasing the temperature, L_Φ is increasing rapidly, which may be interpreted as a consequence of the spins freezing.

Determination of the free spins population

From this measurement, we can extract the magnetic scattering time $\tau_s = L_s^2/D$ with $D = 42$ cm^2/s the diffusion coefficient determined from the resistivity of the sample. The measurement of this scattering time temperature-dependence may give an insight on how the spins are frozen in the sample. In the following, we propose an interpretation that leads to a determination of the concentration of free spins in the spin glass phase.

We consider that the magnetic scattering is governed by an energy exchange between an electron and a free spin impurity, like in the case of the Kondo effect. In this case, the resulting τ_s is directly proportional to the density of magnetic scatterers involved $n_{imp}(T)$. This is theoretically described by the Nagaoka-Suhl formula [90] in the regime $T \geq T_K$, T_K being the Kondo temperature ($T_K = 40$ mK in our alloy).

$$\frac{\hbar}{\tau_s(T)} = \frac{n_{imp}(T)}{\pi \nu_F} \frac{\pi^2 S(S+1)}{\pi^2 S(S+1) + \ln^2 (T/T_K)} \tag{7.3.2}$$

where ν_F is the Fermi density of states, S the spin of the impurity and $n_{imp}(T)$ the density of magnetic impurities participating to the inelastic scattering. As temperature decreases, spins are progressively frozen, and we can consider that the free spins population is reduced.

The above equation can be rewritten in order to allow the determination of the concentration of scattering impurities as a function of temperature

$$c_{imp}(T) = \frac{\tau_\Phi^K}{\tau_s(T)} \frac{\pi^2 S(S+1) + \ln^2(T/T_K)}{\pi^2 S(S+1)} \tag{7.3.3}$$

with $\tau_\Phi^K = 0.58$ ns.ppm the maximum Kondo scattering in Ag (as measured in reference [91]). Therefore we obtain the temperature dependence of c_{imp} presented on figure 7.10.

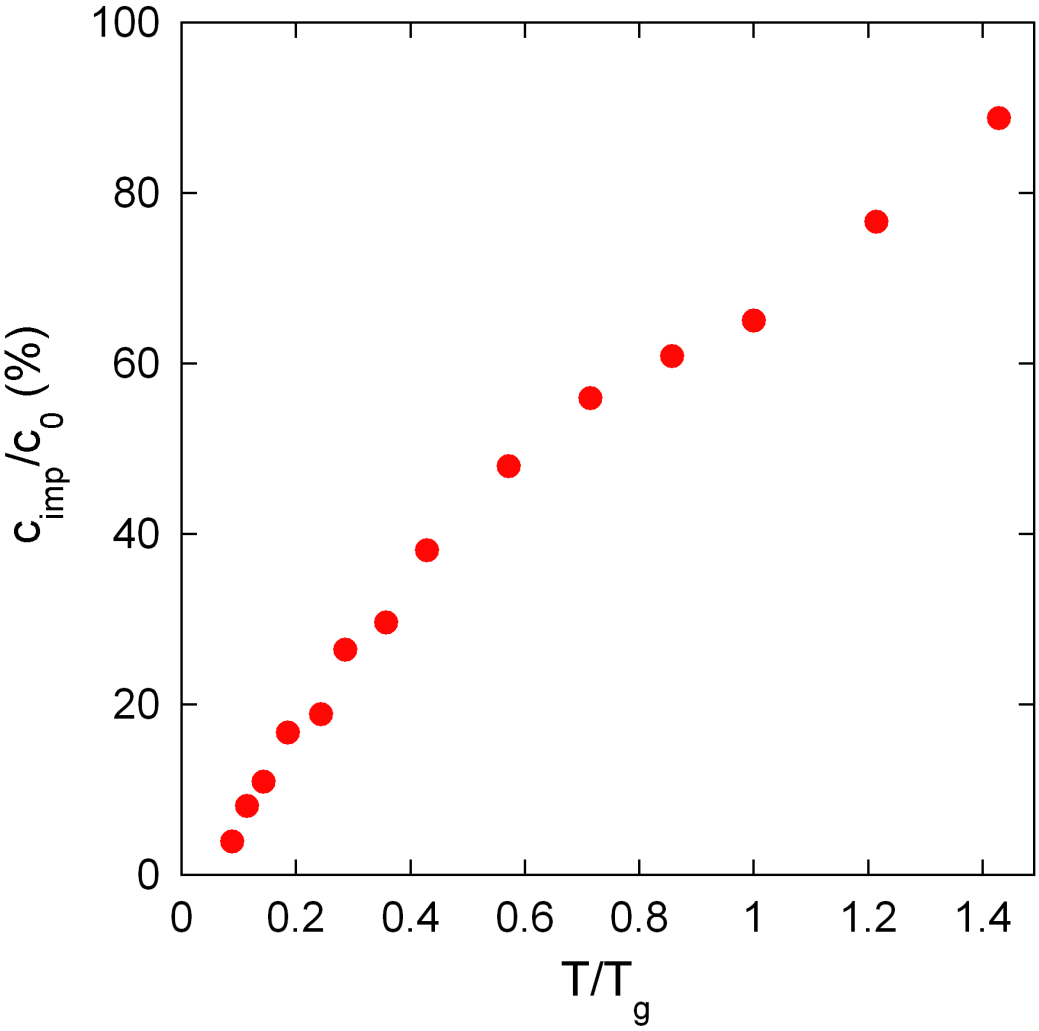

Figure 7.10: *"Free" spin impurities concentration as a function of temperature. The concentration is normalized to the nominal concentration of impurities $c_0 = 700$ ppm, and the temperature is normalized to the spin glass temperature $T_g = 700$ mK.*

We clearly see the freezing of the magnetic impurities in the spin glass phase: the free spins population decreases as the temperature is reduced. In our AgMn:700 ppm alloy, we find about 27 ppm, *i.e.* $c/c_0 = 4\%$ of free spins at the lowest temperature ($T/T_g = 0.09$). At $T = 1$ K, the free spins population increases up to $c/c_0 = 89\%$. Such mesoscopic measurements may provide a unique access to the freezing of the spins as a function of temperature. And the experimental data may thus be compared with theoretical models. In particular, the temperature-dependence of the free spins population should be linked to the temperature-dependence of the internal fields

distribution in the sample. This distribution can give an insight in the underlying interaction mechanisms (short-range or mean-field).

Conclusion

Using UCF, we have performed measurements of the phase coherence length L_Φ in a AgMn:700 ppm spin glass wire. We observe that L_Φ strongly increases with the magnetic field, in agreement with previous works. At low temperature, this enhancement is still present but becomes stepwise. This feature could be attributed to intermediate magnetic excitations of the system, that disappear above a temperature close to T_g. In addition, we are able to extract quantitatively L_Φ from the low-field part of the UCF. We interpret the observed increase of L_Φ as a freezing of the magnetic spins when temperature is reduced. We propose that the L_Φ measured may provide a unique tool to probe the population of free spins in a spin glass.

L'homme le plus simple qui a de la passion persuade mieux que le plus éloquent qui n'en a point.

François de La Rochefoucauld,
Maximes

Chapter 8
Measurement of the magnetofingerprints correlations

We present in this chapter measurements of the correlations between magnetofingerprints obtained in AgMn spin glasses. We studied the sensitivity of the UCF to the spin configuration, and the influence of magnetic field and temperature on this configuration.

8.1 Scaling effects: the route to overlaps

In this section, we consider the question of the sensitivity of our technique to a change in the *spin* configuration of the spin glass. As presented in chapter 3, the correlation coefficient C and the spin overlap q are linked together by a known function of L/L_m, L being the length of the sample and L_m the magnetic length. Indeed, the correlation will be affected by a variation of q only if L/L_m is large: the phase difference between paths encountering a different spin configuration increases with the number of magnetic scattering events. Therefore, we have to test the sensitivity of our technique on *long* wires.

We have thus performed an experimental comparison between pure Ag and AgMn wires. On the one hand, we measure the magnetofingerprints in a pure Ag sample at low temperature. We first take a reference curve, representative of the (non magnetic) disorder configuration, and then we heat up the sample to about 15 K for 15 hours. The sample is heated by using an additional current, as described in chapter 5. We cool down the sample back to the measurement temperature, and we record a second magnetofingerprint. As shown on figure 8.1, the two traces remain highly correlated: the correlation coefficient $C = 0.95$, meaning that we do not modify the disorder (positions of atoms or defects) in the Ag sample. On the other hand, we repeat the same experiment in a long wire ($L \approx 17$ μm) of AgMn spin glass of concentration $c = 400$ ppm ($T_g \approx 400$ mK). We heat up to 15 K (≈ 37 T_g) for 20 min. The two traces obtained before and after the thermal cycle (shown on figure 8.1) are visibly different, the resulting correlation coefficient is $C \approx 0.2$.

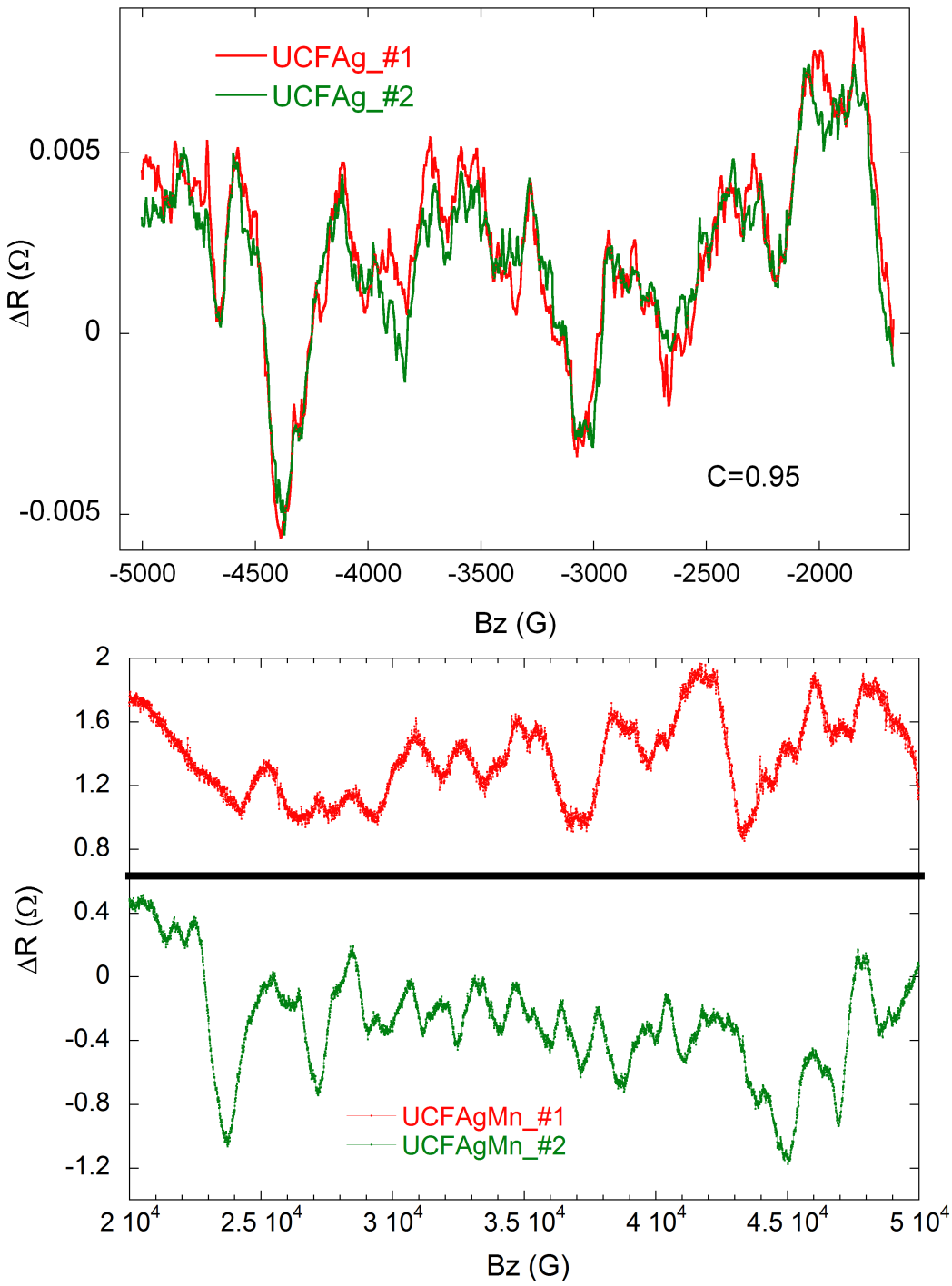

Figure 8.1: *Comparison of the magnetofingerprints obtained before and after a thermal cycle at high temperature. Top: in the Ag sample, the traces remain highly correlated* $C = 0.95$. *Bottom: in the spin glass sample AgMn:400 ppm* ($L \approx 17$ μm), *the fingerprints are visibly different, the correlation is* $C \approx 0.2$.

As a result, the experiment on pure Ag proves that the position of the atoms did not change during the thermal cycle. For the AgMn sample, in strong contrast, the magnetofingerprints clearly change, as the spin configuration has been modified - the orientation of the spins, not their position - at high temperature. This clearly shows that the universal conductance fluctuations are sensitive to the reorganization of the spin configuration.

8.2 Field effects: spin glass rigidity?

An unexpected field robustness

The effect of an external magnetic field on the spin glass phase remains quite beyond a complete understanding. In particular, the pioneering measurements of magnetofingerprints in spin glasses have revealed an unexpected robustness against magnetic field: the magnetofingerprint was not modified, even by applying a magnetic field much larger than the typical spin glass field scale B_g [45], as if the spins were not affected. On the contrary, we have observed in our experimental magnetofingerprints indications that the spins may be polarized by the magnetic field, as discussed in chapter 7. In this section, we investigate the effect of a magnetic field on the spin configuration in spin glass wires.

In the usual view of spin glasses, one expects that a magnetic field larger than B_g should destroy the ordered phase. B_g is defined by $k_B T_g = g\mu B_g$ with k_B the Boltzmann constant, g the Landé factor, and μ the magnetic moment, expressed in units of the Bohr magneton μ_B. In our low concentration alloys, $T_g = 700$ mK leads to $B_g \approx 1000$ G (using $g = 2$ for the electrons and $\mu = 5\ \mu_B$ for Mn).

We have measured magnetofingerprints on a AgMn sample of length $L \approx 17\ \mu$m and concentration $c = 400$ ppm ($T_g \approx 400$ mK). The field is swept from $B_z = 0$ to $B_z = 8$ T, that is 80 times larger than B_g, at a temperature $T = 100$ mK and we repeat the measurement, so that we obtain two magnetofingerprints which are shown on figure 8.2.

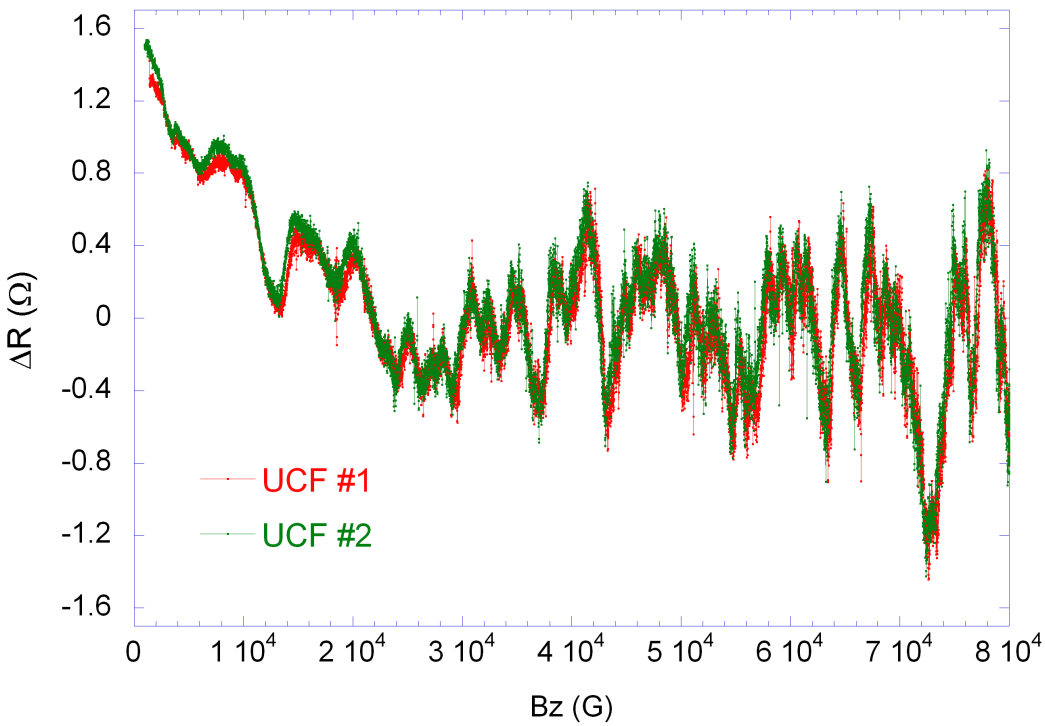

Figure 8.2: *Resistance fluctuations as a function of the magnetic field for a AgMn:400 ppm wire ($L \approx 17\ \mu m$). Two successive traces are shown, separated by a time scale of few hours. Though the system has been brought to a very high field, the trace is highly reproducible.*

The two successive traces are highly reproducible ($C = 0.94$), though in the time between, we have applied a magnetic field much larger than B_g. This high correlation of the UCF may

lead to the conclusion that *the spin configuration does not change even under high magnetic field.* This is very surprising, as it contradicts the usual vision of spin glasses.

Decorrelation of the magnetofingerprints

From the high correlation coefficient, we can estimate that less than 1 % of the spins are rotated by the magnetic field. However, in our signal of figure 8.2, we observe the enhancement of the fluctuations with magnetic field, which is a convincing signature of a polarization effect on the magnetic impurities, as already discussed in chapter 7. Therefore these contradictory results deserve further investigations.

In order to understand more in details the effect of the external magnetic field, we use an additional in-plane field ($X-Y$ field B_{xy}). The perpendicular field B_z is still used to obtain the magnetofingerprints, but under several constant values for B_{xy}. We measure the UCF traces at low temperatures, deep into the spin glass phase $T \ll T_g$, so that the dynamics of the system appear frozen on the time scale of the experiment (which is confirmed by the reproducibility of the curves). We measure successively three magnetofingerprints. We first take a reference magnetofingerprint of the spin configuration, without additional field $B_{xy} = 0$ T. Then, we apply a parallel magnetic field of $B_{xy} = 1$ T, and take the second magnetofingerprint. We switch the parallel field back to $B_{xy} = 0$ T before taking the third trace. Results of this experiment are presented on figure 8.3.

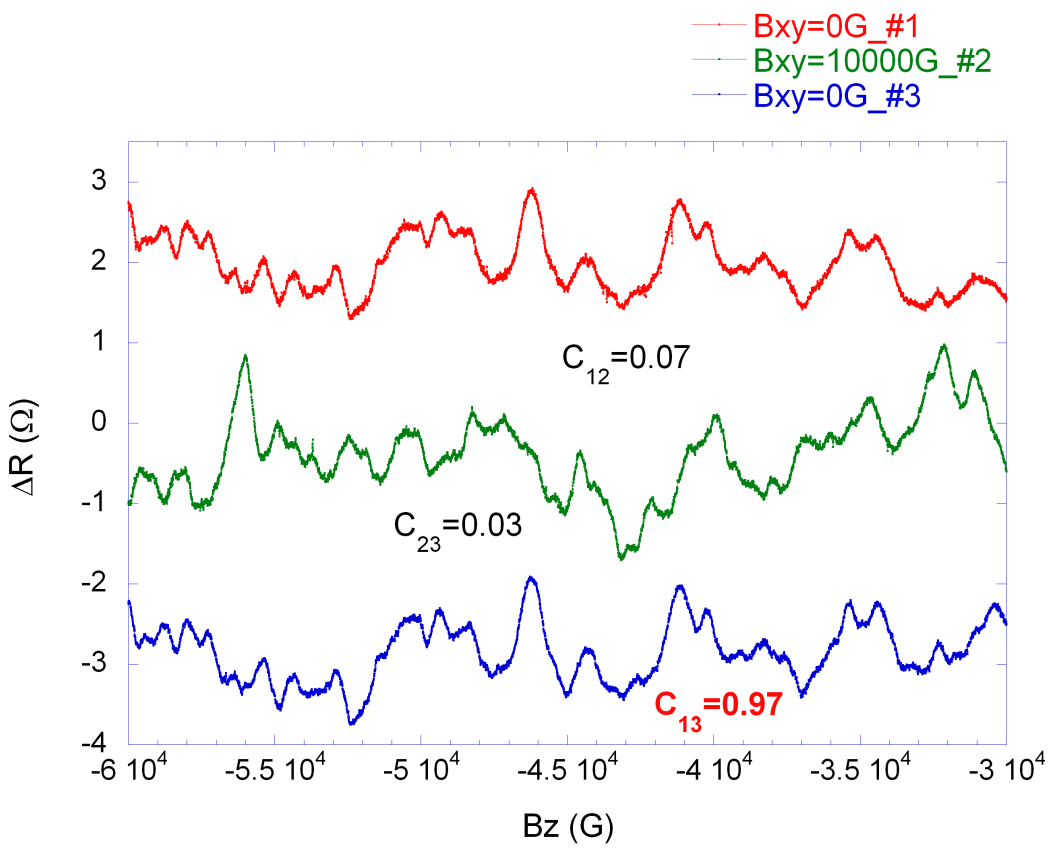

Figure 8.3: *Three successive magnetofingerprints of the spin configuration, taken for different values of the in-plane field B_{xy}. The first trace #1 and the third trace #3 are taken at $B_{xy} = 0$ G whereas the second trace #2 is taken at $B_{xy} = 10000$ G. The correlation between traces is indicated.*

When we apply a large additional magnetic field, the magnetofingerprint is visibly strongly affected: the correlation between traces #1 and #2 gives $C_{12} = 0.07$. The same correlation is found between traces #2 and #3, therefore the parallel field changes significantly the magnetofingerprint. Surprisingly however, we recover exactly the original magnetofingerprint when we switch back the field: the correlation between traces #1 and #3 is $C_{13} = 0.97$. From these data, we could infer that the magnetic field deforms the spin configuration in a *reversible* way.

The effect of the external magnetic field on the magnetofingerprints may have two distinct origins. On the one hand, the parallel magnetic field B_{xy} dephases the electron trajectories as well as B_z, and thus affects the magnetofingerprints. This orbital effect is perfectly reversible. On the other hand, the magnetic field may polarize the spins, which would also affect the magnetofingerprints. In spin glasses, it is theoretically predicted that the UCF are governed by these two effects, and thus by *two field scales* [41]. The first one B_c is attributed to orbital effects, due to the coupling of the electrons to the magnetic flux. The second B_s is the characteristic field scale attributed to the electron scattering off magnetic spins, and is only present in magnetic systems. Consequently, we should have the two effects on our magnetofingerprints.

In order to distinguish which effect is dominant, we investigate the temperature dependence of the typical field scale for the decorrelation of the experimental magnetofingerprints. For orbital effects, the field scale B_c depends on L_Φ, and should thus vary with temperature. For spin effects, we suggest that the field scale B_s is linked to a spin glass feature, and may be independent of T.

We thus repeated the previous experiment, for various values of B_{xy} in a AgMn:700 ppm alloy ($L \approx 17$ μm). We performed two sets of measurements, at $T = 65$ mK and $T = 400$ mK. From these data, we calculated the correlation between the reference magnetofingerprint at $B_{xy} = 0$ G and a given trace taken at B_{xy}. The results are presented on figure 8.4.

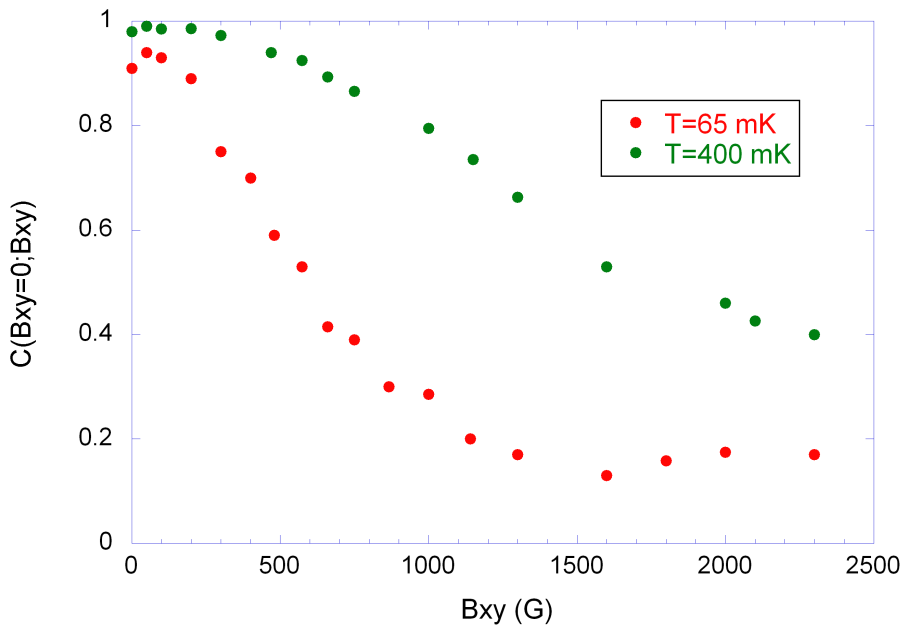

Figure 8.4: *Correlation coefficient $C(B_{xy} = 0; B_{xy})$ in a AgMn:700 ppm alloy ($L \approx 17$ μm), as a function of B_{xy}, for two different temperatures $T = 65$ mK (green) and $T = 400$ mK (red).*

The field scale of the decorrelation is clearly changing with the temperature. The values can be estimated by reading B_{cxy} when $C(B_{xy} = 0; B_{cxy}) = 0.5$. We obtain $B_{cxy}(T = 65\ mK) \approx$ 618 G and $B_{cxy}(T = 400\ mK) \approx$ 1600 G. For comparison, we have performed the same experiment in a non magnetic Ag wire, and the decorrelation field is also depending on temperature in a similar way. As a conclusion, when sweeping the parallel magnetic field, orbital effects prevail on the spin effects ($B_c < B_s$) in our AgMn wire, and the observed reversibility of the magnetofingerprints is attributed to orbital effects.

Discussion and prospects

In order to circumvent the previous issue, we propose to separate out the orbital and magnetic contributions to the UCF. This can be achieved using the Onsager symmetries, as described in chapter 2. One measures the magnetofingerprints in two configurations, between which one has permuted the $I-V$ current-voltage contacts. One can thus construct a quantity which is only depending on the magnetic part of the UCF

$$\Delta R_M = \frac{\Delta R_{IV}(B) - \Delta R_{VI}(-B)}{2} \tag{8.2.1}$$

In principle, this magnetic contribution should directly reflect spin effects in the sample. Note that in order to perform this construction, we have two requirements to fulfill. First, L_Φ has to be larger than L, so that we perform a real four-probe measurement. Second, $L_m \ll L$ is necessary to obtain a good sensitivity of the magnetofingerprints to the spin configurations. As a conclusion, we experimentally need a system where $L_m \ll L < L_\Phi$. As L_m depends on the exchange coupling J, or the impurity concentration, it may eventually be tuned in future experiments, in order to allow for a direct extraction of ΔR_M. Measuring this magnetic component may bring new insight on the influence of a magnetic field, and in particular the physics lying behind the observed robustness upon field cycling.

How can we interpret this robustness with the magnetic field? Let us discuss the field-temperature (mean-field) phase diagram of our spin glass. In AgMn alloys, the presence of random anisotropy should affect this phase diagram [92, 89]. In particular, it enhances the field value required to destroy the spin glass order. Theoretical calculations thus give a critical field which is about 5 B_g at low temperature ($T \leq 0.1T_g$), that is a field about 1 T in our samples.

Experimentally, one usually measures the irreversibility line, that is the line below which the response of the system is different between Field-cooled (FC) and Zero-field-cooled (ZFC) protocols. One thus finds a field line which very rapidly increases in the vicinity of T_g [93, 94] for CuMn and AgMn systems.

Our experiment brings new important information. We observe an increase in the amplitude of the conductance fluctuations as a function of magnetic field, which is a consequence of the polarization of the spins. It suggests that the spin configuration *is affected*: spins are "unlocked", they are not frozen anymore. This polarization starts at a field about $B_1 \simeq 2$ T (see chapter 7).

In addition, our experiment reveals that the spin configuration has not changed after a field cycle at 8 T. The field effect thus appears as reversible; when applying a magnetic field, the system evolves in the phase space along a certain path, and when we decrease the magnetic field, the system evolves back on the same path, so that it comes back to its original state. Such a behavior would imply some memory features in spin glass systems, directly at the microscopic level: each spin evolves back to its original orientation.

As a conclusion, we may infer that we have two different field scales in our system. A field $B > B_1 \simeq 2$ T is sufficient to "unlock" the spins at low temperature, and to start to polarize them. However, a field of 8 T is not strong enough to affect the spin configuration *in an irreversible way*: the system keeps the memory of its original zero-field state, at a microscopic level.

8.3 Temperature effects: a determination of the overlaps?

A natural and simple way to change spin configurations in a spin glass is to cycle the sample to temperatures above T_g.

The sample is heated and quenched by using a DC current as described in chapter 5. Figure 8.5 shows the calibration experimentally obtained for a long wire of AgMn:700 ppm. It allows to convert reliably the heating current I in an effective temperature T for the sample.

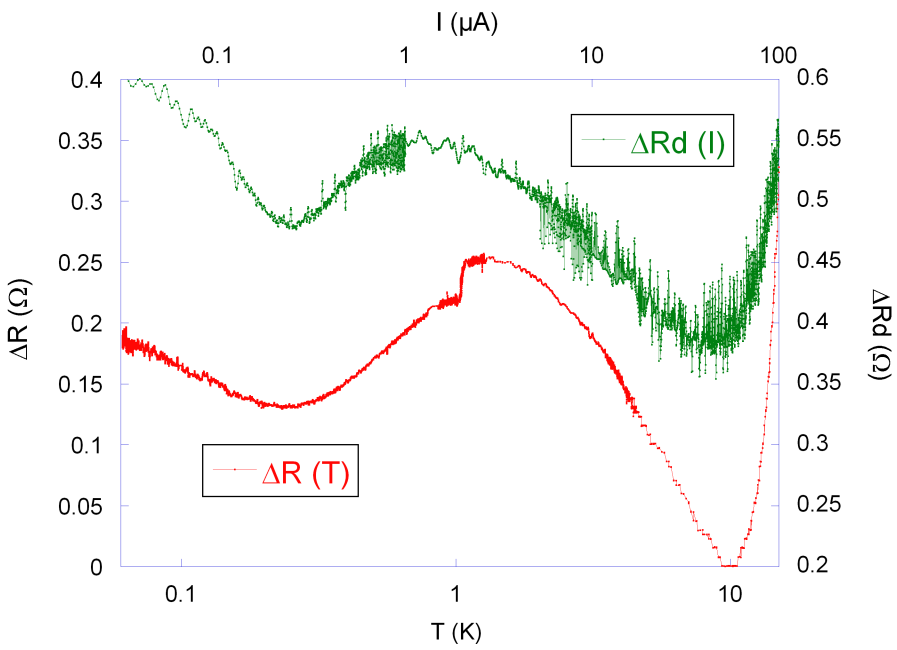

Figure 8.5: *Measurement of the resistance variations $\Delta R(T)$ and $\Delta R_d(I)$. Bottom axis: log scale of T in K. Top axis: log scale of I in μA. The resistance variations are plotted on the same scale and have been shifted for clarity. The two curves show a good agreement, and allow for a determination of T for a given I applied.*

We describe here the protocol that we have used to study the effect of temperature on the spin configurations. All the magnetofingerprints are taken at the same low temperature $T_{meas} = 50$ mK, so that the dynamics is frozen on the time scale of the measurement[1]. From low temperature, we apply a current I_0 in order to heat the sample at a temperature T_0 during a time τ. The system is then quenched down to $T_{meas} < T_g$, the measurement temperature. This thermal cycle can eventually be realized in the presence of a magnetic field B_0. At low temperature, we measure the magnetofingerprint of the spin configuration (n). We can repeat this annealing, quench, measurement procedure in order to obtain the magnetofingerprint $(n+1)$. This protocol is sketched on figure 8.6.

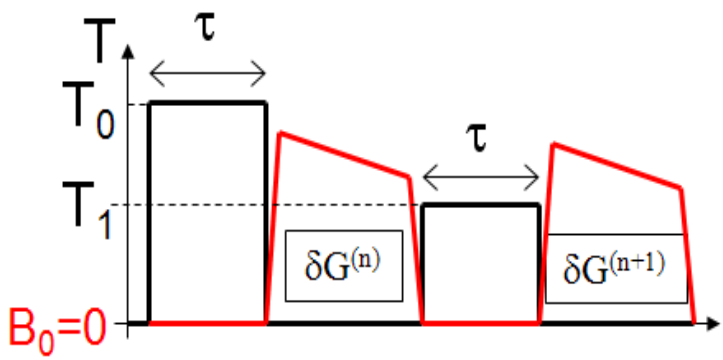

Figure 8.6: *The temperature of the system is raised to T_0 for a time τ at zero magnetic field. The system is then quenched, and the magnetofingerprint is taken. The operation can be repeated, so that we can compare the successive magnetofingerprints. This protocol can be performed for different values of T_0, τ or B_0.*

We have performed this experiment in a long AgMn:400 ppm wire ($L \approx 17$ μm). We expect that the evolution of the spin configuration at high temperature depends on: the annealing temperature T_0, the time τ spent, and the magnetic field B_0. Different magnetofingerprints obtained after an annealing of the sample at $T_0 \gg T_g$ are presented on figure 8.7.

We observe that within this protocol the magnetofingerprints evolve towards a different trace, that is in an *irreversible* way. This behavior is contrasting with the influence of the magnetic field which modifies reversibly the spin configuration. Such an evolution of the traces can be characterized by calculating the correlation $C_{n,n+1}$ between successive magnetofingerprints, as a function of the intermediate annealing temperature T_0. The results, obtained for $\tau = 5$ min and $B_0 = 0$ fixed, are shown on figure 8.8.

We observe that the experimental correlation between magnetofingerprints decreases very slowly with T_0, and remains quite large ($C > 0.5$). Surprinsingly, it appears that the sample has to be heated to temperatures $T_0 \gg T_g$ in order to obtain weakly correlated traces.

[1]We have checked that at such temperatures, the magnetofingerprint is not changing, up to several days.

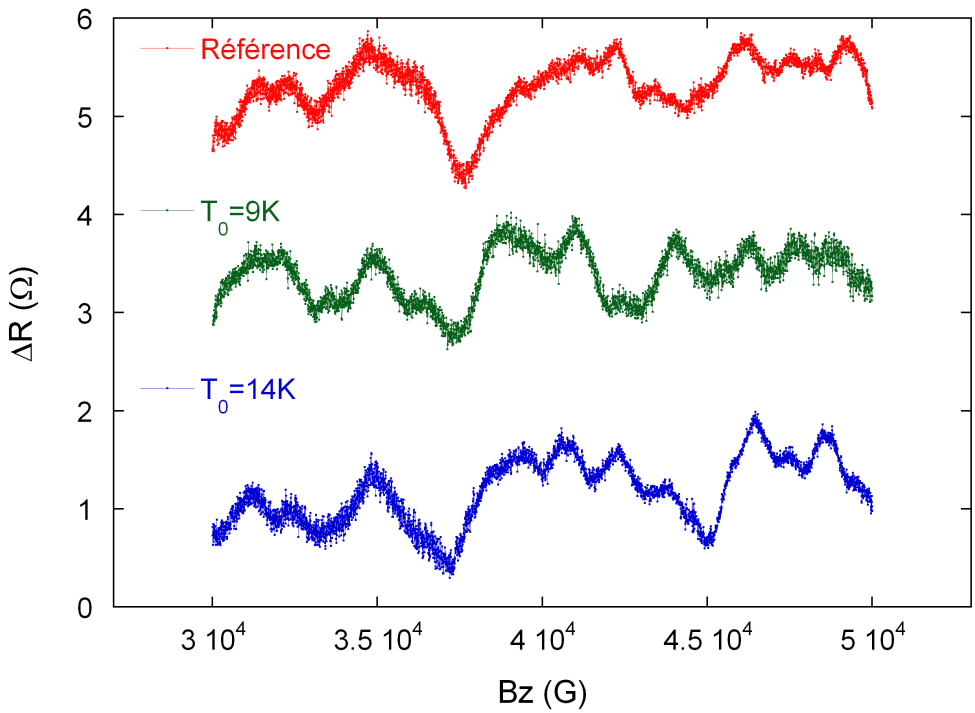

Figure 8.7: *Resistance fluctuations as a function of magnetic field for a AgMn:400 ppm alloy ($L \approx 17\ \mu m$). A reference magnetofingerprint (red curve) is taken. The sample is then annealed at $T_0 = 9\ K$, and the magnetofingerprint is measured (blue curve). The sample is annealed again at $T_0 = 14\ K$, and the magnetofingerprint obtained (green curve). The three traces have been shifted for clarity.*

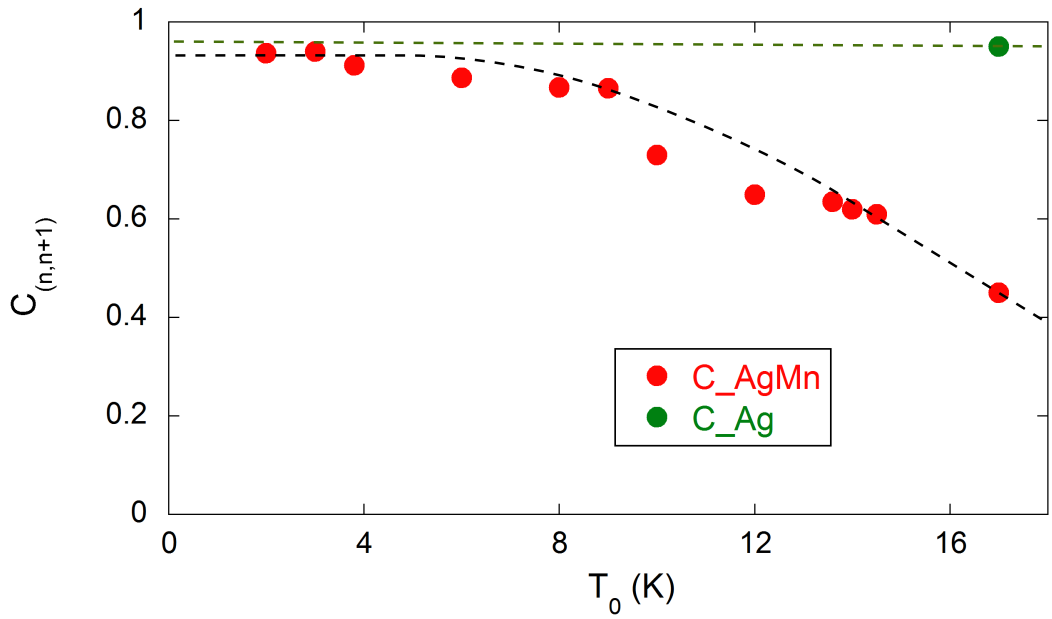

Figure 8.8: *Correlation coefficient of successive magnetofingerprints $C_{n,n+1}$, as a function of the annealing temperature T_0. This correlation is decaying slowly as T_0 increases. For comparison, the green point represents the correlation in the pure Ag sample. The dashed lines are a guide to the eye.*

At this point, it is crucial to ask about the sensitivity of our technique. We have presented in chapter 3 the theoretical link that has been established between the correlation coefficient

C_{12} and the spin overlap q_{12}. C_{12} is obtained experimentally from the magnetofingerprints, and q_{12} represents the overlap between spin configurations. The relation $C_{12}(q_{12})$ strongly depends on the ratio L/L_m. In particular, the correlation at zero overlap $q_{12} = 0$ is not zero, and may indeed be quite large, depending on the value of L/L_m. This dependence of $C(q = 0)$ as a function of the ratio L/L_m is presented on figure 8.9 (top).

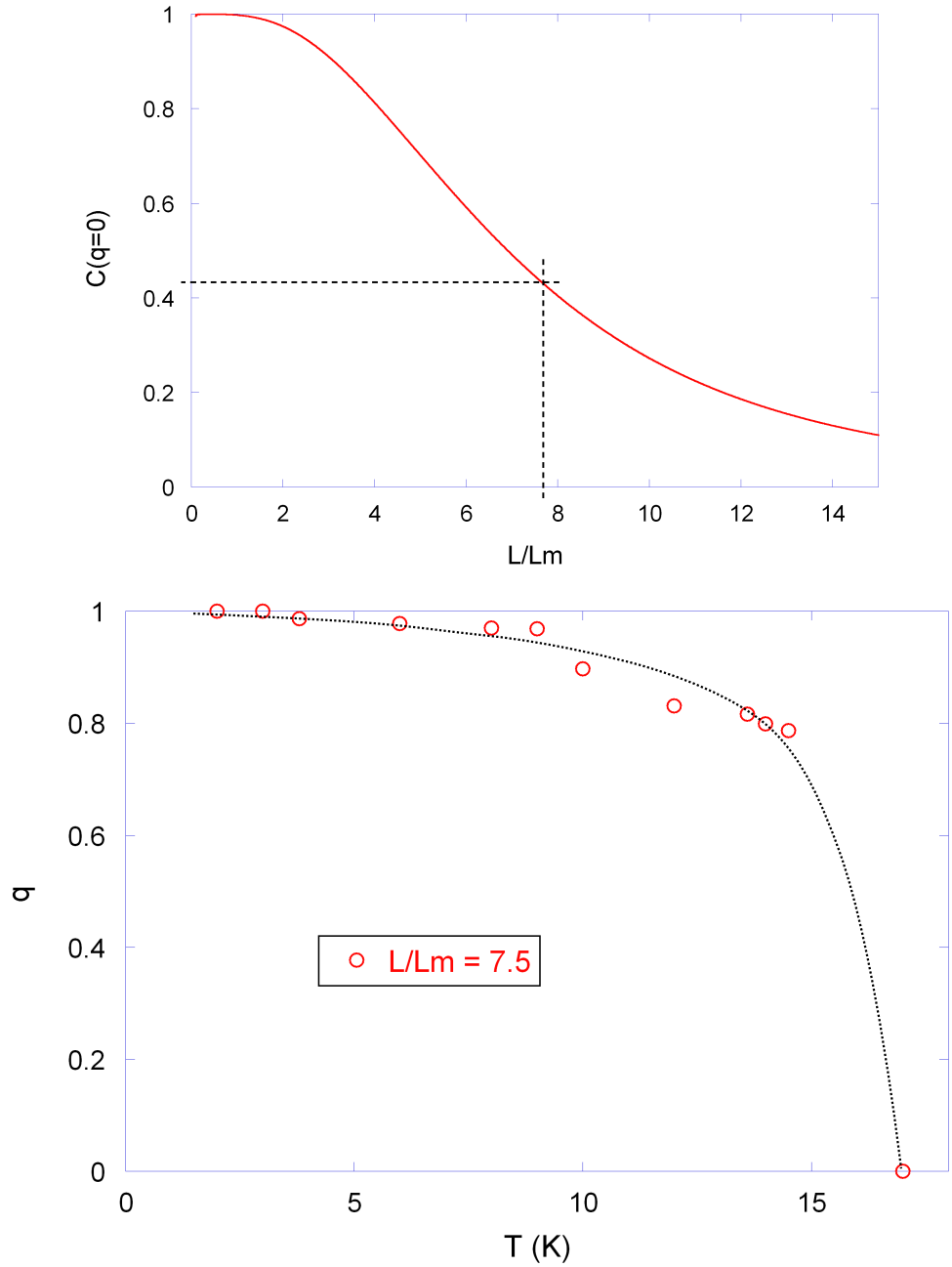

Figure 8.9: *Top: theoretical correlation coefficient at zero overlap $C(q = 0)$ as a function of L/L_m. The minimum experimental decorrelation $C = 0.42$ allows to determine a ratio $L/L_m = 7.5$. Bottom: the spin overlap q extracted from the experimental data using $L/L_m = 7.5$, as a function of T_0 the annealing temperature. The dashed line is a guide to the eye.*

We have thus tried to extract the spin overlap q from the measured correlation C at each temperature T_0. We can roughly estimate the ratio L/L_m by considering the lowest correlation found experimentally $C \approx 0.42$, that we identify as the minimum correlation, that is when all

the spins have rotated ($q = 0$). The curve plotted in figure 8.9 allows to graphically determine L/L_m, assuming that in our case $C(q = 0) = 0.42$. Consequently, we can directly convert the experimental data $C(T_0)$ in $q(T_0)$, which is presented on figure 8.9 (bottom).

The resulting decay of $q(T_0)$ is very sharp, and surprisingly the temperature for which it mainly decreases is much larger than T_g. This suggests that one needs to heat the sample up to very high temperature in order to obtain a low spin overlap. It is worthy to discuss the extraction procedure, which depends crucially on L/L_m. In order to determine this ratio more precisely, one can try to anneal the sample at larger T_0, looking for a saturation of the correlation C. Such saturation would give the base line $C(q = 0)$ for the experiment. From this line, it is thus possible to extract univocally L/L_m. A cross check experiment would be to measure C at a constant value of T_0 (that is a constant q) and as a function of the length L. The scaling function obtained may be compared to theoretical predictions, leaving L_m as a fitting parameter. These experiments may be performed in future works.

From the experimental findings, it remains that the temperature needed to appreciably change the correlation is much larger than T_g. From figure 8.9, we can infer that 80% of the spins need an annealing temperature of $T_0 \approx 15$ K to rotate. This suggests that we may have *another characteristic energy scale* in the system, which governs the "unlocking" of the spin configuration at the microscopic level. For example, it could be attributed to dynamical effects: in our experiment we observe the spins that relax on a time shorter than τ, the annealing time. This surprising result clearly deserve further investigations.

In this experiment, we have used the correlation between disorder magnetofingerprints as a new tool to trace back the spin overlap. Such a direct determination of $q(T)$ allows in principle to distinguish a low-temperature spin glass phase $q = 1$ from a high-temperature paramagnetic phase $q = 0$. It is thus possible to repeat this experiment in the presence of a magnetic field B_0, in order to probe the field-temperature phase diagram of the sample. Using this protocol, one can also investigate the dynamics of the system by varying the annealing time τ. Therefore, such a measurement of the spin overlap q opens a new way to probe the spin glass phase *at the microscopic level.*

Conclusion

In this chapter, we have measured the correlations between experimental magnetofingerprints in a AgMn wire. Using this original tool, we can investigate microscopically the effect of a magnetic field on the spin glass phase. We observe that the magnetofingerprints are deformed in a reversible way by the magnetic field. By measuring the correlations between magnetofingerprints as a function of temperature, we are able to measure the spin overlap $q(T)$. This opens the possibility to study directly the statistical distribution of the order parameter $P(q)$, which is the fundamental quantity characterizing the ground state of spin glasses.

Conclusion

In this work, we have implemented measurements of universal conductance fluctuations in spin glasses. The idea that such mesoscopic phenomena allow to trace back reorganizations in the microscopic disorder has been experimentally validated in a quantitative way. This new and original approach gives access to a direct measurement of fundamental parameters of spin glasses which were not accessible up to now.

We have fabricated mesoscopic spin glass samples in which the electronic phase coherence length is sufficiently large to allow for the measurement of quantum conductance fluctuations. We have developed a strategy of local heating which allows to achieve fast thermal cycling of our sample.

Resistivity measurements in our mesoscopic sample show the usual signatures of a spin glass phase. In addition, our resistivity measurement reveals remanence, appearing below the transition temperature T_g. Such a measurement can be used to determine T_g directly in a mesoscopic wire where usual magnetic susceptibility measurements are not possible, due to their small volume.

The amplitude of universal conductance fluctuations is sensitive to the inelastic scattering of the electrons in the sample, thus allowing for the study of the internal excitations of our spin glass. We have observed the freezing of some excitations of the system in the presence of an external magnetic field. Moreover, this type of measurement gives a new access to important quantities: the determination of the electron phase coherence length in the spin glass may be linked to the population of free spins. This opens new prospects for the study of these systems at a microscopic level.

Universal conductance fluctuations give a magnetofingerprint of the sample disorder. We have studied the correlations between different configurations, in order to extract direct information on how the disorder evolves in the spin glass. We have studied modifications of the magnetic configuration due to an external parameter. If we apply a magnetic field, the magnetofingerprints seem to be modified in a reversible way. However, when we cycle the sample above T_g, the magnetofingerprints are irreversibly affected. From the measurement of the correlation between magnetofingerprints, we can directly extract q, the order parameter of the spin glass phase.

This work opens new ways to numerous prospects on the experimental study of spin glasses using quantum conductance fluctuations. In particular, these measurements allow to access to the order parameter q of the transition. By repeating the experiment under different experimental conditions, we can obtain the statistical distribution $P(q)$ of this parameter, which is the fundamental quantity characterizing the ground state of spin glasses. It is also possible to study the field-temperature phase diagram or the relaxation time in spin glasses directly from

a microscopic point of view. We would like to point out that this experimental approach is not restricted to the study of metals, it can be performed in semi-conducting systems as well. Though we cannot conclude yet between the two main models describing spin glasses, there is a real hope that such measurements of the universal conductance fluctuations may bring important new insights on the nature of the ground state of spin glasses.

Appendix A
Wiring of the fridge

In this appendix, we present the detailed wiring of the dilution fridge.

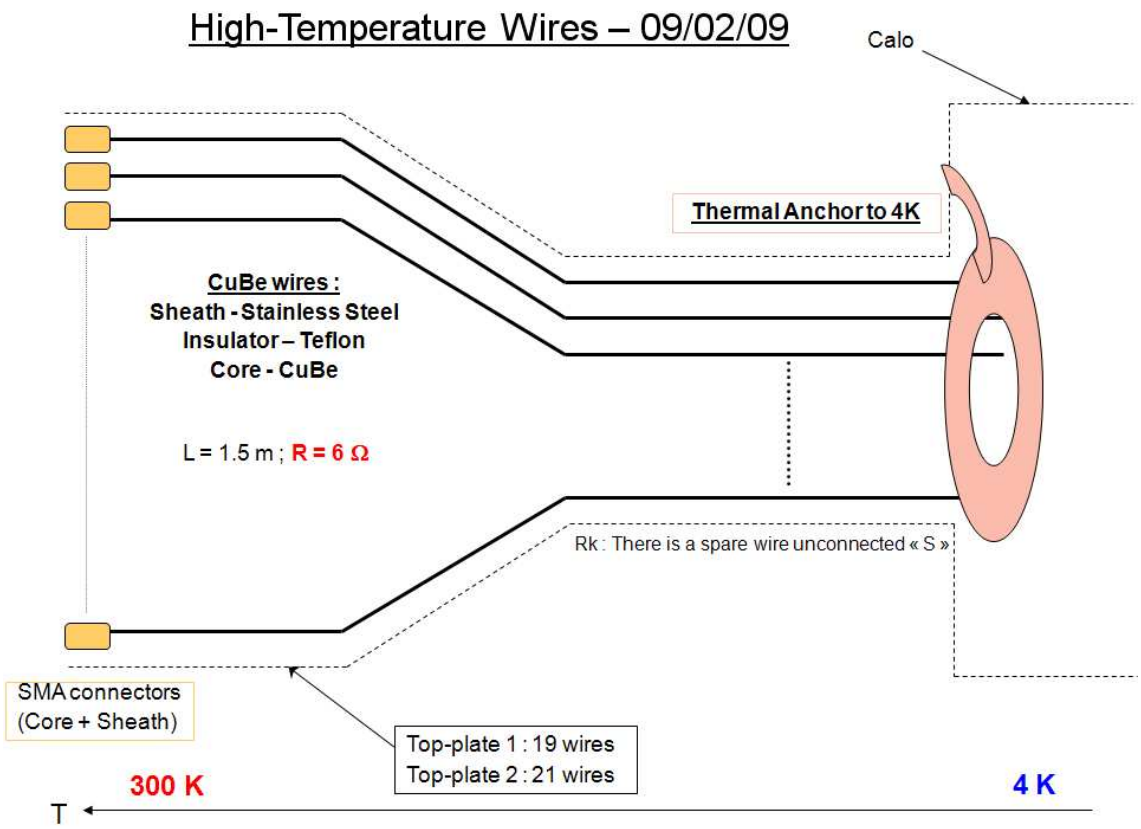

Figure A.1: *High-temperature wiring (from 300 to 4 K) with low resistance wires.*

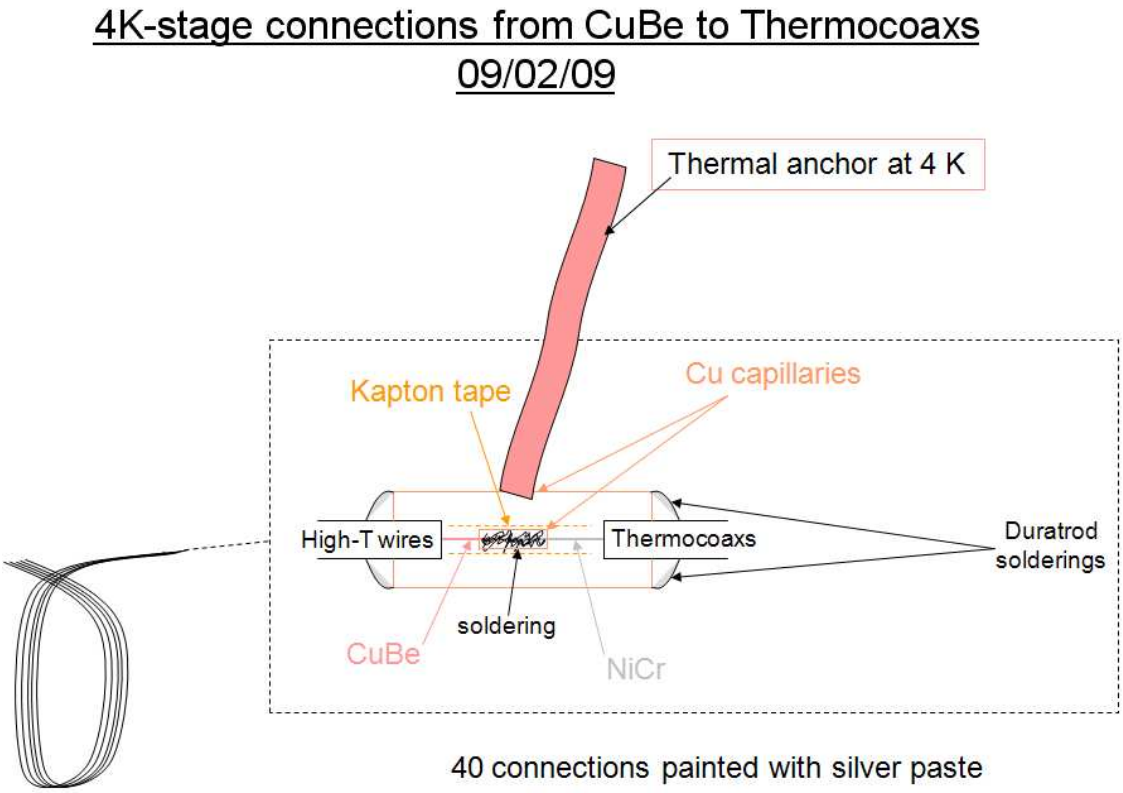

Figure A.2: *Detail of the connection at 4 K between low resistance cables and thermocoaxs. Special care is taken for the thermalization.*

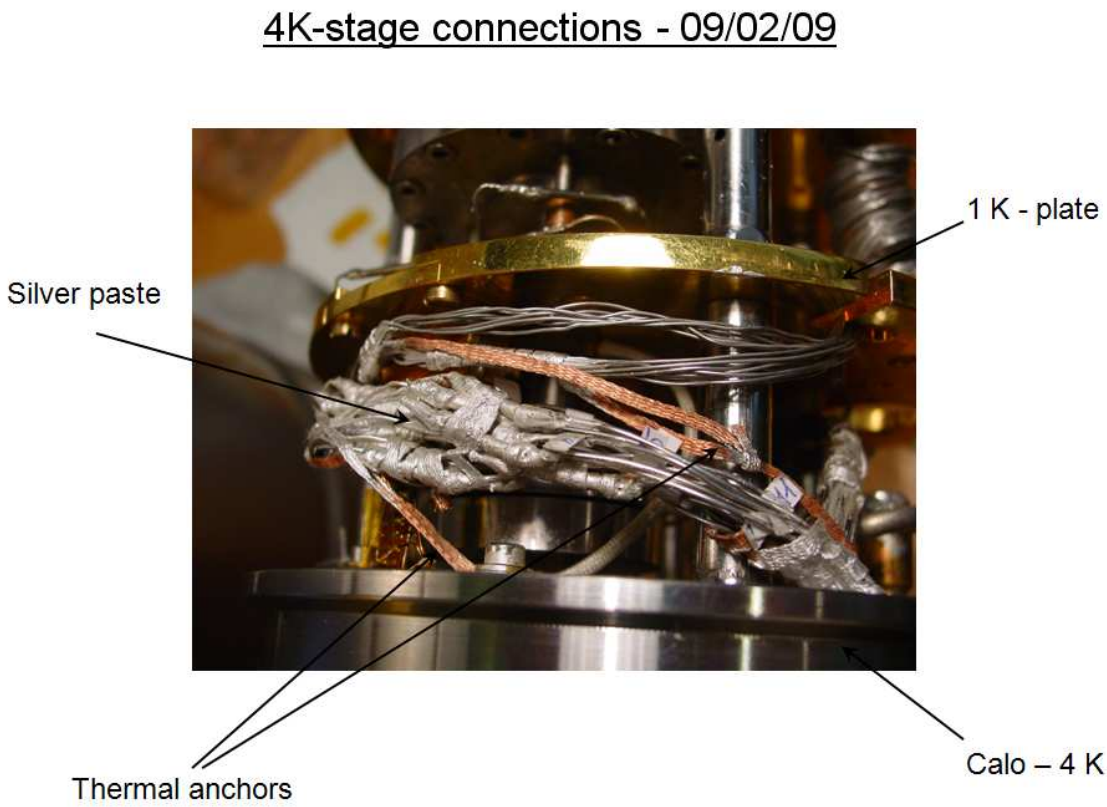

Figure A.3: *Photograph of the 4 K connection between cables.*

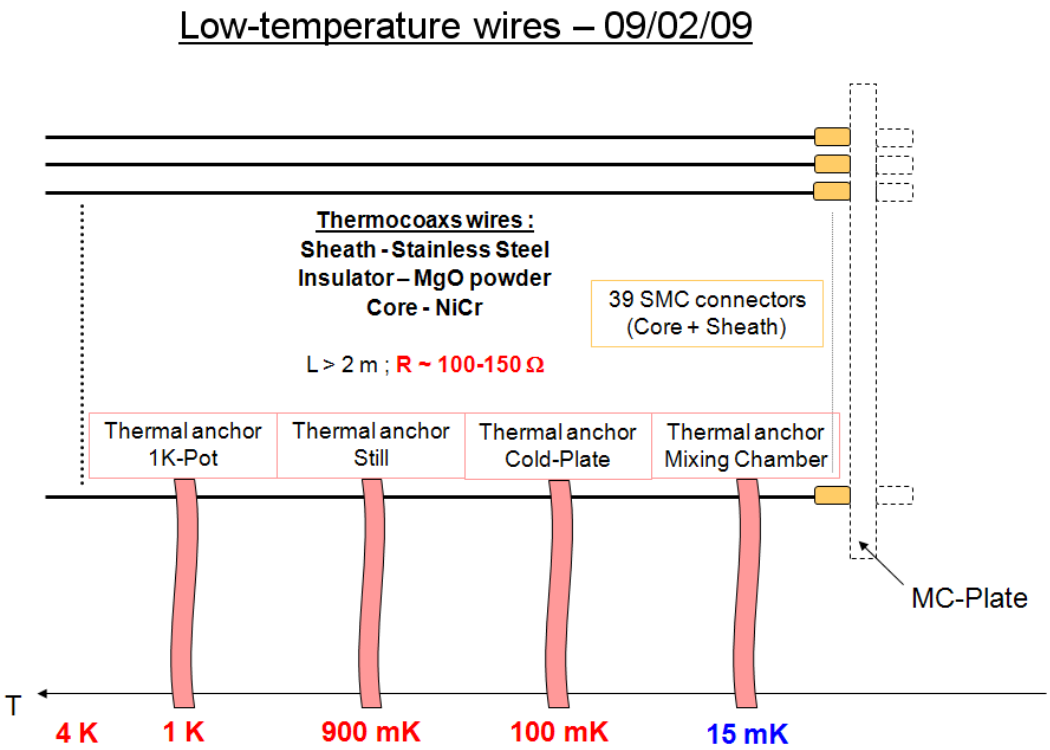

Figure A.4: *Low-temperature wiring (from 4 K down to the mixing chamber plate) with thermocoaxs.*

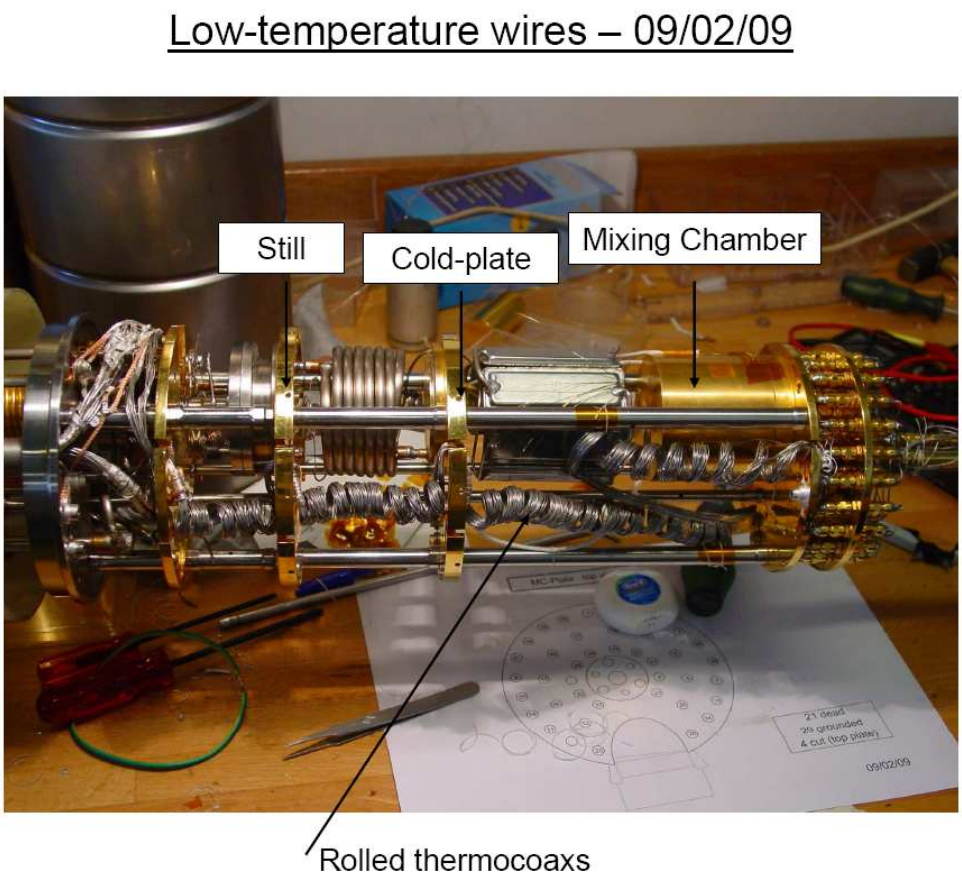

Figure A.5: *Photograph of the low-temperature wiring.*

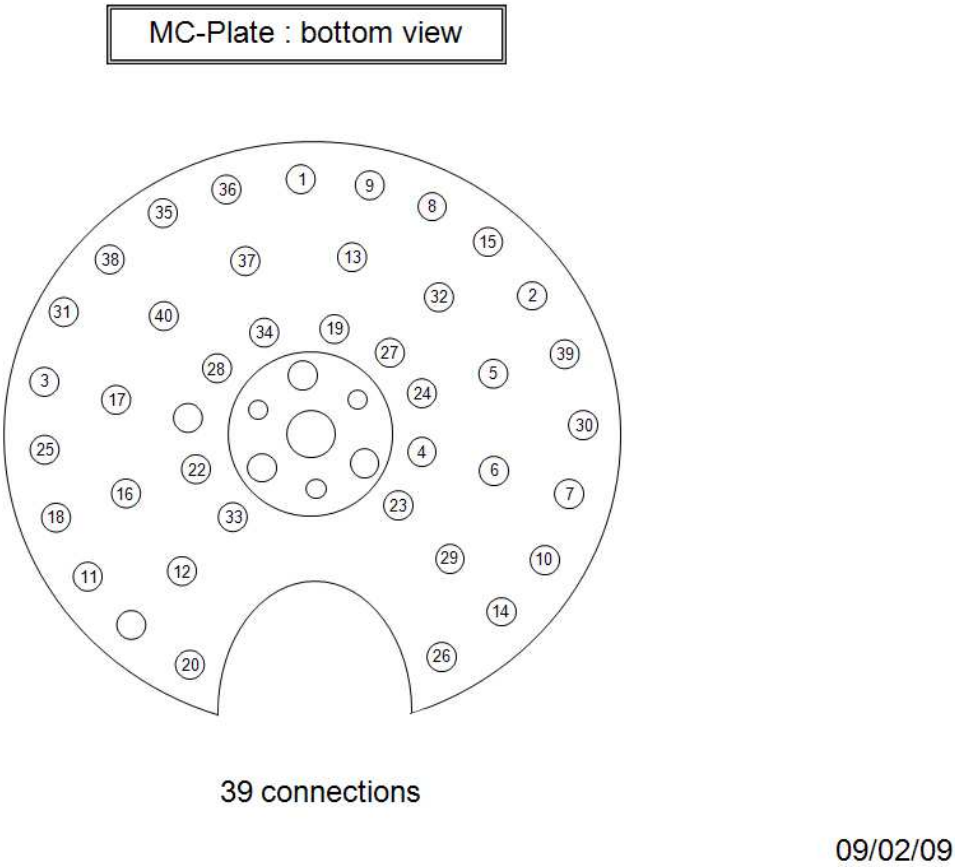

Figure A.6: *Bottom view of the mixing chamber plate.*

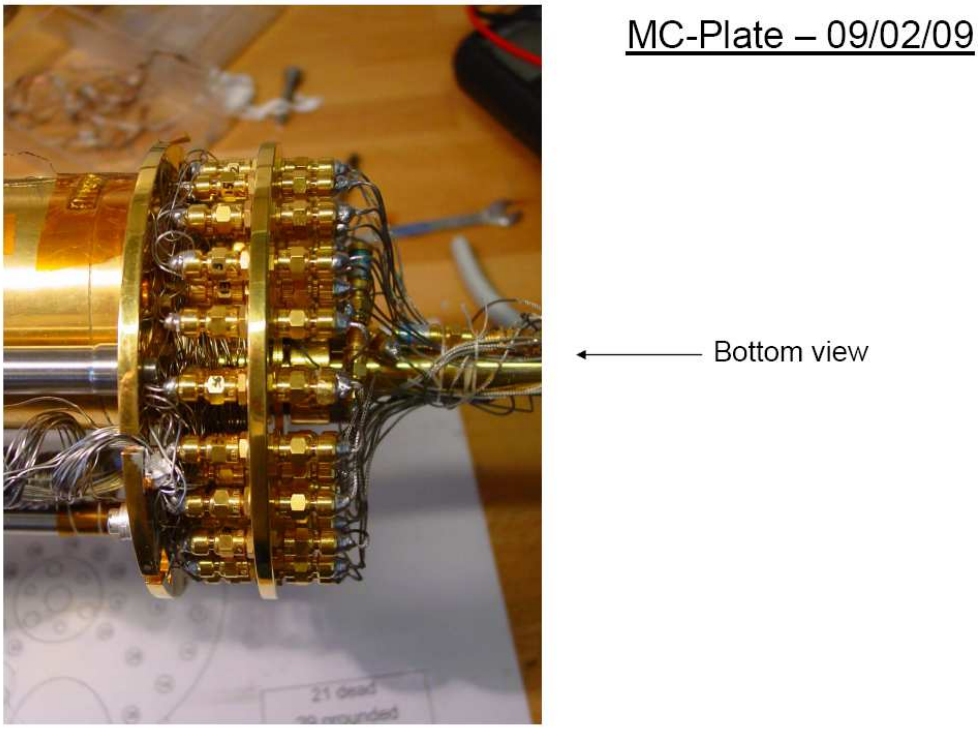

Figure A.7: *Photograph of the mixing chamber plate. The bottom view is on the cold-finger side.*

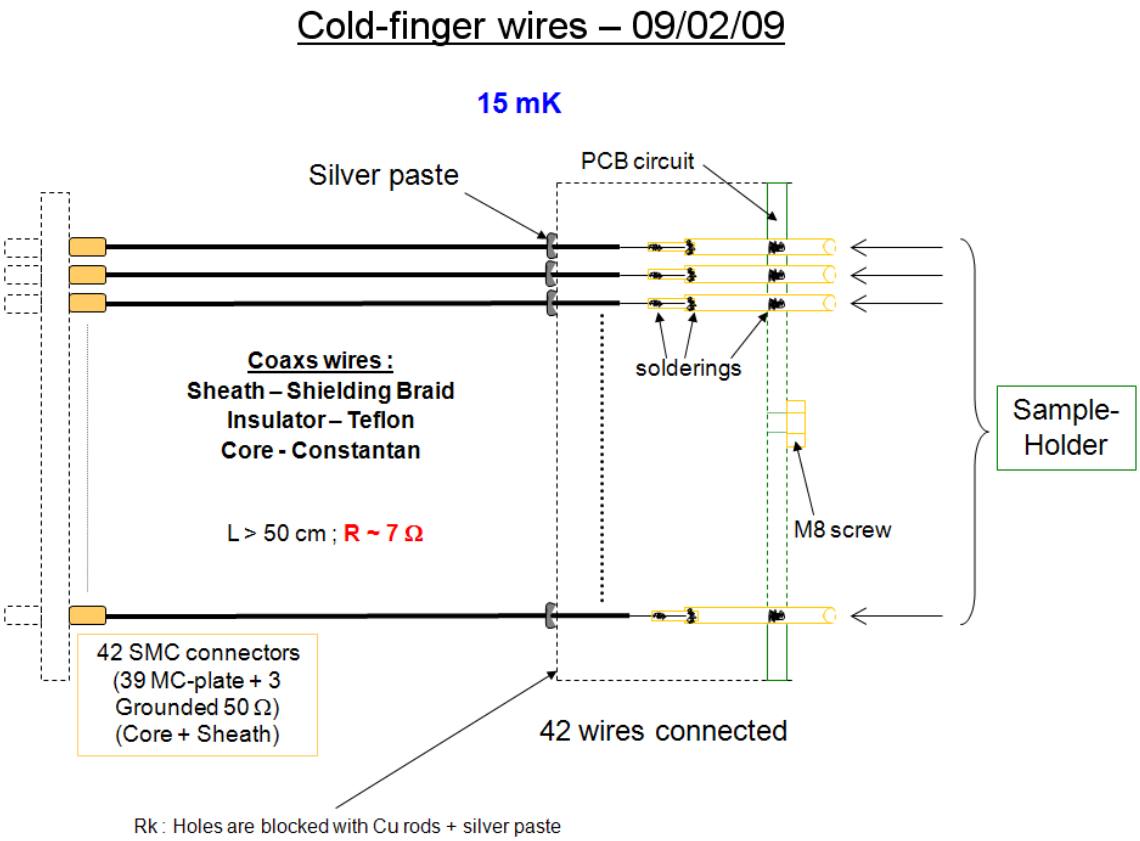

Figure A.8: *Cold-finger wiring with shielded cables.*

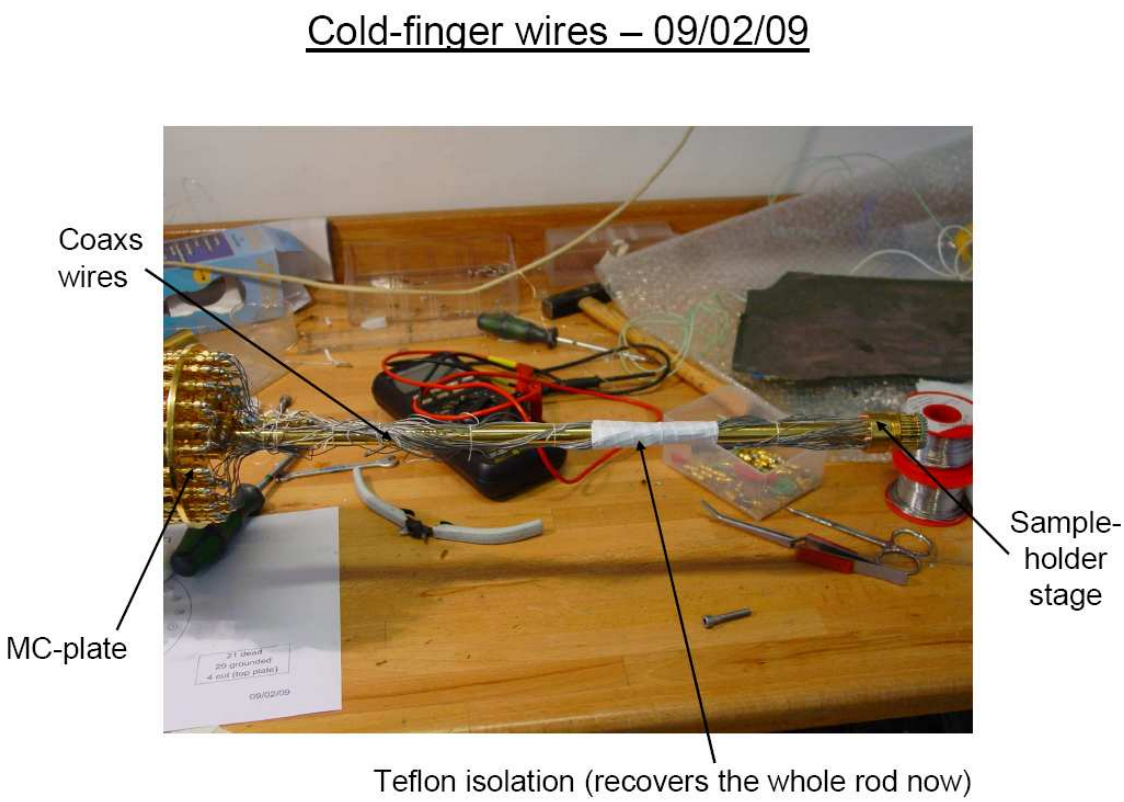

Figure A.9: *Photograph of the cold-finger wiring.*

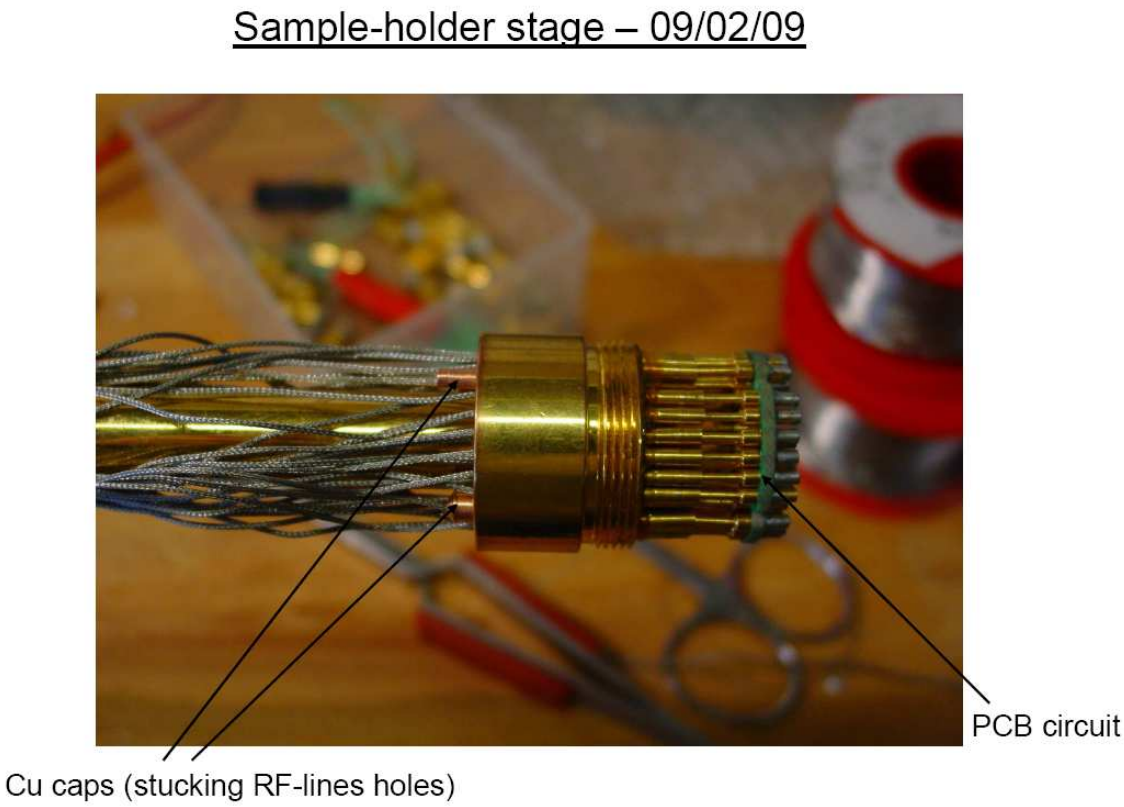

Figure A.10: *Photograph of the sample-holder stage.*

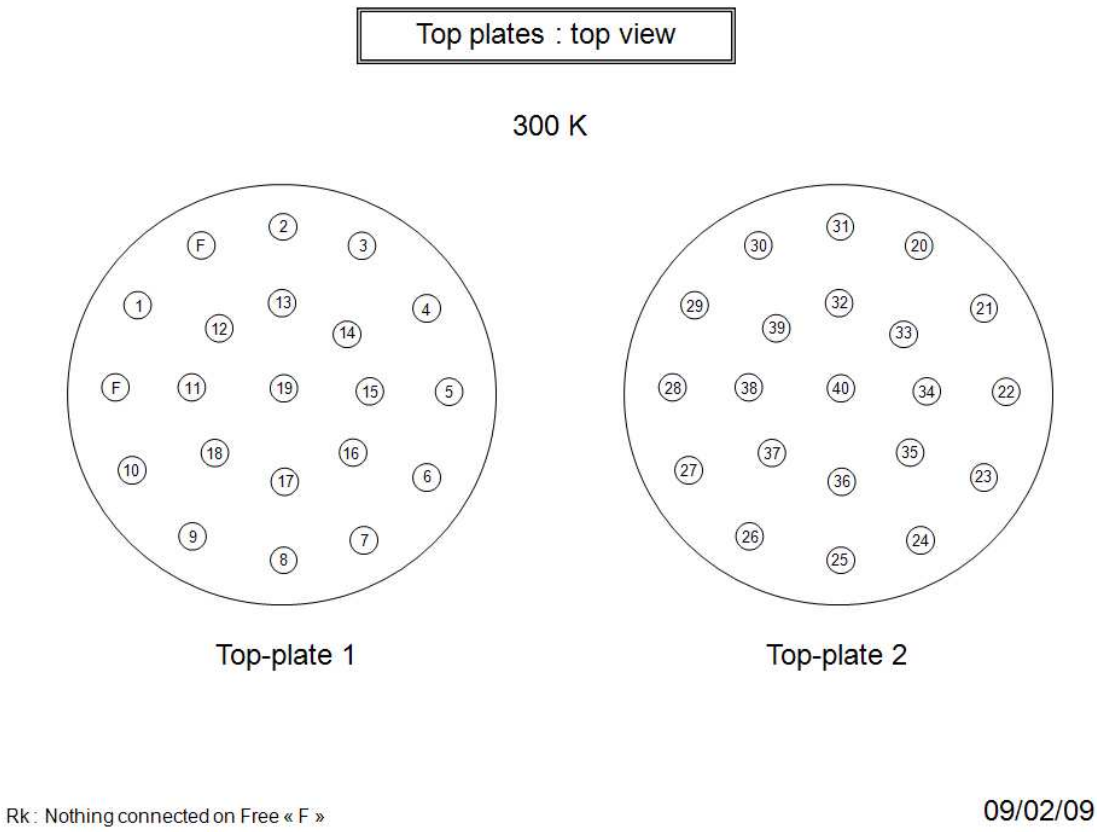

Figure A.11: *Top view of the room-temperature connection plates.*

Appendix B

Extraction of the phase coherence length from the universal conductance fluctuations

We detail here the procedure used to extract the phase coherence length L_Φ in a spin glass sample. The temperature-dependence of the amplitude of the Universal Conductance Fluctuations (UCF) depends on several characteristic lengths: the thermal length L_T defined in chapter 2, the phase coherence length $L_\Phi(T)$ and the length of the sample L. When these lengths are comparable, which is the case in the spin glass sample, the amplitude of the UCF is described by the following formulas [95].

One sets $a = (L/\pi L_\Phi)^2$ and $b = 2(L/\pi L_T)^2$. For a quasi $1d$ sample, the variance of the UCF $\overline{\delta g^2}$, in units of $(e^2/h)^2$, is given by

$$\overline{\delta g^2}(T) = \frac{s^2}{\beta}[2I(a,b) + J(a,b)]$$
$$I(a,b) = \frac{4}{\pi^4}\int_{-\infty}^{\infty} dx F(x) \sum_n \frac{1}{(n^2+a)^2 + x^2 b^2}$$
$$J(a,b) = \frac{4}{\pi^4}\int_{-\infty}^{\infty} dx F(x) \sum_n \frac{(n^2+a)^2 - x^2 b^2}{[(n^2+a)^2 + x^2 b^2]^2}$$

where s is the spin degeneracy and β a numerical factor taking into account time-reversal symmetry. The function $F(x) = (x \coth x - 1)/(\sinh x^2)$. This formula can be computed numerically, and one recovers analytic functions in the asymptotic regimes [30]. As an example, $\overline{\delta g^2} = \frac{2\pi s^2}{3\beta}\frac{L_T^2 L_\Phi}{L^3}$ when $L_T \ll L_\Phi \ll L$.

In our experiment, we have in addition to take into account spin-orbit effects that are not negligible in Ag, and elastic magnetic scattering due to the presence of magnetic impurities. It leads to a modification of the above formulas [96]. These effects can be directly incorporated by setting $d = \frac{4}{3}\left(\frac{L}{\pi L_{so}}\right)^2$ with L_{so} the spin-orbit length and $c = \frac{4}{3}\left(\frac{L}{\pi L_m}\right)^2$ with L_m the magnetic

length. One sets $a_m = a + c + d$, and the resulting variance of the UCF is thus written as

$$\overline{\delta g^2}(T) = \frac{s^2}{\beta}\left(\frac{1}{2}J(a,b) + \frac{3}{2}J(a_m,b)\right) + \frac{s^2}{\beta}\left(\frac{1}{4}I(a,b) + \frac{3}{4}I(a_m,b)\right) \tag{B.0.1}$$

Typically, for the calculation presented in chapter 7, we have used the following parameters. The spin-orbit length $L_{so} \approx 300$ nm is known in Ag [54]. We have evaluated that $L/L_m \approx 1$. The thermal length L_T is calculated at all temperatures. From the experimental amplitude of the UCF $\delta g(T)$, we can thus calculate numerically the corresponding value for L_Φ.

Bibliography

[1] Neil W. Ashcroft and David N. Mermin. *Solid State Physics*. Thomson Learning, Toronto, 1st edition, January 1976.

[2] Charles Kittel. *Introduction to Solid State Physics*. Wiley, 7th edition, July 1995.

[3] K. Binder and A. P. Young. Spin glasses: Experimental facts, theoretical concepts, and open questions. *Rev. Mod. Phys.*, 58(4):801–976, Oct 1986.

[4] K. H. Fisher and J. A. Hertz. *Spin Glasses*. Cambridge University Press, 1991.

[5] J.A. Mydosh. *Spin glasses, An experimental introduction*. Taylor and Francis, London, 1993.

[6] M. Mézard, G. Parisi, and M. Virasoro. *Spin Glass Theory and Beyond*. Wolrd Scientific Publishing Company, 1987.

[7] Gérard Toulouse. Theory of the frustration effect in spin glasses. *Commun. Phys.*, 2:115, 1977.

[8] V. Cannella and J. A. Mydosh. Magnetic ordering in gold-iron alloys. *Phys. Rev. B*, 6(11):4220–4237, Dec 1972.

[9] C. A. M. Mulder, A. J. van Duyneveldt, and J. A. Mydosh. Susceptibility of the cumn spin-glass: Frequency and field dependences. *Phys. Rev. B*, 23(3):1384–1396, Feb 1981.

[10] T. Kasuya. A theory of metallic ferro- and antiferromagnetism on zener's model. *Progress of Theoretical Physics*, 16:45–57, July 1956.

[11] M. A. Ruderman and C. Kittel. Indirect exchange coupling of nuclear magnetic moments by conduction electrons. *Phys. Rev.*, 96(1):99, Oct 1954.

[12] Kei Yosida. Magnetic properties of cu-mn alloys. *Phys. Rev.*, 106(5):893–898, Jun 1957.

[13] J. Souletie and R. Tournier. Specific heat and magnetization in dilute magnetic alloys. *Journal of Low Temperature Physics*, Volume 1:95 – 108, 1969.

[14] E. Vincent, J. Hammann, M. Ocio, J.-P. Bouchaud, and L.F. Cugliandolo. Lecture notes in physics. In M. Rubi, editor, *Complex Behaviour of Glassy Systems*, volume 492, pages 184 – 219. Springer, 1997.

[15] S. F. Edwards and P. W. Anderson. Theory of spin glasses. ii. *Journal of Physics F: Metal Physics*, 6(10):1927, 1976.

[16] Giorgio Parisi. Order parameter for spin-glasses. *Phys. Rev. Lett.*, 50(24):1946–1948, Jun 1983.

[17] S. F. Edwards and P. W. Anderson. Theory of spin glasses. *Journal of Physics F: Metal Physics*, 5(5):965, 1975.

[18] David Sherrington and Scott Kirkpatrick. Solvable model of a spin-glass. *Phys. Rev. Lett.*, 35(26):1792–1796, Dec 1975.

[19] Marek Cieplak and Jayanth R. Banavar. Lower critical dimensionality of heisenberg spin-glasses. *Phys. Rev. B*, 29(1):469–471, Jan 1984.

[20] F. Matsubara, T. Iyota, and S. Inawashiro. Effect of anisotropy on a short-range ±j heisenberg spin glass in three dimensions. *Phys. Rev. Lett.*, 67(11):1458–1461, Sep 1991.

[21] J. R. L. de Almeida and D. J. Thouless. Stability of the sherrington-kirkpatrick solution of a spin glass model. *Journal of Physics A: Mathematical and General*, 11(5):983, 1978.

[22] G. Parisi. Infinite number of order parameters for spin-glasses. *Phys. Rev. Lett.*, 43(23):1754–1756, Dec 1979.

[23] G Parisi. A sequence of approximated solutions to the s-k model for spin glasses. *Journal of Physics A: Mathematical and General*, 13(4):L115, 1980.

[24] G Parisi. The order parameter for spin glasses: a function on the interval 0-1. *Journal of Physics A: Mathematical and General*, 13(3):1101, 1980.

[25] G Parisi. Magnetic properties of spin glasses in a new mean field theory. *Journal of Physics A: Mathematical and General*, 13(5):1887, 1980.

[26] Daniel S. Fisher and David A. Huse. Equilibrium behavior of the spin-glass ordered phase. *Phys. Rev. B*, 38(1):386–411, Jul 1988.

[27] Daniel S. Fisher and David A. Huse. Ordered phase of short-range ising spin-glasses. *Phys. Rev. Lett.*, 56(15):1601–1604, Apr 1986.

[28] Yoseph Imry and Shang-keng Ma. Random-field instability of the ordered state of continuous symmetry. *Phys. Rev. Lett.*, 35(21):1399–1401, Nov 1975.

[29] Silvio Franz, Marc Mézard, Giorgio Parisi, and Luca Peliti. Measuring equilibrium properties in aging systems. *Phys. Rev. Lett.*, 81(9):1758–1761, Aug 1998.

[30] E. Akkermans and G. Montambaux. *Mesoscopic Physics of Electrons and Photons*. Cambridge University Press, 2007.

[31] S. Datta. *Electronic Transport in Mesoscopic Systems*. Cambridge University Press, 1997.

[32] Yoseph Imry. *Introduction to mesoscopic physics second edition*. Oxford University Press, 2002.

[33] B. L. Al'Tshuler. Fluctuations in the extrinsic conductivity of disordered conductors. *Soviet Journal of Experimental and Theoretical Physics Letters*, 41:648, June 1985.

[34] Dominique Mailly and Marc Sanquer. Sensitivity of quantum conductance fluctuations and of 1/f noise to time reversal symmetry. *J. Phys. I France*, 2(4):357–364, 1992.

[35] Y. Aharonov and D. Bohm. Significance of electromagnetic potentials in the quantum theory. *Phys. Rev.*, 115(3):485–491, Aug 1959.

[36] P. A. Lee and A. Douglas Stone. Universal conductance fluctuations in metals. *Phys. Rev. Lett.*, 55(15):1622–1625, Oct 1985.

[37] P. A. Lee, A. Douglas Stone, and H. Fukuyama. Universal conductance fluctuations in metals: Effects of finite temperature, interactions, and magnetic field. *Phys. Rev. B*, 35(3):1039–1070, Jan 1987.

[38] D. J. Thouless. Maximum metallic resistance in thin wires. *Phys. Rev. Lett.*, 39(18):1167–1169, Oct 1977.

[39] M. Büttiker. Four-terminal phase-coherent conductance. *Phys. Rev. Lett.*, 57(14):1761–1764, Oct 1986.

[40] Selman Hershfield. Resistance fluctuations with magnetic impurities in a four-terminal geometry. *Phys. Rev. B*, 44(7):3320–3323, Aug 1991.

[41] B. L. Al'Tshuler and B. Z. Spivak. Variation of the random potential and the conductivity of samples of small dimensions. *ZhETF Pis ma Redaktsiiu*, 42:363, November 1985.

[42] Shechao Feng, Patrick A. Lee, and A. Douglas Stone. Sensitivity of the conductance of a disordered metal to the motion of a single atom: Implications for 1/f noise. *Phys. Rev. Lett.*, 56(18):1960–1963, May 1986.

[43] M. B. Weissman. What is a spin glass? a glimpse via mesoscopic noise. *Rev. Mod. Phys.*, 65(3):829–839, Jul 1993.

[44] N. E. Israeloff, M. B. Weissman, G. J. Nieuwenhuys, and J. Kosiorowska. Electrical noise from spin fluctuations in cumn. *Phys. Rev. Lett.*, 63(7):794–797, Aug 1989.

[45] P. G. N. de Vegvar, L. P. Lévy, and T. A. Fulton. Conductance fluctuations of mesoscopic spin glasses. *Phys. Rev. Lett.*, 66(18):2380–2383, May 1991.

[46] M. B. Weissman. Comment on conductance fluctuations of mesoscopic spin glasses. *Phys. Rev. Lett.*, 68(23):3484, Jun 1992.

[47] David Carpentier and Edmond Orignac. Measuring overlaps in mesoscopic spin glasses via conductance fluctuations. *Physical Review Letters*, 100(5):057207, 2008.

[48] Guillaume Paulin. *Transport electronique et verres de spins*. PhD thesis, Ecole Normale Supérieure de Lyon - Université Lyon 1, 22 juin 2010.

[49] G. Paulin and D. Carpentier. Conductance correlations in a mesoscopic spin glass wire : a numerical landauer study. *ArXiv e-prints*, 0910:4341, October 2009.

[50] A. A. Fedorenko and D. Carpentier. Nonlinear sigma-model study of magnetic dephasing in a mesoscopic spin glass. *EPL (Europhysics Letters)*, 88(5):57009, 2009.

[51] A. C. Hewson. *The Kondo Problem to Heavy Fermions*. Cambridge University Press, 1997.

[52] Laurent Saminadayar, Pritiraj Mohanty, Richard A. Webb, Pascal Degiovanni, and Christopher Bäuerle. Electron coherence at low temperatures: The role of magnetic impurities. *Physica E: Low-dimensional Systems and Nanostructures*, 40(1):12 – 24, 2007. Proceedings of the International Workshop on Quantum Coherence, Noise and Decoherence in Nanostructures.

[53] Benjamin Huard. *Interactions entre électrons, effet Josephson mésoscopique et fluctuations asymétriques du courant*. PhD thesis, Université Paris 6, 2006.

[54] Thibaut Capron, Yasuhiro Niimi, François Mallet, Yannick Baines, Dominique Mailly, Fang-Yuh Lo, Alexander Melnikov, Andreas D. Wieck, Laurent Saminadayar, and Christopher Bäuerle. Low-temperature dephasing in irradiated metallic wires. *Phys. Rev. B*, 77(3):033102, Jan 2008.

[55] J. B. Johnson. Thermal agitation of electricity in conductors. *Phys. Rev.*, 32(1):97, Jul 1928.

[56] H. Nyquist. Thermal agitation of electric charge in conductors. *Phys. Rev.*, 32(1):110–113, Jul 1928.

[57] D. C. Glattli, P. Jacques, A. Kumar, P. Pari, and L. Saminadayar. A noise detection scheme with 10 mk noise temperature resolution for semiconductor single electron tunneling devices. *Journal of Applied Physics*, 81(11):7350–7356, 1997.

[58] A. B. Zorin. The thermocoax cable as the microwave frequency filter for single electron circuits. *Review of Scientific Instruments*, 66(8):4296–4300, 1995.

[59] F. C. Wellstood, C. Urbina, and John Clarke. Hot-electron effects in metals. *Phys. Rev. B*, 49(9):5942–5955, Mar 1994.

[60] M. Henny, H. Birk, R. Huber, C. Strunk, A. Bachtold, M. Krüger, and C. Schönenberger. Electron heating effects in diffusive metal wires. *Applied Physics Letters*, 71(6):773–775, 1997.

[61] F. Pierre, A. B. Gougam, A. Anthore, H. Pothier, D. Esteve, and Norman O. Birge. Dephasing of electrons in mesoscopic metal wires. *Phys. Rev. B*, 68(8):085413, Aug 2003.

[62] Wilfried Rabaud. *Courants Permanents dans des Anneaux Mésoscopiques Connectés*. PhD thesis, Université Joseph Fourier - Grenoble 1, 2001.

[63] Gerd Bergmann. Weak localization in thin films : a time-of-flight experiment with conduction electrons. *Physics Reports*, 107(1):1 – 58, 1984.

[64] Y. Niimi, Y. Baines, T. Capron, D. Mailly, F.-Y. Lo, A. D. Wieck, T. Meunier, L. Saminadayar, and C. Bäuerle. Effect of disorder on the quantum coherence in mesoscopic wires. *Physical Review Letters*, 102(22):226801, 2009.

[65] Shinobu Hikami, Anatoly I. Larkin, and Yosuke Nagaoka. Spin-orbit interaction and magnetoresistance in the two dimensional random system. *Progress of Theoretical Physics*, 63(2):707–710, 1980.

[66] B. L. Altshuler, A. G. Aronov, and D. E. Khmelnitsky. Effects of electron-electron collisions with small energy transfers on quantum localisation. *Journal of Physics C: Solid State Physics*, 15(36):7367, 1982.

[67] I. L. Aleiner and Ya. M. Blanter. Inelastic scattering time for conductance fluctuations. *Phys. Rev. B*, 65(11):115317, Feb 2002.

[68] H. Vloeberghs, J. Vranken, C. van Haesendonck, and Y. Bruynseraede. Destruction of the spin-glass order in thin aufe films. *EPL (Europhysics Letters)*, 12(6):557–562, 1990.

[69] L. Hoines, R. Stubi, R. Loloee, J. A. Cowen, and J. Bass. How thin a spin glass is still a spin glass? *Phys. Rev. Lett.*, 66(9):1224–1227, Mar 1991.

[70] O. Laborde and P. Radhakrishna. Disappearance of interaction effects in dilute gold-iron alloys. *Solid State Communications*, 9:701–703, May 1971.

[71] J. A. Mydosh, P. J. Ford, M. P. Kawatra, and T. E. Whall. Electrical resistivity of aufe alloys in the spin-glass, mictomagnetic, and ferromagnetic regimes. *Phys. Rev. B*, 10(7):2845–2856, Oct 1974.

[72] Ulf Larsen. Resistance maximum in spin glasses. *Phys. Rev. B*, 14(10):4356–4367, Nov 1976.

[73] M. G. Vavilov, L. I. Glazman, and A. I. Larkin. Electron transport and energy relaxation in dilute magnetic alloys. *Phys. Rev. B*, 68(7):075119, Aug 2003.

[74] C. Rizzuto. Formation of localized moments in metals: experimental bulk properties. *Reports on Progress in Physics*, 37(2):147, 1974.

[75] B. L. Al'Tshuler and A. G. Aronov. Magnetoresistance of thin films and of wires in a longitudinal magnetic field. *Soviet Journal of Experimental and Theoretical Physics Letters*, 33:499, May 1981.

[76] F. Mallet, J. Ericsson, D. Mailly, S. Ünlübayir, D. Reuter, A. Melnikov, A. D. Wieck, T. Micklitz, A. Rosch, T. A. Costi, L. Saminadayar, and C. Bäuerle. Scaling of the low-temperature dephasing rate in kondo systems. *Phys. Rev. Lett.*, 97(22):226804, Nov 2006.

[77] P. J. Ford and J. A. Mydosh. Electrical resistivity of noble-metal-host-3 d solute spin-glass alloys. *Phys. Rev. B*, 14(5):2057–2070, Sep 1976.

[78] O. Laborde and P. Radhakrishna. Interaction effects in copper-manganese alloys at low temperatures. *Journal of Physics F: Metal Physics*, 3(9):1731–1737, September 1973.

[79] Shoichi Nagata, P. H. Keesom, and H. R. Harrison. Low-dc-field susceptibility of cumn spin glass. *Phys. Rev. B*, 19(3):1633–1638, Feb 1979.

[80] C. Djurberg, K. Jonason, and P. Nordblad. Magnetic relaxation phenomena in a cumn spin glass. *Eur. Phys. J. B*, 10(1):15–21, 1999.

[81] Petra Erika Jönsson and Hajime Takayama. "glassy dynamics" in ising spin glasses — experiment and simulation—. *Journal of the Physical Society of Japan*, 74(4):1131–1134, 2005.

[82] V. I. Fal'ko. The aharonov-bohm effect in a mesoscopic ring of diluted magnetic alloy. *Journal of Physics: Condensed Matter*, 4(15):3943, 1992.

[83] M. G. Vavilov and L. I. Glazman. Conductance of mesoscopic systems with magnetic impurities. *Phys. Rev. B*, 67(11):115310, Mar 2003.

[84] A. Benoit, D. Mailly, P. Perrier, and P. Nedellec. Effect of magnetic impurities of universal conductance fluctuations. *Superlattices and Microstructures*, 11(3):313 – 316, 1992.

[85] P. Mohanty and R. A. Webb. High-field measurements of electron decoherence time in metallic nanowires: Switching off magnetic impurity spins. *Phys. Rev. Lett.*, 91(6):066604, Aug 2003.

[86] F. Pierre and Norman O. Birge. Dephasing by extremely dilute magnetic impurities revealed by aharonov-bohm oscillations. *Phys. Rev. Lett.*, 89(20):206804, Oct 2002.

[87] A. K. Nigam and A. K. Majumdar. Magnetoresistance in canonical spin-glasses. *Phys. Rev. B*, 27(1):495–511, Jan 1983.

[88] J. J. Smit, G. J. Nieuwenhuys, and L. J. de Jongh. Evidence for mn clustering in dilute cumn alloys from high-field (40 t) magnetization curves at 4.2 k. *Solid State Communications*, 31(4):265 – 270, 1979.

[89] G. Kotliar and H. Sompolinsky. Phase transition in a dzyaloshinsky-moriya spin-glass. *Phys. Rev. Lett.*, 53(18):1751–1754, Oct 1984.

[90] G. Gruner and A. Zawadowski. Magnetic impurities in non-magnetic metals. *Reports on Progress in Physics*, 37(12):1497, 1974.

[91] François Mallet. *Transport quantique et effet Kondo*. PhD thesis, Université Joseph Fourier, 2007.

[92] Marc Gabay and Gérard Toulouse. Coexistence of spin-glass and ferromagnetic orderings. *Phys. Rev. Lett.*, 47(3):201–204, Jul 1981.

[93] Dorothée Petit, L. Fruchter, and I. A. Campbell. Ordering in heisenberg spin glasses. *Phys. Rev. Lett.*, 88(20):207206, May 2002.

[94] G. G. Kenning, D. Chu, and R. Orbach. Irreversibility crossover in a cu:mn spin glass in high magnetic fields: Evidence for the gabay-toulouse transition. *Phys. Rev. Lett.*, 66(22):2923–2926, Jun 1991.

[95] Gilles Montambaux. Conductance fluctuations in quasi-1d wires: full temperature and l_Φ dependences. Private communication.

[96] Guillaume Paulin and David Carpentier. Conductance fluctuations. Private communication.

Résumé

Le verre de spin est une phase de la matière dans laquelle le désordre magnétique est gelé. Étant considéré comme un système modèle des verres en général, il a fait l'objet de nombreux travaux théoriques et expérimentaux. Les recherches ont convergé vers deux principales descriptions de l'état fondamental du système diamétralement opposées. D'une part, la solution "champ-moyen" nécessite une brisure de symétrie non triviale, et l'état fondamental est composé de multiples états organisés en une structure hiérarchique. D'autre part, une approche de "gouttelettes", fondée sur la dynamique hors-équilibre d'un état fondamental unique. La validation expérimentale d'une de ces deux théories nécessite une observation détaillée de l'échantillon au niveau microscopique. La physique mésoscopique, basée sur les effets d'interférences électroniques, propose un outil unique pour accéder à cette configuration microscopique des impuretés : les fluctuations universelles de conductance. En effet, ces fluctuations représentent une empreinte unique du désordre dans l'échantillon. Ce travail présente la mise en œuvre de mesures de fluctuations de conductance universelles dans les verres de spin. Les effets d'interférences électroniques étant sensibles aux processus de décohérence du verre de spin, ils donnent accès expérimentalement à de nouvelles quantités concernant les excitations du système. La mesure des corrélations entre les empreintes du désordre permet quant à elle d'explorer sous un angle nouveau l'ordre non conventionnel de cet état vitreux.
Mots-clefs : Physique Mésoscopique, Transport Électronique Cohérent, Fluctuations Universelles de Conductance, Verres de Spin, Systèmes Désordonnés, Cohérence Quantique, Nanostructures Métalliques, Recouvrement de Spins, Empreinte Magnétique.

Abstract

The spin glass is a state of matter in which the magnetic disorder is quenched. Being considered as a model system for glasses in general, it has been extensively studied, both theoretically and experimentally. The research have converged towards two main descriptions of the fundamental state of the system that are clearly antagonist. On the one hand, the "mean-field" solution has a non trivial broken symmetry, and the ground state is composed of multiple states in a hierarchical structure. On the other hand, a magnetic "droplet" model, based on the off-equilibrium dynamics of a unique ground state. The experimental validation of one of these two theories requires a detailed observation of the sample at the microscopic level. Mesoscopic physics, which deals with interference effects of the electrons, proposes a unique tool to access to this microscopic configuration of the impurities: the universal conductance fluctuations. Indeed, these fluctuations represent a unique fingerprint of the sample disorder. This work presents the implementation of universal conductance fluctuations measurements in spin glasses. The electron interference effects being sensitive to the decoherence processes of the spin glass, they give access experimentally to new quantities related to the excitations of the system. The measurement of correlations between the disorder fingerprints allow to explore under a new perspective the non conventional order of this glassy state.
Keywords: Mesoscopic Physics, Coherent Electron Transport, Universal Conductance Fluctuations, Spin Glasses, Disordered Systems, Quantum Coherence, Metallic Nanostructures, Spin Overlap, Magnetofingerprint.